Measurements of water isotope composition and depth variation reveal strong influence of hydroclimate on water balance and water levels of shallow lakes in the Peace-Athabasca Delta (northern Alberta, Canada)

by

Arisha Imran

A thesis
presented to the University of Waterloo
in fulfilment of the
thesis requirement for the degree of
Master of Science
in
Biology (Water)

Waterloo, Ontario, Canada, 2024

© Arisha Imran 2024

Author's Declaration

This thesis consists of material all of which I authored or co-authored: see Statement of Contributions included in the thesis. This is a true copy of the thesis, including any required final revisions, as accepted by my examiners.

I understand that my thesis may be made electronically available to the public.

Statement of Contributions

I am the sole author of Chapter 1 and Chapter 4, which were written under the supervision of Professor Roland Hall and Professor Brent Wolfe and not intended for publication.

Chapter 2 has been published as: Imran, A., Neary, L. K., Falcone, M. D., Wolfe, B. B., Hall, R. I., 2024. Value of long-term isotope monitoring of an index lake for tracking changes in lake water balances across a northern freshwater landscape. *Journal of Hydrology: Regional Studies*, 53, 101765. https://doi.org/10.1016/j.ejrh.2024.101765.

CRediT author statement for Chapter 2: **Arisha Imran**: Conceptualization, Data curation, Formal analysis, Investigation, Methodology, Visualization, Writing – original draft; **Laura K. Neary**: Investigation, Writing – review & editing; **Matthew D. Falcone**: Formal Analysis, Investigation, Writing – review & editing; **Brent B. Wolfe**: Conceptualization, Funding acquisition, Methodology, Investigation, Project administration, Resources, Supervision, Writing – review & editing; **Roland I. Hall**: Conceptualization, Funding acquisition, Methodology, Investigation, Project administration, Resources, Supervision, Writing – review & editing.

Chapter 3 has been prepared as a manuscript written for publication as a peer-reviewed scientific journal paper: Imran, A., Neary, L. K., Hall, R. I., Wolfe, B. B. Overlooked and underrated: Snowmelt runoff rivals influence of river floodwaters on lake-level rise at a cold region freshwater delta. This manuscript will be submitted after the thesis defence.

CRediT author statement for Chapter 3: **Arisha Imran**: Conceptualization, Data curation, Formal analysis, Investigation, Methodology, Visualization, Writing – original draft; **Laura K. Neary**: Investigation, Data curation, Writing – review & editing; **Roland I. Hall**: Conceptualization, Funding acquisition, Methodology, Project administration, Resources, Supervision, Writing – review & editing; **Brent B. Wolfe**: Conceptualization, Funding acquisition, Methodology, Project administration, Resources, Supervision, Writing – review & editing.

Abstract

Shallow water bodies are abundant, productive ecosystems in northern high-latitude regions where they provide habitat for fauna and hold socio-economic and cultural importance for remote communities. In northeastern Alberta, the Peace-Athabasca Delta (PAD), located within Wood Buffalo National Park (WBNP), is a large (~6000 km^2) inland freshwater-rich landscape with an abundance of shallow lakes that is listed as a Ramsar Wetland of International Importance and contributes to WBNP's UNESCO World Heritage status. However, concerns have long persisted about the effects of primarily hydroelectric regulation of Peace River flow and climate change on widespread drawdown of lake water-levels in the delta. In response to these concerns, and pressures from local communities and an international agency, a federal Action Plan was developed with goals to improve aquatic ecosystem monitoring at the PAD. Despite considerable prior study, this requires better understanding of hydrological processes that influence lake water balances and water levels in the delta and advancement of methodological approaches. A 7-year research project was launched in 2015 to inform the design of a long-term aquatic ecosystem monitoring program at the PAD. Research presented in this thesis is an outcome of two key observations that were made during the last two years (2020-2021) of that project, which provided opportunity to explore the influence of unusually high relative humidity on isotope-based lake water-balance modelling and the influence of snowmelt runoff on lake depth when widespread ice-jam flooding occurred.

For two decades, the isotope composition of an index lake (informally named 'PAD 18') provided a constant and reliable estimate of δ_{SSL} (i.e., the water isotope composition of a terminal basin where evaporation = inflow), a key parameter used in an isotope framework for water-balance modelling of lakes at the PAD. In 2020-2021, a sudden and unprecedented shift occurred in the isotope composition of PAD 18, which required closer examination of the isotope framework to ensure accurate assessments of lake water balances. The shift in isotope composition of PAD 18 coincided with an increase in relative humidity by 4.6% from 66.2% (2015-2019) to 70.8% (2020-2021). An independent calculation of $\delta_{SSL,}$ using formulation by Gonfiantini (1986) and flux-weighted air temperature and relative humidity from 2020-2021, was determined to be equivalent to the observed isotope composition of PAD 18 during 2020-2021, confirming the shift in isotope

composition reflected re-equilibration of the lake water with the atmosphere following the rise in relative humidity. The importance of accurate characterization of δ_{SSL} for isotope mass-balance modelling is demonstrated by estimating evaporation-to-inflow (E/I) ratios for 61 lakes across the PAD in July 2021 using the previous 2015-2019 isotope framework and the new 2020-2021 isotope framework. Results show differences between the two frameworks are minor when E/I ratios are low, but they become consequential when E/I ratios are high because of the non-linear effect of relative humidity on isotope framework parameters. Appropriate parametrization for isotope mass-balance modelling is critical for monitoring agencies utilizing isotope-based techniques at the PAD, and elsewhere. Thus, re-evaluation of isotope framework parameters may become increasingly important as climate warming fosters greater variability of meteorological conditions.

Snowmelt runoff is well-recognized for sustaining shallow waterbodies across semi-arid and sub-humid northern regions where evaporation rates are high. At the PAD, however, the influence of snowmelt runoff from within the delta remains largely unknown because the attention on drawdown of perched lakes has focused almost exclusively on alteration of the ice-jam flood regime. During spring of 2020, extensive ice-jam flooding occurred which raised water levels in flooded lakes across the PAD, but water levels rose also in many non-flooded lakes, providing an opportunity to explore the role of snowmelt runoff on lake levels. Using measurements of water depth and water isotope compositions, the contributions from snowmelt runoff and river floodwaters to lake-level rise were quantified at 52 lakes and spatial patterns were explored. Results reveal that the lake-level rise from snowmelt runoff at non-flooded lakes rivals the rise caused by floodwaters at flooded lakes. Geospatial analyses show lake-level rise by snowmelt was greatest in the northern Peace sector and the southwestern margin in the southern Athabasca sector where greater topographic relief and denser vegetation enhance snow accumulation via redistribution of snow by wind from adjacent flat, sparsely vegetated terrain. In contrast, the rise due to floodwater input was greatest in lower lying flood-prone central areas of the Athabasca sector. Exploration of meteorological records since 1963 reveal that similar contributions of snowmelt runoff to lake-level rise as occurred in 2020 were likely common between the early 1960s and late 1980s but only once since 1987 (2018), suggesting that reduced input from snowmelt runoff has contributed to drawdown of shallow perched lakes in recent decades.

Concern for drawdown of water levels in the PAD have prompted a need for enhanced monitoring of lake water balances and water levels, especially as mitigative actions are considered. The research presented in this thesis advances knowledge about the influence of shifts in relative humidity on isotope-based modelling of lake water balances and the role of snowmelt runoff on lake depth. The novel integration of water isotope composition and water depth measurements demonstrated here provides opportunity for assessing the success of mitigative actions such as strategic water releases from the W.A.C. Bennett Dam located upstream of the delta to enhance ice-jam flooding. While long-term aquatic ecosystem monitoring programs must be built on a foundation of knowledge generated through primary research, systematic and repeated measurements over sufficient scales of space and time may also trigger new research that leads to important new discoveries, as revealed in this thesis.

Acknowledgements

The completion of this thesis would not be possible without the support of so many people.

To Brent and Roland – Thank you for taking the time and care to mentor me through this journey, and most importantly, believing in me. You've allowed me to take ownership of my work, which has taught me to trust myself and grow into the scientist I am today. Your encouragement has pushed me beyond limits I did not know I could reach.

To Laura Neary – Thank you for being my mentor, collaborator, and most importantly my friend. I am forever grateful to have you by my side.

To Meredith Watson – You and I are the same person, but different font. Your understanding and support through the good and bad times has meant the world to me and I'm so grateful to have you in my life.

To Laura Anderson – I've appreciated your kindness so much throughout my degree and have made so many fun memories with you in the field.

To current and past members of the Hall/Wolfe lab – Thank you for helping me with my work in any way possible.

To Isabel Jorgensen, Julie DePauw, Lauren Banks, and Taylor Virgin – You are the best things to come out of the Water program/SWIGS! Thank you for being so supportive and giving me not only some perspective, but also some wonderful memories and friendships.

To Aeliya Husain, Rachel To, Akanksha Krishnan, Angela Wang, and Huma Javed – My lifelong pals! Even though we all live in different cities, you have always been close in my heart. Thank you for caring throughout my degree and my life.

To my family and most importantly my parents, Maliha and Imran – Thank you for your constant love and support, even when you didn't understand my work. I would not have made it this far in life without you, and I owe this success to you both.

To the Peace-Athabasca Delta – This landscape has inspired me in many ways throughout my work. It has been such a privilege to have visited the delta, and most importantly, contribute knowledge towards understanding it a bit better.

The research presented in this thesis was supported by grants to co-supervisors Roland I. Hall and Brent B. Wolfe from NSERC (Northern Research Chair, Collaborative Research and Development, Discovery and Northern Research Supplement programs), Alberta Environmental Monitoring, Evaluation & Reporting Agency (now Alberta Environment and Protected Areas), British Columbia Hydro and Power Authority, Canadian Natural Resources Limited, Suncor Energy Incorporated, the Government of Ontario's Premier's Research Excellence Award Program, the Canada Foundation for Innovation New Opportunities Fund, Polar Continental Shelf

Project of Natural Resources Canada, Northern Water Futures of the Global Water Futures Program, the Northern Scientific Training Program of Indian and Northern Affairs Canada (2000–2003) and Polar Knowledge Canada (2016–2019), and Parks Canada Agency (2020–2021).

Table of Contents

Author's Declaration ii

Statement of Contributions iii

Abstract iv

Acknowledgements vii

List of Figures xi

List of Tables xvi

Chapter 1 | Introduction 1

Chapter 2 | Value of long-term isotope monitoring of an index lake for tracking changes in lake water balances across a northern freshwater landscape 6

2.1 Introduction 6

2.2 Methods 11

2.2.1 Study site 11

2.2.2 Sample collection and analysis 12

2.2.3 Meteorological data 13

2.2.4 Water isotope measurements and re-evaluation of isotope framework parameters for 2020-2021 14

2.3 Results and discussion 16

2.3.1 Verifying PAD 18 as a suitable index lake 16

2.3.2 Long-term monitoring of PAD 18 from 2000-2006 and 2014-2019 19

2.3.3 Development of a new isotope framework for 2020-2021 20

2.4 Conclusions and Recommendations 29

2.5 References 32

Chapter 3 | Overlooked and underrated: Snowmelt runoff rivals influence of river floodwaters on lake-level rise at a cold region freshwater delta 38

3.1 Introduction 38

3.2 Methods 43

3.2.1 Study Area 43

3.2.2 Meteorological conditions prior to and during the 2020 freshet 44

3.2.3 Field work and laboratory analyses 46

3.2.4 Data analyses 48

3.2.4.1 Analysis of water isotope composition 48

3.2.4.2 Identification of flooded lakes 49

3.2.4.3 Quantifying the proportion of input from snowmelt and river floodwater to the flooded lakes 50
3.2.4.4 Determination of lake-level change 52
3.2.4.5 Estimating the lake-level rise due to input of snowmelt versus floodwater 53
3.2.4.6 Geospatial analyses 53
3.3 Results 54
3.3.1 Flood status of lakes in 2020 54
3.3.2 Quantifying the proportion of input from floodwaters and snowmelt to the lakes that flooded in spring 2020 56
3.3.3 Comparison of lake-level rise by input from snowmelt versus river floodwaters in 2020 59
3.4 Discussion 64
3.5 Implications and recommendations 68
3.6 References 70
Chapter 4 | Conclusions and Recommendations 83
References (Chapters 1 and 4) 87
Appendices 94
Appendix 1 (Chapter 2) 94
Appendix 2 (Chapter 3) 101

List of Figures

Figure 1.1: Upper maps show location of the Peace-Athabasca Delta (PAD; red) in northern Alberta, Canada, within Wood Buffalo National Park (WBNP). Hydroelectric (rectangles) and oil sands mining projects (1985-2015; orange; sourced from: http://osip.alberta.ca/Library/Browser) are depicted within the watersheds of the Peace River (light pink) and Athabasca River (light purple). Lower map shows locations of the lake (black circles) and river (black triangles) sites where samples were collected for the research reported in this thesis. PAD shapefile (black outline) delineates the area used for geospatial analyses. 5

Figure 2.1: Schematic $\delta^{18}O$-$\delta^{2}H$ diagram identifying key reference lines and isotope parameters used in isotope mass-balance studies. The three linear relations displayed are: 1) the Global Meteoric Water Line (GMWL), which represents the observed relation between $\delta^{18}O$ and $\delta^{2}H$ in amount-weighted annual precipitation worldwide ($\delta^{2}H = 8\ \delta^{18}O + 10$; Craig, 1961; Rozanski et al., 1993), 2) the Local Meteoric Water Line (LMWL), which represents the region-specific distribution of the isotope composition of precipitation, and 3) the Local Evaporation Line (LEL), which represents the evaporative trajectory of lake surface water (δ_L) fed by waters of mean annual isotope composition of precipitation (δ_P). Key points along the LEL include δ_{SSL} which represents the special case of a terminal (i.e., closed-drainage) basin in isotopic and hydrologic steady-state fed by waters of mean annual isotope composition of precipitation (δ_P), and δ^* which represents the theoretical limiting isotope composition of a desiccating water body. The isotope composition of atmospheric moisture (δ_A) and the ice-free season atmospheric moisture (δ_{As}) is commonly assumed to be in equilibrium with δ_P and the isotope composition of ice-free season precipitation (δ_{Ps}), respectively. Evaporation-to-inflow (E/I) ratios can be calculated using the coupled-isotope tracer approach of Yi et al. (2008) to estimate the isotope composition of input water (δ_I) and by incorporating the isotope composition of evaporated vapour (δ_E)..... 8

Figure 2.2: Location of lake 'PAD 18' and Fort Chipewyan at the Peace-Athabasca Delta (PAD), Alberta, Canada. Top right panel shows a 3D elevation map of PAD 18 and its position within the landscape that is elevated beyond the influence of river floodwaters. High-resolution digital elevation model data source: Environment and Climate Change Canada (https://open.canada.ca/data/en/dataset/03568324–1a8b-4c00-8650-f5c35f6e0bff). Bottom right panel shows an aerial photograph of PAD 18 in September 2020, courtesy of Parks Canada staff. 11

Figure 2.3: Water isotope compositions of evaporation pan (grey circles; including tap water [open circle in the bottom panel] used to fill the pan) maintained at Fort Chipewyan, Lake Athabasca (black triangles), and PAD 18 (black circles) in 2003 (for locations, see Figure 2.1). Top panel shows time series of $\delta^{18}O$ values of water from the evaporation pan and PAD 18. Black dashed line in the top panel indicates average $\delta^{18}O$ of PAD 18 in 2003 (-9.47‰) and grey dashed line indicates average $\delta^{18}O$ of the evaporation pan at equilibrium (-9.03‰). Bottom panel shows evolution of pan water isotope compositions towards equilibrium with the atmosphere and PAD 18 isotope compositions in $\delta^{18}O$-$\delta^{2}H$ space. Evaporation pan and PAD 18 data are from Falcone (2007). Lake Athabasca data are from Wolfe et al. (2012). 18

Figure 2.4: Time series of $\delta^{18}O$ for PAD 18 sampled during ice-free seasons of 2000-2006 and 2014-2021. Connecting lines are for each sampling year. Average ice-free season flux-weighted

relative humidity of each sampling year is shown in the colour palette (see Table 2.2). Dashed lines indicate average δ_{SSL} values estimated from the isotope compositions of PAD 18 from 2000-2006 and 2014-2019 ($\delta^{18}O$ = -9.15‰) and from 2020-2021 ($\delta^{18}O$ = -10.30‰), and the horizontal grey bars indicates one standard deviation about the average, respectively. Dark grey line segments represent δ_{SSL} values derived using Equation 2 for each sampling year. 23

Figure 2.5: In **a)**, the isotope compositions of PAD 18 during 2015-2019 (grey circles) and 2020-2021 (orange circles) are displayed alongside the average isotope composition of PAD 18 from 2020-2021 (blue triangle) on the predicted LEL based on meteorological conditions during 2015-2019 as reported in Remmer et al. (2020a). In **b)**, the isotope compositions of PAD 18 in 2020-2021 (orange circles) and the average value (blue triangle) are compared to δ_{SSL} (black circle behind blue triangle) calculated using Equation 2. In **c)**, the predicted LEL is displayed for 2020-2021 using the average isotope composition of PAD 18 as δ_{SSL} and incorporating meteorological conditions from 2020-2021 (blue circles and line; LEL: $\delta^2H = 4.30\ \delta^{18}O - 62.85$) and compared to the 2015-2019 LEL (black circles and lines; LEL: $\delta^2H = 4.27\ \delta^{18}O - 63.47$). See Table 2.3 for isotope and hydroclimate parameters associated with isotope frameworks presented in a) and c). 24

Figure 2.6: The distribution of evaporation-to-inflow (E/I) ratios derived from lake water isotope compositions from the Peace-Athabasca Delta (PAD) in July 2021.**a)** boxplots comparing the distribution of E/I ratios computed using the 2015-2019 isotope framework (purple boxplots) and 2020-2021 isotope framework (teal boxplots) for lakes in the Athabasca sector and Peace sector. **b)** isoscapes displaying spatial interpolation of E/I ratios calculated using the 2015-2019 isotope framework as presented in Remmer et al. (2020a) (left panel) and the 2020-2021 isotope framework (right panel). Warm-toned colours represent higher E/I ratios and cool-toned colours represent lower E/I ratios based on a scale from 0-1.5. 28

Figure 2.7: Aerial photograph of PAD 33 (May 27, 2023) displaying visible evidence of water-level drawdown. 29

Figure 3.1: Maps displaying **a)** location of the Peace-Athabasca Delta (PAD) within Wood Buffalo National Park (WBNP) in northern Alberta, Canada, and the watersheds of the Peace (light blue) and Athabasca (light purple) rivers; **b)** spatial interpolation (by inverse distance weighting; Moran's I = -0.15, p = 0.15) of the magnitude of lake-level change (m) between September 2019 and May 2020 for 58 lakes where measurements were obtained using water-depth loggers and/or spot depth measurements; **c)** water extent (dark blue) in spring 2020 based on false colour satellite imagery (Sentinel-2) obtained on May 24 (from https://apps.sentinel-hub.com/eo-browser/). ... 41

Figure 3.2: Maps displaying **a)** variation of ground elevation (masl) and **b)** vegetation cover across the PAD. Panels a) and b) show the locations of the 59 lakes (black circles) and 4 river sites (black triangles) sampled for water isotope composition in May 2020. Water-depth loggers were deployed at these lakes in May through September of 2019 and 2020. High-resolution digital elevation model data (4-m resolution) were sourced from Environment and Climate Change Canada and are accessible at https://open.canada.ca/data/en/dataset/03568324-1a8b-4c00-8650-f5c35f6e0bff. Vegetation data from circa 2017 were sourced from French et al. (2022) and are accessible at https://daac.ornl.gov/. 45

Figure 3.3: Graphs showing temporal variation of meteorological variables between fall of 2019 and spring of 2020. **a)** Air temperature (°C) expressed as daily (thin black line) and monthly means (black circles) recorded at station "Fort Chipewyan RCS" at the Fort Chipewyan airport, Alberta, Canada (Climate ID: 3072659) compared to Climate Normal (1981-2010) for the 31-day running mean (thick black line) and monthly mean (dashed line) and associated variability (1 standard deviation unit; grey band) at station "Fort Chipewyan A" near the airport (Climate ID: 3072658). Spring isotherm date (red circle) is the date when the 31-day running mean is above 0°C. **b)** Daily modelled snow water equivalent (SWE; mm; black line) and daily rainfall (mm; vertical blue bars) between September 1, 2019 and May 31, 2020 compared to the median (dashed line) and interquartile range (grey band) of long-term daily modelled SWE for 1991-2020, with the spring isotherm date (red circle). Daily rainfall data represent precipitation when average daily mean air temperature exceeded 0°C at Fort Chipewyan airport (Climate ID: 3072659). Daily SWE data are averaged from ten townships (T110R07W4, T110R08W4, T112R05W4, T112R07W4, T112R08W4, T112R10W4, T113R05W4, T113R10W4, T115R07W4, T115R08W4) and sourced from Alberta's AgroClimatic Information Service (https://www.alberta.ca/acis-find-historic-climate-data). **c)** Wind rose plot indicating wind direction and speed patterns at 10-m height recorded during the estimated snowfall period (October 1, 2019 – April 15, 2020), at Fort Chipewyan airport (Climate ID: 3072659). The wind rose plot was extracted from Alberta's AgroClimatic Information Service (https://www.acis.alberta.ca/acis/wind-rose.jsp). Temperature and SWE plots were created using the package 'ggplot2' in RStudio (version 2023.03.0+386) using packages lubridate (v.1.9.1; Grolemund and Wickham, 2011), zoo (v.1.8-11; Zeileis and Grothendieck, 2005), and ggplot2 (v.3.4.4; Wickham, 2016)..... 47

Figure 3.4: Schematic $\delta^{18}O$-$\delta^{2}H$ diagram identifying key reference lines and isotope parameters used in isotope mass-balance studies alongside isotope compositions of two hypothetical lakes; one that received primarily river floodwaters (δ_{L-1}) and one that received primarily snowmelt (δ_{L-2}). The three linear relations displayed are: 1) the Local Meteoric Water Line (LMWL), which represents the region-specific distribution of the isotope composition of precipitation (rain, snow), 2) the Local Evaporation Line (LEL), which represents the evaporative trajectory of lake surface water (δ_L) fed by waters of mean annual isotope composition of precipitation (δ_P), and 3) a river – snow Meteoric Water Line segment between the isotope composition of river water (δ_{River}) and snow (δ_{Snow}), which defines the potential range of the isotope composition of input water (δ_I) for lakes fed by mixtures of river water and snowmelt, as determined by the intersection of a lake-specific evaporation line between the isotope composition of evaporated vapour (δ_E) and δ_L, based on Remmer et al. (2020a) and the coupled-isotope tracer approach of Yi et al. (2008). Shaded regions in the polygon represent zones where δ_I will primarily reflect inputs of river floodwaters (blue), snowmelt (pink), or a 50% mixture (white) based on the position of δ_L in $\delta^{18}O$-$\delta^{2}H$ space. Key reference parameters used in isotope mass-balance studies include δ_{SSL}, which represents the special case of a terminal (i.e., closed-drainage) basin in isotopic and hydrologic steady-state (evaporation = inflow) fed by δ_P, and δ^* which represents the theoretical limiting isotope composition of a desiccating water body..... 51

Figure 3.5: Isotope compositions of 58 lakes, 1 index lake (PAD 18 which approximates δ_{SSL}; Imran et al., 2024 [Chapter 2]), and 4 river sites sampled in May 2020 plotted in reference to the predicted LEL based on meteorological conditions during 2020-2021, as reported in Imran et al. (2024 [Chapter 2]). **a)** Top panels show isotope compositions of flooded lakes (blue circles), non-

flooded lakes (orange circles), and rivers (blue triangles) in the Peace sector (left panel) and Athabasca sector (right panel). **b)** Bottom panels display the estimated isotope compositions of input water (δ_I) of flooded lakes on snow-river Meteoric Water Line segments between the isotope composition of snow (pink circle) and the respective river (blue triangle) for the Peace sector (left panel) and Athabasca sector (right panel). The isotope composition of the Athabasca River is estimated from its distributary channels (Embarras River, Mamawi Creek, Fletcher Channel). . 55

Figure 3.6: Map showing geospatial interpolation (by inverse distance weighting) of isotope-inferred percent river floodwater input to flooded lakes in spring 2020 (Moran's $I = 0.40$, $p<0.01$) compared to the spring 2018 flood extent (dashed line) in the Peace-Athabasca Delta. Spring 2018 flood extent is from Remmer et al. (2020a), with modifications that include constraining the interpolation to within the study area extent and using inverse distance weighting..... 58

Figure 3.7: Distribution of lake-level rise at 52 lakes in spring 2020 in the Peace-Athabasca Delta. **a)** Bar plots showing the rise in lake level between September 2019 and May 2020 and the amount attributable to snowmelt (pink) and river floodwater (blue) in the (left panel) Peace sector (n=23) and (right panel) Athabasca sector (n=29). Lakes are arranged in descending order by total lake-level rise. Medians for the total lake-level rise (dashed line) are displayed for the Peace sector (0.31 m) and Athabasca sector (0.41 m). **b)** Boxplots showing the distribution of lake-level rise in (left panel) lakes across both sectors attributable to snowmelt input in non-flooded lakes (n=27), river floodwaters in flooded lakes (n=25), and snowmelt input in flooded lakes (n=25), (middle panel) the lakes in the Peace sector attributable to snowmelt input in non-flooded lakes (n=19), river floodwaters in flooded lakes (n=4), and snowmelt input in flooded lakes (n=4), and (right panel) the lakes in the Athabasca sector attributable to snowmelt input in non-flooded lakes (n=8), river floodwaters in flooded lakes (n=21), snowmelt input in flooded lakes (n=21). Mann-Whitney U tests (snowmelt input in non-flooded lakes vs river input in flooded lakes; snowmelt input in non-flooded lakes vs flooded lakes) and a paired-samples Wilcoxon signed ranks test (river input vs snowmelt input in flooded lakes) were conducted on the entire set of study lakes across both sectors (differences are identified by the letters in the left panel). 61

Figure 3.8: Maps showing spatial interpolation (by inverse distance weighting) of the **a)** magnitude of lake-level change (m) between September 2019 and May 2020 (Moran's $I = -0.15$, $p = 0.15$) for lakes where measurements were obtained using water-depth loggers and/or spot depth measurements lake-level rise (m); lake-level rise (m) in spring 2020 attributable to input of **b)** snowmelt (Moran's $I = 0.31$, $p<0.01$) and **c)** river floodwater (Moran's $I = 0.04$, $p = 0.54$). Lakes where water level declined were assigned a value of zero for spatial interpolations in panels in b) and c) and are indicated as red circles. 63

Figure 3.9: Long-term trends captured with generalized additive models (GAMs; grey line; shaded region represents 95% confidence interval) of peak snow water equivalent (SWE) values between Feb 15 – April 28 (top panel) and rate of melt (mm/day; i.e., total number of days for peak SWE to reach zero; middle panel) from 1963 – 2020. Daily SWE data are averaged from ten townships (T110R07W4, T110R08W4, T112R05W4, T112R07W4, T112R08W4, T112R10W4, T113R05W4, T113R10W4, T115R07W4, T115R08W4) and sourced from Alberta's AgroClimatic Information Service (https://www.alberta.ca/acis-find-historic-climate-data). Bottom panel shows temporal variation of surface water extent (ha) in the Peace-Athabasca Delta from 1984 – 2020, as reported in WBNP (2022), based on Global Surface Water (LANDSAT Satellite 30 m resolution)

derived from May or June images (dashed line shows the simple linear regression). Data for bottom panel were provided by Parks Canada and presented as shown in WBNP (2022). 67

List of Tables

Table 2.1: Isotope data ($\delta^{18}O$, $\delta^{2}H$, d-excess) of tap water, rainfall, evaporation pan, and PAD 18 in Fort Chipewyan (Alberta, Canada), May – August 2003. 17

Table 2.2: Isotope data ($\delta^{18}O$, $\delta^{2}H$, d-excess) of PAD 18 from 2000-2006 and 2014-2021, and ice-free season flux-weighted air temperature (°C) and relative humidity (%). 21

Table 2.3: Isotope framework parameters and the LEL slopes and intercepts based on i) meteorological conditions during 2015-2019 using a long-term (2000-2015) average isotope composition of PAD 18 for δ_{SSL} (Remmer et al., 2020a), and ii) meteorological conditions during 2020-2021 and the average isotope composition of PAD 18 for δ_{SSL} during 2020-2021. δ_{SSL} value for 2015-2019 framework is based on water isotope compositions of PAD 18 collected during 2000-2006 and 2014-2015. Note, all parameters are expressed in decimal notation when applied in Equations 3 and 4. 27

Chapter 1 | Introduction

Shallow lakes are an abundant and characteristic feature of northern landscapes where they provide key ecosystem services that support wildlife and local communities (Schindler and Smol, 2006; Medeiros et al., 2017). Because of their small water volumes, northern shallow lakes have been recognized as sentinels for detecting hydrologic changes caused by multiple stressors, including effects of climate change and industrial development (Smol, 2016; Saros et al., 2023). In recent decades, high latitude regions have experienced some of the greatest warming on Earth, resulting in increased evaporation, altered precipitation patterns, and degradation of permafrost (Rouse et al., 1997; Schindler and Donahue, 2006; Schindler and Smol, 2006; AMAP, 2021; IPCC, 2021). Hydrological changes have been documented at shallow lakes in several landscapes of northern Canada and Alaska in response to climatic trends. For instance, warmer air temperatures have lengthened the ice-free season and increased evaporative water loss. At Cape Herschel (Nunavut), these changes have promoted the desiccation of shallow high Arctic ponds (Smol and Douglas, 2007). A study conducted in the Old Crow Flats (Yukon) and the Hudson Bay Lowlands (Manitoba) identified the vulnerability of shallow subarctic lakes to desiccation when low snowmelt runoff becomes insufficient to offset evaporation during the summer (Bouchard et al., 2013). Increases in amount of rainfall at the Old Crow Flats in northern Yukon and Hudson Bay Lowlands in northern Manitoba have resulted in more positive water balances in shallow lakes and ponds (Macrae et al., 2018; MacDonald et al., 2021). Increased thawing of permafrost has resulted in lake drawdown via vertical and lateral drainage (i.e., Marsh et al., 2009; Lantz and Turner, 2015; Tondu et al., 2016). However, thaw of permafrost has also led to greater hydrologic connectivity of waterbodies with the landscape (Wolfe et al., 2011), and permafrost meltwater has been identified as an additional input source to lake water balances (Gibson et al., 2016a). Climate models predict that global warming will lead to increases of extreme meteorological events, which raises concern for alteration of water balance and depth of shallow lakes in northern regions (Prowse et al., 2009; Walsh et al., 2020, IPCC, 2021). The rapid expansion of industrial activities further adds to the growing alarm about future surface water sustainability in northern landscapes (Schindler and Donahue, 2006; Schindler and Smol, 2006).

The Peace-Athabasca Delta (PAD), located in northeastern Alberta, is a freshwater-rich landscape where concern has grown for decades about drawdown of water levels in the abundant shallow lakes in response to changes in climate and upstream industrial activities (Figure 1.1) (PADPG, 1973; Prowse and Conly, 2002; Schindler and Donahue, 2006; Wolfe et al., 2012; Beltaos, 2014; Kay et al., 2019). Spanning an area of 6,000 km^2 between the terminus regions of the Athabasca River and Peace River at the western end of Lake Athabasca, the PAD is one of the world's largest freshwater boreal deltas (Timoney, 2013). The large size and its physical and ecological features have garnered the PAD recognition as a Ramsar Wetland of International Importance (Timoney, 2013). The ecological features include that the PAD is one of the most important waterfowl nesting and staging areas in North America, with 400,000 to 1 million waterfowl visiting during spring and fall migrations, provides the nesting grounds for the only known breeding population in central Canada of the vulnerable Peregrine Falcon (*Falco peregrinus*), and contains the largest undisturbed grass and sedge meadows in North America that support bison populations. About 80% of the PAD is protected within Wood Buffalo National Park (WBNP), where its 'Outstanding Universal Value' contributes importantly to the park's World Heritage status (WBNP, 2019). The delta holds importance for the Mikisew Cree First Nation (MCFN), Athabasca Chipewyan First Nation (ACFN), and Fort Chipewyan Métis Nation for access to traditional lands which hold economic, cultural, and spiritual values and sustain their way of life (MCFN, 2014; Vannini and Vannini, 2019; ACFN, 2021). Since the late 1960s, however, concern has been expressed about a reduction in the frequency of large-scale ice-jam floods and widespread drawdown of water levels in the delta's lakes and wetlands (PADPG, 1973; PADTS, 1996; Prowse and Conly, 1998; WHC/IUCN, 2017). Declines in flood frequency and water levels have been attributed to regulation of Peace River flow for hydroelectricity by the W.A.C. Bennett Dam located 1,100 km upstream, water withdrawals by oil sands mining along the Athabasca River and other human activities, and climate change (Peters and Prowse, 2001; Wolfe et al., 2006; Sauchyn et al., 2015; Kay et al., 2019; Lamontagne et al., 2021). Concern for widespread lake drying has intensified since the approval, construction, and operation of BC Hydro's Site C hydroelectric dam upstream of the PAD on the Peace River (MCFN, 2014). In 2014, the MCFN submitted a petition to UNESCO to add WBNP to the list of World Heritage 'in Danger', citing in part, the degradation of the PAD by industrial activities (MCFN, 2014; WHC/IUCN, 2017). Following the petition, UNESCO issued 17 recommendations, and two of

them identified the need for improved hydrological and ecological monitoring of the delta's aquatic ecosystems (WHC/IUCN, 2017). In response to these recommendations, a federal Action Plan was developed that focused on research and monitoring of processes driving hydrologic changes at the PAD (WBNP, 2019). One of the goals of the Action Plan is "to enhance monitoring and to improve the assessment of current and future water quantity conditions in the Peace and Athabasca River Basins" (WBNP, 2019; pg. 48).

In response to the need for an aquatic ecosystem monitoring program at the PAD, multi-faceted research was undertaken during 2015-2021 at ~60 lakes and 9 rivers that spanned the delta's broad hydroecological gradients (Neary et al., 2024; Figure 1.1). During this 7-year period, seasonal (spring, summer, fall) measurements of water isotope composition and hourly measurements of water depth provided information on the influences of river flooding, precipitation, and evaporation on lake water balances and water levels (Remmer et al., 2020a,b; Neary et al., 2021). As demonstrated at the PAD and elsewhere, repeated measurements of water isotope composition were used because they identify the influential sources of water input (e.g., snowmelt, rainfall, river floodwaters) and water loss (e.g., evaporation) and quantify variation in lake water balances over space and time (Clark and Fritz, 1997; Edwards et al., 2004; Wolfe et al., 2007; Brock et al., 2009; Anderson et al., 2013; Brooks et al. 2014; Turner et al., 2014; Gibson et al., 2016b,c; MacDonald et al., 2017, 2021; Narancic et al., 2017; Remmer et al., 2020a,b). Water isotope tracers possess distinct advantages when assessing hydrological change at a landscape scale within remote regions. For example, sampling is much less field intensive than conventional hydrologic monitoring methods, the small volumes of water needed (~30 ml) can be collected rapidly collected at each site, and the analyses are cost-effective (Neary et al., 2024). Potential drawbacks are that each sample provides a snapshot of recent hydrological processes that occurred during weeks preceding sample collection, which may underrepresent influence of short-lived events. Also, metrics derived from the data cannot always be used to quantify changes in lake depth, which is often a primary variable of interest (Edwards et al., 2004). Depth loggers were deployed to continuously measure variations in water depth, which enabled an ability to capture the timing and influence of hydrological processes operating at short time scales (e.g., substantial rainfall events, open-water flooding) and quantify the influence of evaporation on lake-level drawdown during the open-water season (Neary et al., 2021).

I began my MSc research late in the above 7-year research project, at a time when relative humidity and precipitation rose suddenly to above average (Neary et al., 2024). While the implications of the shift in meteorological conditions were unknown to us at the time, ongoing measurement of water isotope composition revealed a sudden and sustained decline in 2020 and 2021 at an elevated lake (informally named 'PAD 18') that had long served as an 'index lake' for isotope mass-balance modelling of lakes within the PAD. The change in isotope composition of PAD 18 required further assessment of the isotope framework that was relied upon for estimating water balances of the other deltaic lakes. The shift in water isotope composition was unprecedented since sampling began in 2000, which raised questions about whether PAD 18 remained a reliable index lake. The investigation into the cause of the shift in isotope composition of PAD 18, which is detailed in Chapter 2, entitled "Value of long-term isotope monitoring of an index lake for tracking changes in lake water balances across a northern freshwater landscape", reveals the effects of a rise in relative humidity on the isotope composition of the lake water and the consequences for isotope mass-balance modelling. In the spring of 2020, ice-jams formed in the Peace and Athabasca rivers that triggered widespread flooding of the landscape. Water depth loggers had been installed into 59 lakes during the open-water season of 2019, before the flooding occurred, and in May of 2020 shortly after the flooding. Water levels were observed to increase in the flooded lakes. Unexpectedly, however, substantial water-level rises were also observed at many of the lakes which did not receive input of floodwater, raising the possibility that input of snowmelt, an understudied hydrological process in northern floodplains, may also contribute importantly to maintenance of water levels during the open-water season by offsetting losses to evaporation. This observation provided opportunity to integrate measurements of water isotope composition and water-depth to quantify the role of snowmelt runoff on lake depth, which is detailed in Chapter 3, entitled "Overlooked and underrated: Snowmelt runoff rivals influence of river floodwaters on lake-level rise at a cold region freshwater delta". A synthesis of the findings from both data chapters is summarized in Chapter 4, along with implications for management decisions.

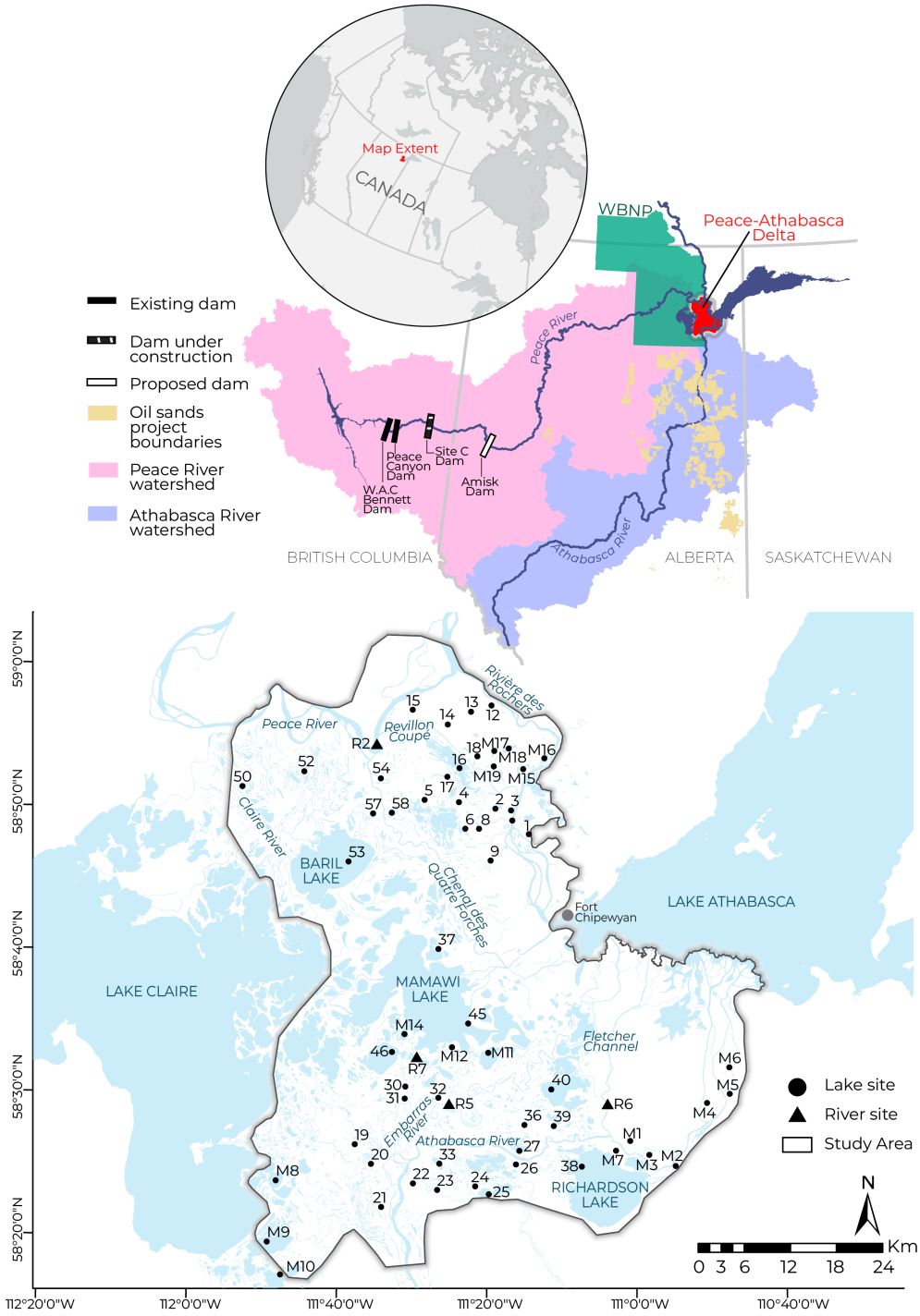


Figure 1.1: Upper maps show location of the Peace-Athabasca Delta (PAD; red) in northern Alberta, Canada, within Wood Buffalo National Park (WBNP). Hydroelectric (rectangles) and oil sands mining projects (1985-2015; orange; sourced from: http://osip.alberta.ca/Library/Browser) are depicted within the watersheds of the Peace River (light pink) and Athabasca River (light purple). Lower map shows locations of the lake (black circles) and river (black triangles) sites where samples were collected for the research reported in this thesis. PAD shapefile (black outline) delineates the area used for geospatial analyses.

Chapter 2 | Value of long-term isotope monitoring of an index lake for tracking changes in lake water balances across a northern freshwater landscape

Citation: Imran, A., Neary, L. K., Falcone, M. D., Wolfe, B. B., Hall, R. I., 2024. Value of long-term isotope monitoring of an index lake for tracking changes in lake water balances across a northern freshwater landscape. *Journal of Hydrology: Regional Studies*, 53, 101765. https://doi.org/10.1016/j.ejrh.2024.101765.

2.1 Introduction

Stable isotopes of oxygen (^{18}O, ^{16}O) and hydrogen (^{2}H, ^{1}H) in water are valuable tracers for characterizing the influence of hydrological processes on lake water balances (Gonfiantini, 1986; Gat, 1995, 1996; Clark and Fritz, 1997; Gibson and Edwards, 2002; Yi et al., 2008). Water isotope tracers are also considered ideal for hydrological monitoring purposes because the approach is cost-effective and less field-intensive than conventional methods, which offers a distinct advantage in remote regions that are poorly instrumented and where baseline hydrological data are limited or difficult to acquire (Edwards et al., 2004; Wolfe et al., 2007; Gibson and Reid, 2014). For example, several studies conducted across lake-rich landscapes in northern Canada have demonstrated the value of using water isotope tracers to track responses of water balances of lakes to ongoing climate change and other potential stressors (Gibson and Edwards, 2002; Gibson et al., 2002; St. Amour et al., 2005; Brock et al., 2007; Wolfe et al., 2007; Turner et al., 2010; MacDonald et al., 2017; Remmer et al., 2018; Wan et al., 2020; Gibson et al., 2022; Wilcox et al., 2022), which have also served as the foundation for the development and application of long-term aquatic ecosystem monitoring programs (Tondu et al., 2013; Remmer et al., 2020a,b; MacDonald et al., 2021).

Interpretation of lake water isotope compositions in conventional $\delta^{18}O$-$\delta^{2}H$ [1] space against the backdrop of an 'isotope framework' consisting of reference lines and parameters is key to evaluating influence of hydrological processes (Figure 2.1). The systematic coupling between hydrogen and oxygen isotope composition in the global water cycle is revealed by a strong linear

[1] Isotope compositions are expressed as δ-values, representing deviations in per mil (‰) from Vienna Standard Mean Ocean Water (VSMOW), such that $\delta_{sample} = [(R_{sample}/R_{VSMOW}) - 1] \times 10^3$ where R is the $^{18}O/^{16}O$ or $^{2}H/^{1}H$ ratio in the sample and VSMOW, on a scale normalized to values of Standard Light Antarctic Precipitation (−55.5‰ for $\delta^{18}O$; −428‰ for $\delta^{2}H$) (Coplen, 1996).

relationship between $\delta^{18}O$ and $\delta^{2}H$ of precipitation, termed the Global Meteoric Water Line (GMWL), and is approximated by $\delta^{2}H = 8\ \delta^{18}O + 10$ (Craig, 1961; Rozanski et al., 1993). Although the GMWL serves as an important reference line for understanding spatial patterns in meteoric waters, it can differ from a Local Meteoric Water Line (LMWL) that accounts for influence of local climatic factors such as the origin of vapour mass and subsequent variations by secondary processes of re-evaporation and mixing (Rozanski et al., 1993; Clark and Fritz, 1997). The isotope composition of water that has undergone evaporation within a region will lie on a trajectory along a Local Evaporation Line (LEL), which characterizes the relative influence of evaporation controlled by local atmospheric conditions including relative humidity, temperature, and the isotope composition of atmospheric moisture (δ_A) (Clark and Fritz, 1997; Gibson and Edwards, 2002; Edwards et al., 2004; Yi et al., 2008). The global and local meteoric water lines (MWLs) and the LEL serve as important references in an isotope framework for evaluating lake water balances, as the isotope composition of a given lake in relation to the MWLs and the LEL in $\delta^{2}H$-$\delta^{18}O$ space can provide information about input sources and influence of evaporation, respectively (Clark and Fritz, 1997). Commonly, the LEL is determined empirically by applying a linear regression through measured lake water isotope compositions in a region. With this approach, intersection of the LEL with the GMWL (or LMWL) is often used to estimate the mean annual isotope composition of precipitation (δ_P). Alternatively, the LEL can be predicted using the linear resistance model of Craig and Gordon (1965) and incorporating local meteorological data and modelled or measured isotope values, including an independent estimate of δ_P. Predicting the LEL offers the advantage of evaluating lake water isotope data independently with respect to their position along (degree of evaporation) and about (i.e., above/below; influence of input sources such as rainfall, snowmelt or groundwater) the LEL (MacDonald et al., 2017). Based on the departure of the isotope composition of a given lake in $\delta^{18}O$-$\delta^{2}H$ space relative to the MWLs, the water balance can be expressed as an evaporation-to-inflow (E/I) ratio via isotope mass-balance modelling (Gonfiantini, 1986; Gibson and Edwards, 2002; Edwards et al., 2004; Gibson et al., 2016). E/I ratios have proven to be a highly informative metric for capturing snapshots of the hydrological conditions of lakes in many regions, but their derivations are sensitive to appropriate characterization of model parameters (Gibson and Edwards, 2002; Brooks et al., 2014; Cui et al., 2017; Remmer et al., 2020a).

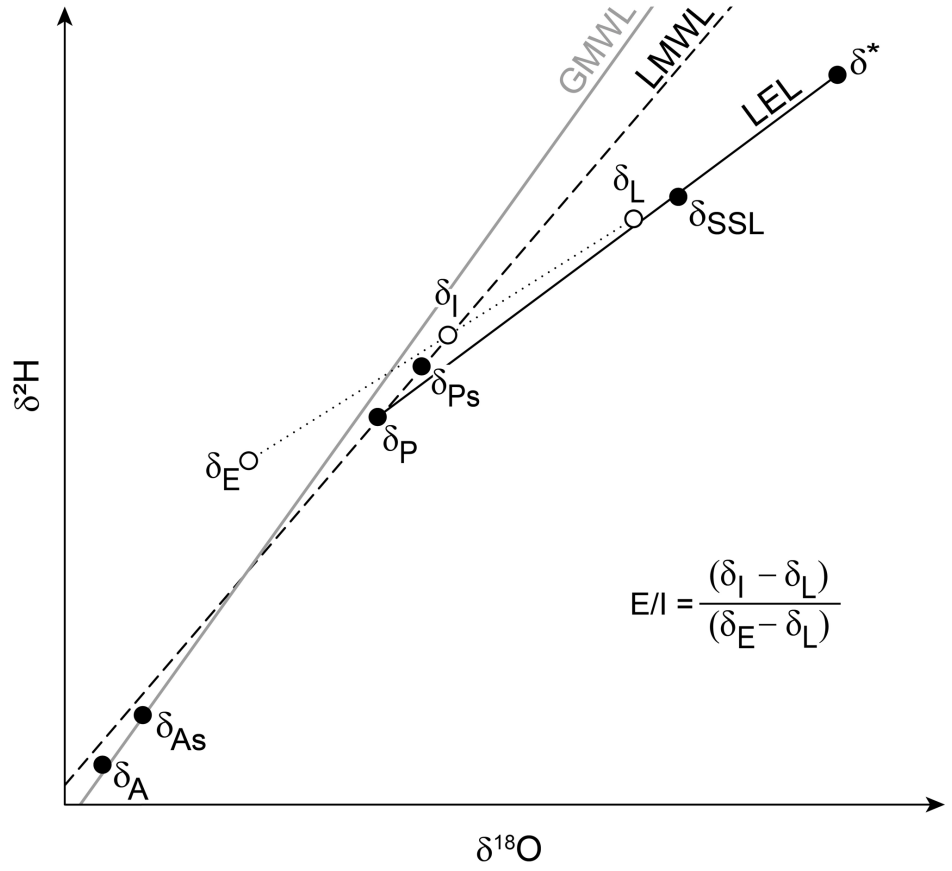


Figure 2.1: Schematic $\delta^{18}O$-$\delta^{2}H$ diagram identifying key reference lines and isotope parameters used in isotope mass-balance studies. The three linear relations displayed are: 1) the Global Meteoric Water Line (GMWL), which represents the observed relation between $\delta^{18}O$ and $\delta^{2}H$ in amount-weighted annual precipitation worldwide ($\delta^{2}H = 8\ \delta^{18}O + 10$; Craig, 1961; Rozanski et al., 1993), 2) the Local Meteoric Water Line (LMWL), which represents the region-specific distribution of the isotope composition of precipitation, and 3) the Local Evaporation Line (LEL), which represents the evaporative trajectory of lake surface water (δ_L) fed by waters of mean annual isotope composition of precipitation (δ_P). Key points along the LEL include δ_{SSL} which represents the special case of a terminal (i.e., closed-drainage) basin in isotopic and hydrologic steady-state fed by waters of mean annual isotope composition of precipitation (δ_P), and δ^* which represents the theoretical limiting isotope composition of a desiccating water body. The isotope composition of atmospheric moisture (δ_A) and the ice-free season atmospheric moisture (δ_{As}) is commonly assumed to be in equilibrium with δ_P and the isotope composition of ice-free season precipitation (δ_{Ps}), respectively. Evaporation-to-inflow (E/I) ratios can be calculated using the coupled-isotope tracer approach of Yi et al. (2008) to estimate the isotope composition of input water (δ_I) and by incorporating the isotope composition of evaporated vapour (δ_E).

The isotope composition of evaporated vapour (δ_E) from a lake is a fundamental component for isotope mass-balance calculations of E/I ratios, and requires measurements of air temperature, relative humidity, isotope composition of the lake water (δ_L), and δ_A (Figure 2.1; Craig and

Gordon, 1965; Gonfiantini, 1986; Edwards et al., 2004; Yi et al., 2008). In northern regions with ice-covered seasons, the isotope composition of atmospheric moisture during the ice-free season (δ_{As}) is recommended for model parameterization as the duration of ice cover and seasonality can affect the flux-weighted atmospheric parameters and can differ from mean annual values (Gibson, 2002; Gibson et al., 1999; 2002). All parameters used for calculating δ_E can be measured directly, except for δ_{As} for which sample collection is logistically challenging (Welhan and Fritz, 1977; Gibson et al., 1999). Typically, δ_{As} can be estimated indirectly by assuming isotope equilibrium between average ice-free season precipitation (i.e., rainfall; δ_{Ps}) and atmospheric moisture, but this method can lead to uncertainties as δ_{Ps} can be highly variable in northern regions over different timescales reflecting synoptic-scale variations in local climate (St. Amour et al., 2005; Kershaw et al., 2022). Alternatively, δ_{As} may be explicitly derived from maintaining a constant-volume evaporation pan to simulate a lake at steady-state under local atmospheric conditions (IAEA, 1981; Gibson et al., 1999; Turner et al., 2010; Tondu et al., 2013; MacDonald et al., 2021). Using an evaporation pan, however, requires careful maintenance and continuous sampling (Welhan and Fritz, 1977; Allison et al., 1979a,b; Gibson et al., 1999; MacDonald et al., 2021). Another approach to constrain δ_{As} is to use the isotope composition of a terminal 'index' lake (δ_{SSL}), where evaporation equals inflow (E/I = 1) (Dinçer, 1968; Yi et al., 2008; Remmer et al., 2018, 2020a,b). The index lake method, first suggested by Dinçer (1968), is preferable for estimating δ_{SSL} and subsequently δ_{As} because it relies on a naturally occurring terminal basin at hydrologic and isotopic steady-state, allowing for potentially more accurate assessment of lake water balances of nearby lakes subject to the same atmospheric conditions and exchange processes. While an index lake may not be present in every study region, the usefulness and preference of this approach for anchoring isotope mass-balance calculations has been demonstrated in many studies (Gat and Levy, 1978; Kebede et al., 2001, 2009; Yi et al., 2008; Gibson and Reid, 2014; Remmer et al., 2018, 2020a,b).

Application of isotope mass-balance models has been a key feature of hydrological studies of lakes in the Peace-Athabasca Delta (PAD), an important freshwater landscape located in Wood Buffalo National Park (WBNP) in northern Alberta, Canada, where concerns have persisted about effects of multiple potential stressors on lake-level drawdown (Timoney, 2013; MCFN, 2014;

WHC/IUCN 2017, 2022; WBNP 2019). Use of water isotope tracers has captured snapshots of lake water balances and their influential hydrological processes including the extent and magnitude of flooding and evaporation (Wolfe et al., 2007, 2008; Yi et al., 2008; Remmer et al., 2018, 2020a,b). In 2000, an initial landscape-scale assessment of lake water balances using isotope-inferred estimates of E/I ratios provided a first-order characterization of lake basin drainage types (Wolfe et al., 2007). In that study, δ_{As} was assumed to be in equilibrium with δ_{Ps} because an index lake had not yet been recognized as a potential approach for defining δ_{As}. After several years of field observations, a relatively deep terminal lake, elevated above the reach of episodic floodwaters (informally named 'PAD 18'; Figure 2.2), was identified as a suitable index lake for the region based on near-constant isotope composition (Yi et al., 2008) and supported by isotope monitoring of a constant-volume evaporation pan in 2003 (Falcone, 2007). Recently, PAD 18 has served as a valuable index lake to inform isotope mass-balance calculations for lakes in the PAD (Remmer et al., 2018, 2020b), including a 5-year (2015-2019) synthesis incorporating over 1000 water isotope measurements (Remmer et al., 2020a).

Ongoing monitoring of the water isotope composition of PAD 18 in 2020 and 2021, however, revealed distinctly lower values than observed during the previous five years and previous decade, which prompted an investigation of the ongoing suitability of PAD 18 as an index lake and its utility for continued isotope mass-balance parameterization. Here, our objective is to determine if a shift in atmospheric conditions, mainly an increase in relative humidity of ~5% during 2020 and 2021 and assuming re-equilibration with the atmosphere, can fully account for the change in isotope composition of PAD 18 (and thus, δ_{SSL}), and the extent to which this has a measurable influence on estimates of E/I ratios of lakes in the PAD. Findings highlight the value of an index lake and the importance of re-evaluating parameterization of isotope mass-balance models for ongoing quantification of lake water balances and long-term aquatic ecosystem monitoring in the region.

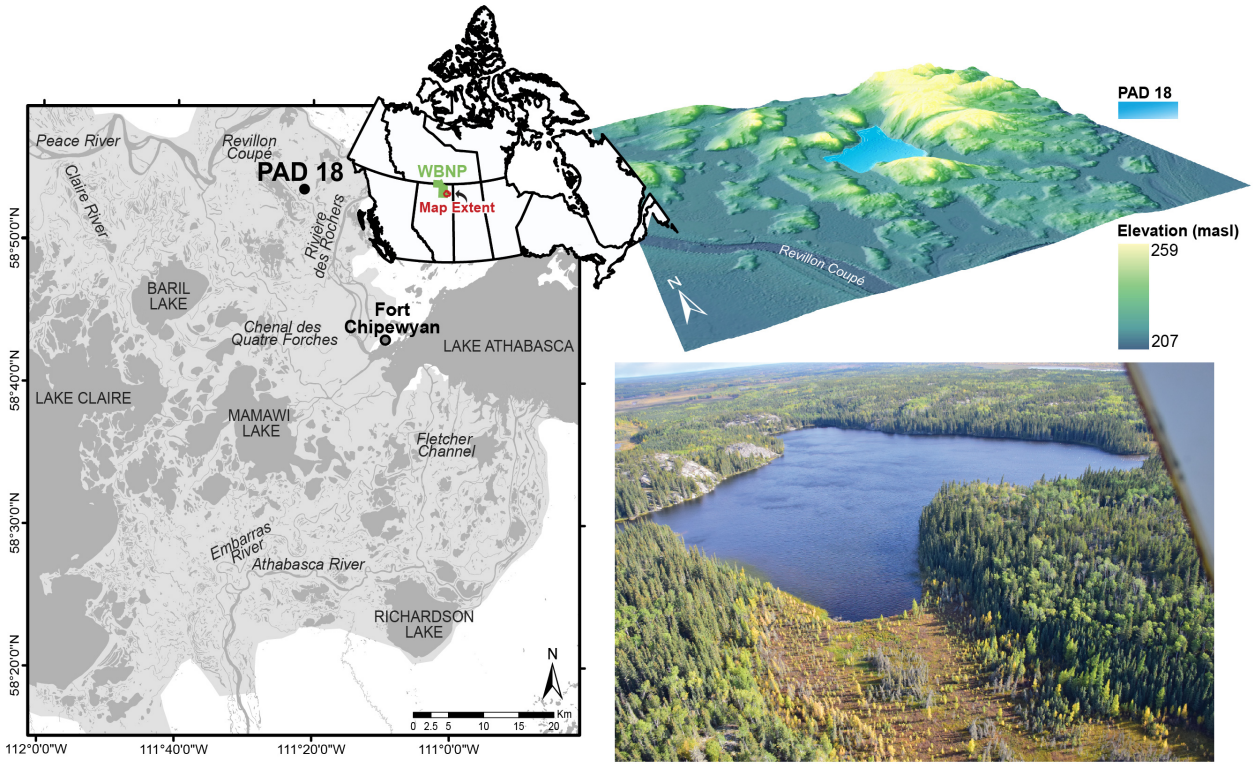


Figure 2.2: Location of lake 'PAD 18' and Fort Chipewyan at the Peace-Athabasca Delta (PAD), Alberta, Canada. Top right panel shows a 3D elevation map of PAD 18 and its position within the landscape that is elevated beyond the influence of river floodwaters. High-resolution digital elevation model data source: Environment and Climate Change Canada (https://open.canada.ca/data/en/dataset/03568324–1a8b-4c00-8650-f5c35f6e0bff). Bottom right panel shows an aerial photograph of PAD 18 in September 2020, courtesy of Parks Canada staff.

2.2 Methods

2.2.1 Study site

PAD 18 (58°53.71' N, 111°21.45' W), a terminal 8-m deep lake (30 ha in surface area), is perched on Canadian Shield bedrock above the reach of river floodwaters that variably influence the water balance of lower lying lakes of the PAD (Figure 2.2). The steep-sided morphometry of the PAD 18 basin restricts littoral zones to a narrow margin around the lake circumference, and mature conifer forest surrounds the lake. Although depth measurements were routinely obtained during water sampling visits since October 2000, we cannot reliably detect lake-level changes based on these data because of differences in location of sampling and the bathymetric variation across the basin. However, observations of the lake level relative to a high-water mark on shoreline bedrock exposures at PAD 18, supported by photographic evidence, reveal minimal inter-annual

variation (± 0.2 m) in water levels both in the early 2000s (Falcone, 2007; Yi et al., 2008) and more recently (Appendix 1).

2.2.2 Sample collection and analysis

Water samples for analysis of oxygen and hydrogen isotope composition were collected from PAD 18 on 46 occasions during ice-free seasons of 2000-2006 and 2014-2021. From 2000-2006, PAD 18 was sampled at irregular intervals. In 2014, PAD 18 was sampled once in late May, whereas from 2015-2021, sampling regularly occurred three times per year (or four times in 2015) during the spring, summer and fall when a network of ~60 other lakes were also sampled that span a broad range of hydrological connectivity with rivers and distributaries. Samples were collected mid-lake at ~10 cm below the water surface from a float-equipped helicopter and stored in sealed 30 ml high-density polyethylene bottles. All samples were analyzed at the University of Waterloo – Environmental Isotope Laboratory (UW – EIL). The samples collected before 2014 were measured by continuous flow isotope ratio mass spectrometry (CF-IRMS), whereas samples collected from 2014-2021 were measured by off-axis integrated cavity output spectroscopy (O-AICOS). For samples measured by CF-IRMS, oxygen isotope values were determined using conventional CO_2-equilibration on a multi-flow system coupled with a GV Instruments Isoprime (MF-GVI-Isoprime), and deuterium was analyzed by hot chromium reduction on a High Temperature Euro Vector EA coupled with a GV Instruments Isoprime (HT-EA-Isoprime). For oxygen and deuterium values measured by O-AICOS, a Los Gatos Research Triple Liquid Water Isotope Analyzer (LGR T-LWIA 45-EP) was used. Analytical uncertainties are ± 0.2‰ for $\delta^{18}O$ and ± 2‰ for $\delta^{2}H$ for samples analyzed by CF-IRMS and ± 0.2 ‰ for $\delta^{18}O$ and ± 0.8 ‰ for $\delta^{2}H$ for samples analyzed by O-AICOS.

A constant-volume class-A evaporation pan was maintained in the backyard of a WBNP research facility in Fort Chipewyan from May 21 – August 24, 2003. The results have been previously reported in a MSc thesis (Falcone, 2007), and they are included here because of their fundamental importance. The pan, a steel cylinder approximately 25 cm deep and 123 cm in diameter with a capacity of 220 L, received measured volumes of tap water to maintain the water level at 19 cm depth on a fixed-point gauge after evaporation or was bailed after rainfall occurred.

Pan water samples were collected every 4-23 days, a tap water sample was collected on June 5, and rainfall samples were collected on 20 different occasions. Tap water used to refill the pan is sourced from Lake Athabasca, which is a large open-drainage lake with continuous connections to active river channels. Measurement of water isotope composition of Lake Athabasca during the equivalent time period in 2003 as the evaporation pan experiment showed minimal variation (May 26, 2003: $\delta^{18}O$ = -18.08‰, $\delta^{2}H$ = -141.85‰; August 8, 2003: $\delta^{18}O$ = -17.08‰, $\delta^{2}H$ = -139.93‰; Wolfe et al., 2012). Pan water, tap water, and rainfall samples were analyzed for $\delta^{2}H$ and $\delta^{18}O$ by CF-IRMS at the UW – EIL using methods described above.

2.2.3 Meteorological data

Annual ice-free season (May-September) relative humidity and air temperature based on evaporation flux-weighted mean hourly values and weighted monthly estimates of potential evapotranspiration, which are used to calculate parameters in the isotope framework, were determined for sampling periods of 2000-2006 and 2014-2021 based on using formulations of Thornthwaite (1948) and meteorological data for Fort Chipewyan from Environment and Climate Change Canada (https://climate.weather.gc.ca/) and the National Research Council of Canada (https://nrc.canada.ca/en/research-development/products-services/software-applications/sun-calculator/). Hourly relative humidity and air temperature data for 2000-2006 were obtained from Environment and Climate Change Canada station 3072658, whereas data for 2014-2021 were obtained from stations 71305 and 71056, which are all located at the Fort Chipewyan airport. Note station 71056 was used in instances (August 2015; 2018-2019) when data were not available at station 71305. Meteorological data for the isotope framework for 2015-2019 used average flux-weighted relative humidity and temperature data for that period, as reported in Remmer et al. (2020a). Meteorological calculations follow methods detailed in the Supplementary Information for Remmer et al. (2020a).

2.2.4 Water isotope measurements and re-evaluation of isotope framework parameters for 2020-2021

Deuterium excess (d-excess) was calculated to indicate the degree of evaporative isotopic enrichment (i.e., the lower the d-excess, the greater the influence of evaporation) for the tap water, rainfall, and pan water samples from 2003, and all PAD 18 water samples from 2000-2006 and 2014-2021 using Dansgaard (1964):

$$d - excess = \delta^2 H - 8\delta^{18} O \quad (1)$$

To assess a decrease in isotopic ratios of oxygen and hydrogen of PAD 18 during 2020-2021, the isotope composition of a theoretical terminal lake in the PAD at steady state was independently estimated using the equation of Gonfiantini (1986), which is based on the linear resistance model of Craig and Gordon (1965):

$$\delta_{SSL} = \alpha^* \delta_I (1 - h + \varepsilon_K) + \alpha^* h \delta_{As} + \alpha^* \varepsilon_K + \varepsilon^* \quad (2)$$

where h is the relative humidity, δ_I is the isotope composition of input water, ε_K is the kinetic separation factor between liquid and vapour phases, α^* is the equilibrium-liquid vapour isotopic fractionation factor, δ_{As} is the isotope composition of atmospheric moisture for the ice-free season, and δ^* is the equilibrium separation factor between liquid and vapour phases. For calculation of δ_{SSL}, which lies on the LEL, the isotope composition of input water was assumed to be equal to the isotope composition of precipitation ($\delta_I = \delta_P$). We used the isotope composition of precipitation as reported in Remmer et al. (2020a), which was derived from a global model (Online Isotopes in Precipitation Calculator; Bowen and Revenaugh, 2003; IAEA/WMO, 2015; Bowen, 2016). The ε_K parameter is humidity dependent, whereas α^* and δ^* are temperature dependent, and were calculated using empirical equations (Gonfiantini, 1986; Horita and Wesolowski, 1994). Average flux-weighted relative humidity and air temperature for the open-water seasons in 2020-2021 were used in Equation 2 for the independent calculation of δ_{SSL}. The isotope composition of δ_{As} used in Equation 2 was adopted from the 2015-2019 framework in Remmer et al. (2020a), as it was assumed initially that this value did not change in 2020-2021. Equations for parameters used for

the isotope framework (α^*, δ^*, and ε_K) are detailed in the Supplementary Information of Remmer et al. (2020a).

As detailed in the Results and Discussion below, following confirmation that the isotope composition of PAD 18 during 2020-2021 was virtually equivalent to δ_{SSL} independently determined using Equation 2, a new isotope framework for 2020-2021 was refined by re-calculating δ_{As} using the equation from Gibson et al. (1999), a rearrangement of Equation 2:

$$\delta_{As} = [(\delta_{SSL} - \varepsilon^*)/\alpha^* - \varepsilon_k - \delta_P(1 - h + \varepsilon_k)]/h \quad (3)$$

For the 2020-2021 isotope framework, the isotope composition of a lake approaching complete desiccation (δ^*), the uppermost endpoint on the LEL, was calculated using average flux-weighted relative humidity and air temperature for 2020-2021, δ_{As} determined using Equation 3, and the equation from Gonfiantini (1986):

$$\delta^* = (h \cdot \delta_{As} + \varepsilon_K + \varepsilon^*/\alpha^*)/(h - \varepsilon_K - \varepsilon^*/\alpha^*) \quad (4)$$

E/I ratios were calculated for 61 lakes in the PAD in July 2021 from lake water isotope compositions using a coupled isotope tracer method (Yi et al., 2008), which assumes the isotope composition of input water (δ_I) lies on the LMWL, for both the isotope framework parameters reported in Remmer et al. (2020a) for 2015-2019 and the new 2020-2021 isotope framework presented below. E/I ratios were determined using Equation 5 (Gonfiantini, 1986; Gibson and Edwards, 2002):

$$E/I = (\delta_I - \delta_L)/(\delta_E - \delta_L) \quad (5)$$

where δ_E was determined using Equation 6 (Craig and Gordon, 1965):

$$\delta_E = [(\delta_L - \varepsilon^*)/\alpha^* - h\delta_{As} - \varepsilon_K]/(1 - h + \varepsilon_K) \quad (6)$$

E/I ratios derived from both frameworks were compared using boxplots, and interpolated maps ('isoscapes') generated using ordinary kriging, which is consistent with Remmer et al. (2020a) and supported by statistically significant values of Moran's *I* ($p < 0.05$) (ArcMap V.10.8.2.). Note, Equations 2-4 and 6 are formulated for parameters expressed in decimal notation.

2.3 Results and discussion

2.3.1 Verifying PAD 18 as a suitable index lake

During May-August 2003, repeated sampling of an evaporation pan maintained in Fort Chipewyan was conducted to provide an estimate of δ_{SSL} and to compare the results to measurements of the isotope composition of PAD 18 (Table 2.1; Figure 2.3). During the first ~5 weeks, the isotope composition of the evaporation pan evolved from tap water (sourced by Lake Athabasca) that was used to fill the pan to more isotopically enriched values as the pan equilibrated with the atmosphere. The isotope composition and d-excess value of the sample collected on June 23 ($\delta^{18}O$ = -10.86‰, $\delta^{2}H$ = -116.07‰; d-excess = -29.19‰) appear to show minimal change from the previous sample collected on June 19 ($\delta^{18}O$ = -10.87‰, $\delta^{2}H$ = -116.89‰; d-excess = -29.93‰). However, this is due to an influential rain event (10.9 mm; $\delta^{18}O$ = -16.63‰, $\delta^{2}H$ = -123.57‰; d-excess = 9.47‰) on June 22-23 that temporarily stabilized the isotope composition of the pan. Although several other rain events occurred (Table 2.1), none appear to have had any measurable effect on the isotopic evolution or steady-state composition of the evaporation pan. Isotope equilibrium between the pan and the atmosphere was attained by July 12, as subsequent samples collected for the next 6 weeks until August 24 resulted in near-constant isotope compositions and d-excess values (average: $\delta^{18}O$ = -9.03 ± 0.31‰, $\delta^{2}H$ = -105.30 ± 1.62‰; d-excess = -33.04 ± 1.37‰). Previous evaporation pan studies conducted in Yellowknife and Lupin (Northwest Territories, Canada) by Gibson et al. (1999) and in the Old Crow Flats (Yukon, Canada) by Tondu et al. (2013) and Turner et al. (2010; 2014), under atmospheric conditions similar to the PAD, also showed rapid isotopic enrichment occurred during the first 4 weeks and the pan equilibrated with the atmosphere after the fifth week of deployment. Notably, the average isotope composition and d-excess value of the evaporation pan upon reaching equilibration with the atmosphere ($\delta^{18}O$ = -9.03‰, $\delta^{2}H$ = -105.30‰; d-excess = -33.04‰) was almost identical to the average isotope composition of PAD 18 in 2003 ($\delta^{18}O$ = -9.47‰, $\delta^{2}H$ = -105.11‰; d-excess = -29.33‰).

Table 2.1: Isotope data ($\delta^{18}O$, $\delta^{2}H$, d-excess) of tap water, rainfall, evaporation pan, and PAD 18 in Fort Chipewyan (Alberta, Canada), May – August 2003.

	Date	$\delta^{18}O$ (‰)	$\delta^{2}H$ (‰)	d-excess (‰)
Tap Water	June 5	-16.82	-140.59	-6.03
Rainfall	June 3	-17.56	-141.29	-0.81
	June 10	-17.29	-140.74	-2.42
	June 16	-19.13	-154.75	-1.71
	June 18	-14.89	-124.65	-5.53
	June 23	-16.63	-123.57	9.47
	June 25	-16.78	-132.39	1.85
	June 27	-17.01	-138.40	-2.32
	June 28	-16.84	-129.83	4.89
	July 3	-16.51	-133.47	-1.39
	July 5	-15.68	-121.00	4.44
	July 6	-15.66	-120.00	5.28
	July 15	-16.71	-137.66	-3.98
	July 18	-13.70	-112.25	-2.65
	July 22	-14.88	-119.64	-0.60
	July 23	-15.50	-122.72	1.28
	July 24	-15.04	-111.47	8.85
	July 30	-14.47	-116.46	-0.70
	August 15	-17.45	-144.36	-4.76
	August 18	-14.10	-115.60	-2.80
	August 20	-20.47	-167.94	-4.18
Evaporation Pan	May 21	-15.83	-134.11	-7.47
	May 31	-13.29	-125.95	-19.63
	June 5	-12.45	-123.33	-23.73
	June 10	-11.98	-120.38	-24.54
	June 19	-10.87	-116.89	-29.93
	June 23	-10.86	-116.07	-29.19
	July 12	-9.05	-104.74	-32.34
	July 18	-9.28	-105.81	-31.57
	August 10	-8.59	-103.41	-34.69
	August 24	-9.21	-107.24	-33.56
PAD 18	May 22	-9.60	-105.50	-28.70
	May 28	-9.73	-105.59	-27.75
	June 25	-9.53	-106.12	-29.88
	July 24	-9.26	-103.43	-29.35
	August 15	-9.24	-104.90	-30.98

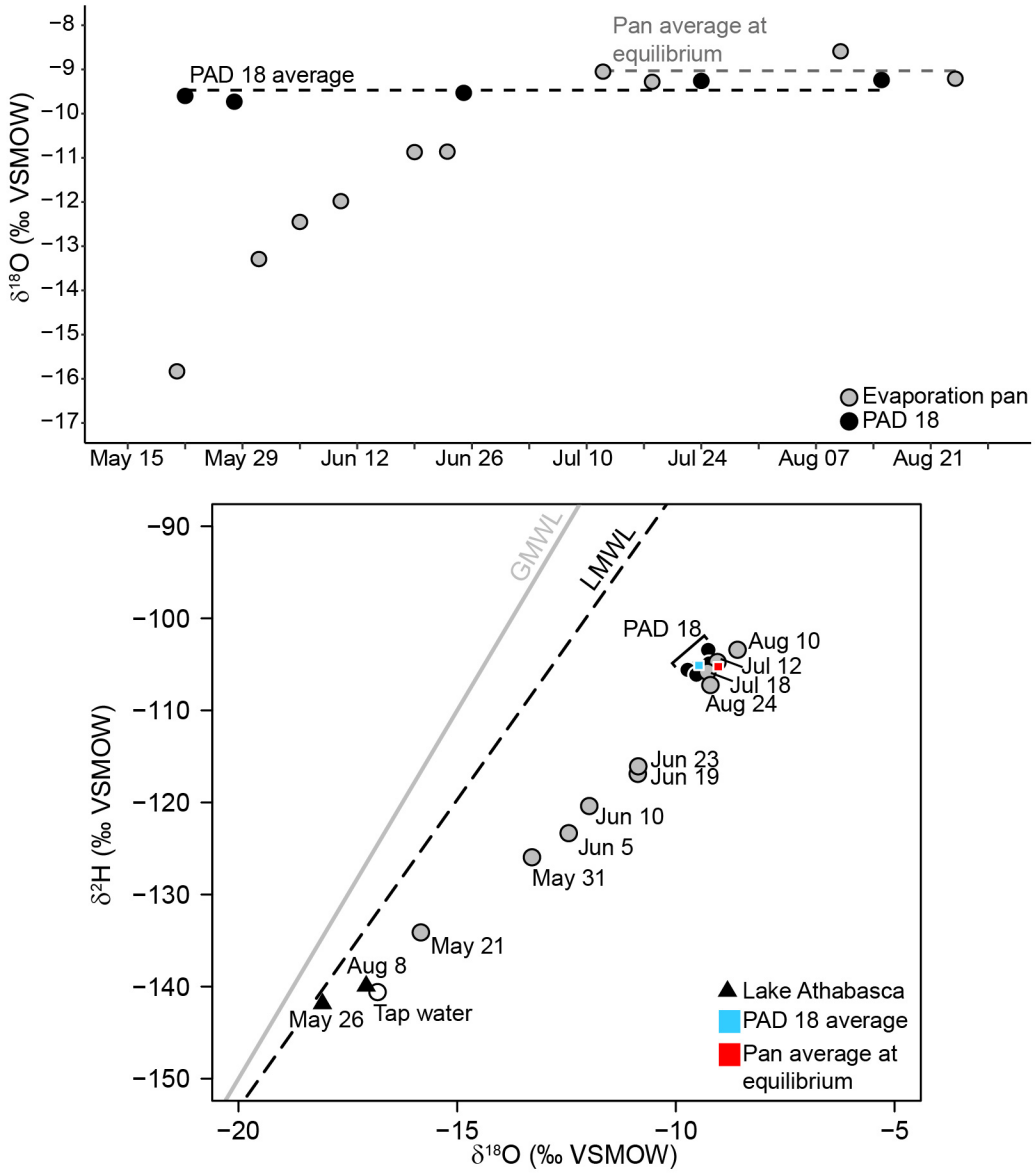


Figure 2.3: Water isotope compositions of evaporation pan (grey circles; including tap water [open circle in the bottom panel] used to fill the pan) maintained at Fort Chipewyan, Lake Athabasca (black triangles), and PAD 18 (black circles) in 2003 (for locations, see Figure 2.1). Top panel shows time series of $\delta^{18}O$ values of water from the evaporation pan and PAD 18. Black dashed line in the top panel indicates average $\delta^{18}O$ of PAD 18 in 2003 (-9.47‰) and grey dashed line indicates average $\delta^{18}O$ of the evaporation pan at equilibrium (-9.03‰). Bottom panel shows evolution of pan water isotope compositions towards equilibrium with the atmosphere and PAD 18 isotope compositions in $\delta^{18}O$-$\delta^{2}H$ space. Evaporation pan and PAD 18 data are from Falcone (2007). Lake Athabasca data are from Wolfe et al. (2012).

These results supported the use of PAD 18 as an index lake (i.e., δ_{SSL}) for estimating δ_{As} using Equation 3 and subsequent isotope mass-balance applications in the PAD (Yi et al., 2008; Remmer et al., 2018, 2020a,b).

2.3.2 Long-term monitoring of PAD 18 from 2000-2006 and 2014-2019

Repeated measurements of the isotope composition and d-excess values of PAD 18 during 2000-2006 and 2014-2019 reveal minimal variation and a long-term average ($\delta^{18}O$ = -9.15 ± 0.42‰, $\delta^{2}H$ = -103.92 ± 1.76‰; d-excess = -30.56 ± 2.88‰) close to the average value obtained during 2003 ($\delta^{18}O$ = -9.47 ± 0.22‰, $\delta^{2}H$ = -105.11 ± 1.03‰; d-excess = -29.33 ± 1.22‰) when the evaporation pan experiment was conducted, demonstrating the value and consistency of PAD 18 to serve as a long-term index lake (Table 2.2; Figure 2.4). Independent calculation of δ_{SSL} for each sampling year using Equation 2, incorporating flux-weighted relative humidity and air temperature of the respective year, and a constant value of δ_{As} from Remmer et al. (2020a) revealed extremely good agreement overall between the measured values at PAD 18 (average $\delta^{18}O$ = -9.14 ± 0.46‰) and those derived using Equation 2 (average $\delta^{18}O$ = -9.24 ± 0.50‰) during 2000-2006 and 2015-2019. Minor differences (<1‰) on an annual basis are likely due to small variation in δ_{As}. During this time, ice-free season flux-weighted relative humidity ranged from 63.0-70.5%, but was on average nearly identical between the two main sampling intervals, 2000-2006 (66.4%) and 2014-2019 (66.2%). There were, however, a few short-lived instances when hydrologic steady-state conditions for a terminal basin were likely not maintained at PAD 18 (i.e., $E/I \neq 1$). For instance, isotope compositions from May 2003, May 2005, May 2014, and May 2017 were low and briefly outside the range of variability, likely due to input of isotopically depleted precipitation in the spring just prior to sampling. In contrast, isotope compositions from later during the ice-free seasons in October 2000 and August 2001 were high and also briefly outside the range of variability, likely in response to short-lived changes in local atmospheric conditions (i.e., air temperature, relative humidity, δ_{As}) that increased evaporation. Strong evaporative enrichment during summer 2001 was also evident at other perched basins in the PAD (see Wolfe et al., 2005; 2008). Despite these few transient instances of variation outside the long-term average, the isotope composition of PAD 18 remained within one standard deviation ($\delta^{18}O$ ± 0.42‰) for 32

of the 39 samples collected over 13 years (2000-2006, 2014-2019).

2.3.3 Development of a new isotope framework for 2020-2021

Following minimal year-to-year variation in isotope composition and d-excess value of PAD 18, consistently low isotope compositions outside the range defined by the long-term standard deviation were obtained during 2020-2021 (average: $\delta^{18}O$ = -10.30 ± 0.41‰, $\delta^{2}H$ = -108.29 ± 1.80‰; d-excess = -25.93 ± 1.71‰; Figure 2.4). Unlike previous short-lived occurrences when hydrologic steady-state conditions were likely not maintained, low isotope compositions persisted for two years, resulting in the longest duration of deviation from the long-term average since sampling began in 2000. Further exploration of these results in $\delta^{18}O$-$\delta^{2}H$ space reveals that the isotope compositions and the average value of PAD 18 in 2020-2021 are distinctly lower than isotope compositions of PAD 18 during 2015-2019, yet they continue to lie on the 2015-2019 isotope framework LEL established by Remmer et al. (2020a; Figure 2.5a). Cumulative precipitation (January 1 – September 30) in 2020 (486.4 mm) substantially exceeded the climate normal (291.4 mm; Neary et al., 2023) and could provide an explanation for the change in isotope composition of PAD 18. However, cumulative precipitation in 2021 (290.6 mm; Neary et al., 2023) was near the climate normal yet PAD 18 remained isotopically depleted compared to prior years. Thus, changes in cumulative precipitation seem unlikely to provide an explanation for the shift in isotope composition during both years. Alternatively, the higher flux-weighted relative humidity in 2020 (71.9%) and 2021 (69.9%) and their average (70.8%) in comparison to 2015-2019 (66.2%) may explain the low observed isotope compositions of PAD 18. Interestingly, the average flux-weighted relative humidity in 2003 (70.5%) was similar to that in 2020-2021, but the average isotope composition of PAD 18 remained largely within the one-standard deviation of the long-term average, which we speculate may be due to a compensating shift in δ_{As}. Calculations show that only a slight increase of 0.91‰ and 2.57‰ in $\delta^{18}O_{As}$ and $\delta^{2}H_{As}$, respectively, is required to offset the effects of higher relative humidity during 2003 on the isotope composition of PAD 18.

Table 2.2: Isotope data ($\delta^{18}O$, $\delta^{2}H$, d-excess) of PAD 18 from 2000-2006 and 2014-2021, and ice-free season flux-weighted air temperature (°C) and relative humidity (%).

Sampling Date	$\delta^{18}O$ (‰)	$\delta^{2}H$ (‰)	d-excess (‰)	T (°C)	h (%)
25-October-2000	-8.18	-104.15	-38.71	13.60	63.7
06-March-2001	-8.97	-105.75	-33.99		
03-June-2001	-8.99	-103.50	-31.58	15.02	67.1
27-August-2001	-7.62	-101.70	-40.74		
03-June-2002	-9.07	-101.84	-29.28		
25-July-2002	-8.81	-100.65	-30.17	13.84	67.0
25-August-2002	-8.77	-101.93	-31.77		
21-September-2002	-9.02	-100.62	-28.46		
30-April-2003†	-10.45	-109.23	-25.63		
22-May-2003	-9.60	-105.50	-28.70		
28-May-2003	-9.73	-105.59	-27.75	14.04	70.5
25-June-2003	-9.53	-106.12	-29.88		
24-July-2003	-9.26	-103.43	-29.35		
15-August-2003	-9.24	-104.90	-30.98		
04-June-2004	-9.36	-107.97	-33.09		
18-July-2004	-8.98	-104.02	-32.18	13.32	64.5
23-September-2004	-8.93	-103.90	-32.46		
16-May-2005	-9.74	-103.63	-25.71		
18-July-2005	-9.34	-104.74	-30.02	12.95	68.1
14-September-2005	-9.58	-105.69	-29.05		
01-June-2006	-9.37	-108.15	-33.19		
20-July-2006	-9.27	-104.07	-29.91	15.25	63.9
01-September-2006	-9.10	-105.08	-32.28		
31-May-2014	-10.03	-107.19	-26.95	15.50	65.5
26-May-2015	-9.10	-102.93	-30.13		
28-June-2015	-8.79	-102.11	-31.79	14.76	66.9
27-July-2015	-9.11	-102.62	-29.74		
15-September-2015	-9.04	-102.42	-30.10		
29-June-2016	-9.32	-103.73	-29.17		
27-July-2016	-9.24	-102.51	-28.59	15.27	69.1
28-September-2016	-9.14	-102.93	-29.81		
16-May-2017	-9.69	-104.88	-27.36		
12-July-2017	-8.88	-102.74	-31.70	15.40	65.4
12-September-2017	-8.70	-102.48	-32.88		
15-May-2018	-9.39	-104.72	-29.60		
10-July-2018	-9.20	-104.68	-31.08	14.76	63.0
11-September-2018	-9.39	-103.52	-28.40		
13-May-2019	-9.29	-104.35	-30.03	13.42	67.5

† Isotope composition excluded from Figure 2.4 and 2.5 as ice was present on the lake when sampling occurred.

12-July-2019	-9.05	-102.87	-30.47		
11-September-2019	-9.19	-103.43	-29.91		
26-May-2020	-10.22	-108.02	-26.26		
29-July-2020	-10.02	-106.09	-25.93	14.27	71.9
15-September-2020	-9.81	-106.99	-28.51		
25-May-2021	-10.95	-111.22	-23.62		
20-July-2021	-10.18	-108.17	-26.73	15.13	69.9
13-September-2021	-10.59	-109.27	-24.55		

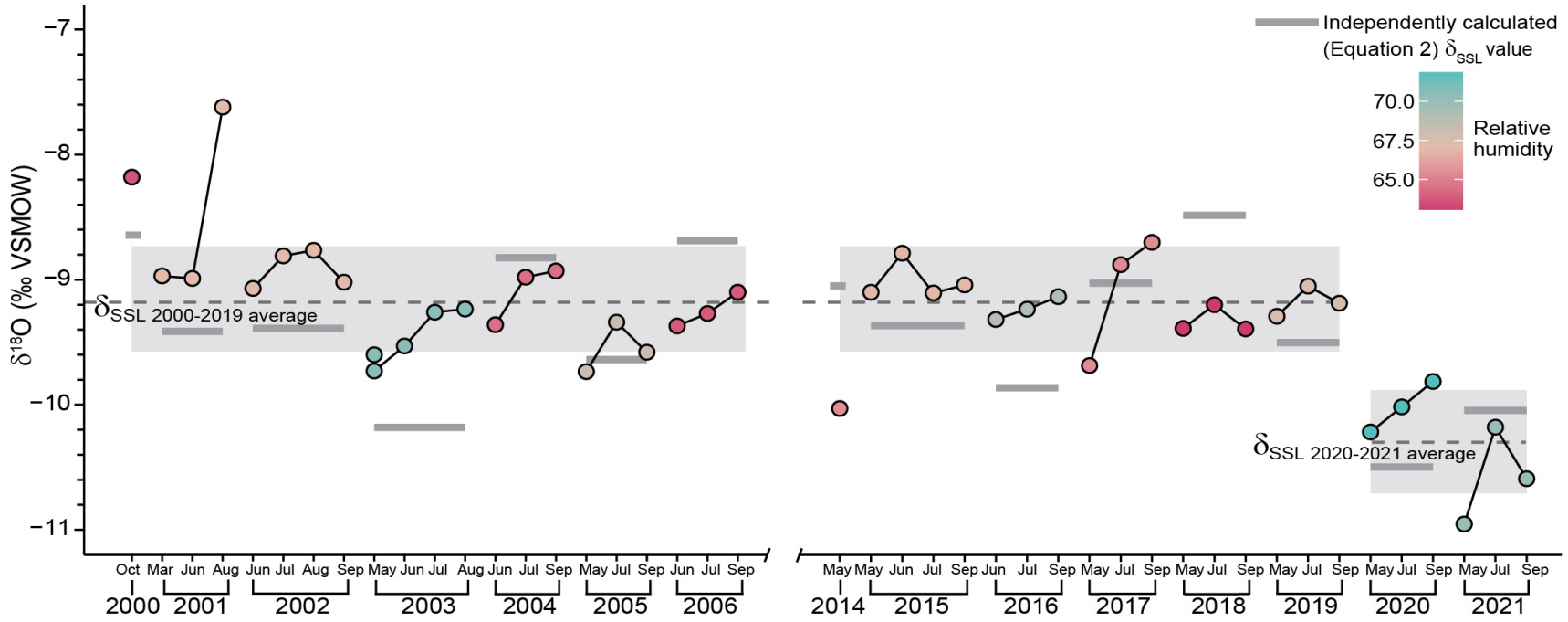


Figure 2.4: Time series of $\delta^{18}O$ for PAD 18 sampled during ice-free seasons of 2000-2006 and 2014-2021. Connecting lines are for each sampling year. Average ice-free season flux-weighted relative humidity of each sampling year is shown in the colour palette (see Table 2.2). Dashed lines indicate average δ_{SSL} values estimated from the isotope compositions of PAD 18 from 2000-2006 and 2014-2019 ($\delta^{18}O$ = -9.15‰) and from 2020-2021 ($\delta^{18}O$ = -10.30‰), and the horizontal grey bars indicates one standard deviation about the average, respectively. Dark grey line segments represent δ_{SSL} values derived using Equation 2 for each sampling year.

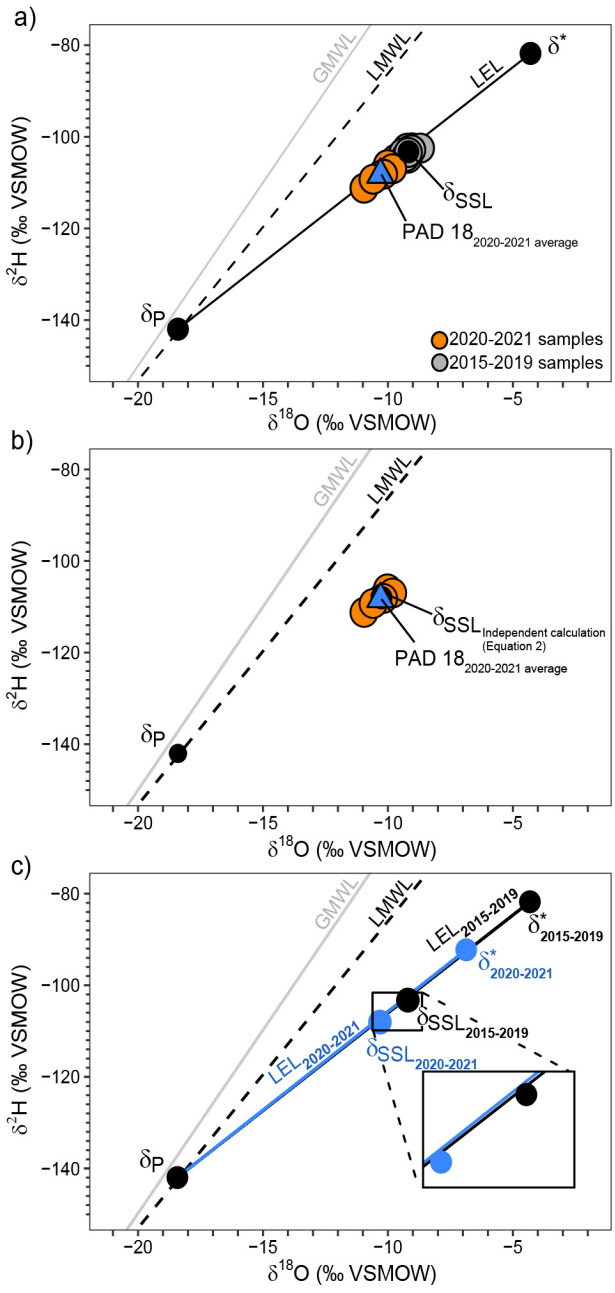


Figure 2.5: In **a)**, the isotope compositions of PAD 18 during 2015-2019 (grey circles) and 2020-2021 (orange circles) are displayed alongside the average isotope composition of PAD 18 from 2020-2021 (blue triangle) on the predicted LEL based on meteorological conditions during 2015-2019 as reported in Remmer et al. (2020a). In **b)**, the isotope compositions of PAD 18 in 2020-2021 (orange circles) and the average value (blue triangle) are compared to δ_{SSL} (black circle behind blue triangle) calculated using Equation 2. In **c)**, the predicted LEL is displayed for 2020-2021 using the average isotope composition of PAD 18 as δ_{SSL} and incorporating meteorological conditions from 2020-2021 (blue circles and line; LEL: $\delta^2H = 4.30\ \delta^{18}O - 62.85$) and compared to the 2015-2019 LEL (black circles and lines; LEL: $\delta^2H = 4.27\ \delta^{18}O - 63.47$). See Table 2.3 for isotope and hydroclimate parameters associated with isotope frameworks presented in a) and c).

To determine if the higher relative humidity in 2020-2021 can account for the shift in isotope composition of PAD 18, δ_{SSL} was independently determined (Equation 2) using average flux-weighted relative humidity and temperature for 2020-2021 and δ_{As} derived from the 2015-2019 isotope framework (Remmer et al., 2020a) and compared to the measured isotope composition of PAD 18 in 2020-2021. The resulting δ_{SSL} value ($\delta^{18}O$ = -10.26‰; $\delta^{2}H$ = -107.99‰) was near-identical to the average isotope composition of PAD 18 during 2020-2021 (average: $\delta^{18}O$ = -10.30 ± 0.41‰; $\delta^{2}H$ = -108.29 ± 1.80‰; Figure 2.5b), which strongly suggests PAD 18 re-equilibrated to different atmospheric conditions in 2020-2021 that resulted in less kinetic isotope fractionation (i.e., evaporative enrichment). In other words, PAD 18 remained at hydrologic and isotopic steady-state for a terminal basin, but under a higher relative humidity. This discovery led to the development of a new 2020-2021 isotope framework, which incorporates the average isotope composition of PAD 18 in 2020-2021 as δ_{SSL}. The new δ_{SSL} value and use of 2020-2021 air temperature and relative humidity data, subsequently yielded a virtually equivalent δ_{As} value (Equation 3), lower δ^{*} value (Equation 4), and marginally steeper LEL slope than the previous 2015-2019 framework (Table 2.3; Figure 2.5c). Minimal difference in δ_{As} and temperature between the two frameworks further validates the increase in relative humidity as a plausible primary cause for the change in the isotope composition of PAD 18.

We evaluated the importance of the new 2020-2021 isotope framework by comparing the E/I ratios in July 2021 at 61 lakes with values derived using the 2015-2019 isotope framework (Figure 2.6). For both isotope frameworks, E/I ratios are higher for lakes in the northern Peace sector than in the southern Athabasca sector (Figure 2.6a). This is consistent with knowledge that water balance of lakes in the Peace sector is more strongly influenced by evaporation, whereas lakes in the Athabasca sector are more prone to flooding (Prowse and Conly, 1998; Wolfe et al., 2007; Timoney, 2013; Neary et al., 2021, 2023). The two frameworks result in small differences in E/I ratios in the Athabasca sector (mean E/I ratio = 0.18 and 0.21 for the 2015-2019 and 2020-2021 isotope frameworks, respectively), but larger differences in the Peace sector (mean E/I ratio = 0.34 and 0.43 for the 2015-2019 and 2020-2021 isotope frameworks, respectively). This is an outcome of the non-linear effect of relative humidity on modelled E/I ratios. For example, at an E/I ratio of 0.4 using the 2015-2019 isotope framework, the difference between the 2015-2019

isotope framework and the 2020-2021 isotope framework is 0.14, whereas the difference rises to 0.41 at an E/I ratio of 0.7. The non-linear relation between E/I ratios produced by the two frameworks result in meaningful differences in the spatial distribution of lake water balances displayed in the isoscapes in the northwestern region of the Peace sector (Figure 2.6b). Here, values generated using the 2020-2021 isotope framework demonstrate measurably greater influence of evaporation than using the 2015-2019 isotope framework. This is a critical feature because, by incorporating the 2020-2021 isotope framework, E/I ratios of lakes in the northwestern region of the Peace sector capture the leading edge of what may be the potential re-emergence of the importance of evaporation across much of the PAD following an unusually wet interval. Indeed, this region was also revealed as a hotspot of evaporative water loss in the 5-year time-series of isoscapes reported by Remmer et al. (2020a) between 2015-2019. Support for ongoing use of the 2020-2021 isotope framework is provided by recent measurement of the isotope composition of 'PAD 33' in late May 2023 ($\delta^{18}O$ = -9.58‰; $\delta^{2}H$ = -103.82‰), a lake located in the Athabasca sector of the PAD long observed to experience strong variation in lake water balance and water level. The E/I ratio of PAD 33 is 1.09 using the 2020-2021 isotope framework, whereas the E/I ratio is 0.68 using the 2015-2019 isotope framework. Clearly, the former is more aligned with evidence in aerial imagery of evaporative lake-level drawdown of PAD 33 (Figure 2.7). Of note, isotope composition in May 2023 at PAD 18 ($\delta^{18}O$ = -10.60‰; $\delta^{2}H$ = -111.82‰) remains low relative to the long-term average. Based on this collective evidence, the 2020-2021 isotope framework anchored by the lower PAD 18 isotope composition as δ_{SSL} more suitably captures the effects of evaporation on lake water balance in the PAD since 2020 and avoids underestimating E/I ratios for lakes most prone to evaporative drawdown.

Table 2.3: Isotope framework parameters and the LEL slopes and intercepts based on i) meteorological conditions during 2015-2019 using a long-term (2000-2015) average isotope composition of PAD 18 for δ_{SSL} (Remmer et al., 2020a), and ii) meteorological conditions during 2020-2021 and the average isotope composition of PAD 18 for δ_{SSL} during 2020-2021. δ_{SSL} value for 2015-2019 framework is based on water isotope compositions of PAD 18 collected during 2000-2006 and 2014-2015. Note, all parameters are expressed in decimal notation when applied in Equations 3 and 4.

Parameter	2015-2019 framework	2020-2021 framework	Source
h (%)	66.2	70.8	ECCC, NRCC
T (°C)	14.62	14.72	ECCC, NRCC
α^* (^{18}O, ^{2}H)	1.0103, 1.0909	1.0103, 1.0908	Horita and Wesolowski (1994)
ε^* (^{18}O, ^{2}H) (‰)	10.30, 90.90	10.26, 90.77	
ε_k (^{18}O, ^{2}H) (‰)	4.79, 4.22	4.14, 3.64	Gonfiantini (1986)
δ_{As} (^{18}O, ^{2}H) (‰)	-26.84, -203.18	-26.89, -203.58	Gibson et al. (1999); Eq. 3
δ_P (^{18}O, ^{2}H) (‰)	-18.4, -142	-18.4, -142	OIPC (Bowen and Revenaugh, 2003; IAEA/WMO, 2015; Bowen, 2016)
δ^* (^{18}O, ^{2}H) (‰)	-4.30, -81.82	-6.84, -92.29	Gonfiantini (1986); Eq. 4
δ_{SSL} (^{18}O, ^{2}H) (‰)	-9.18, -104.26	-10.30, -108.29	PAD 18
LEL slope	4.27	4.30	
LEL intercept	-63.47	-62.85	

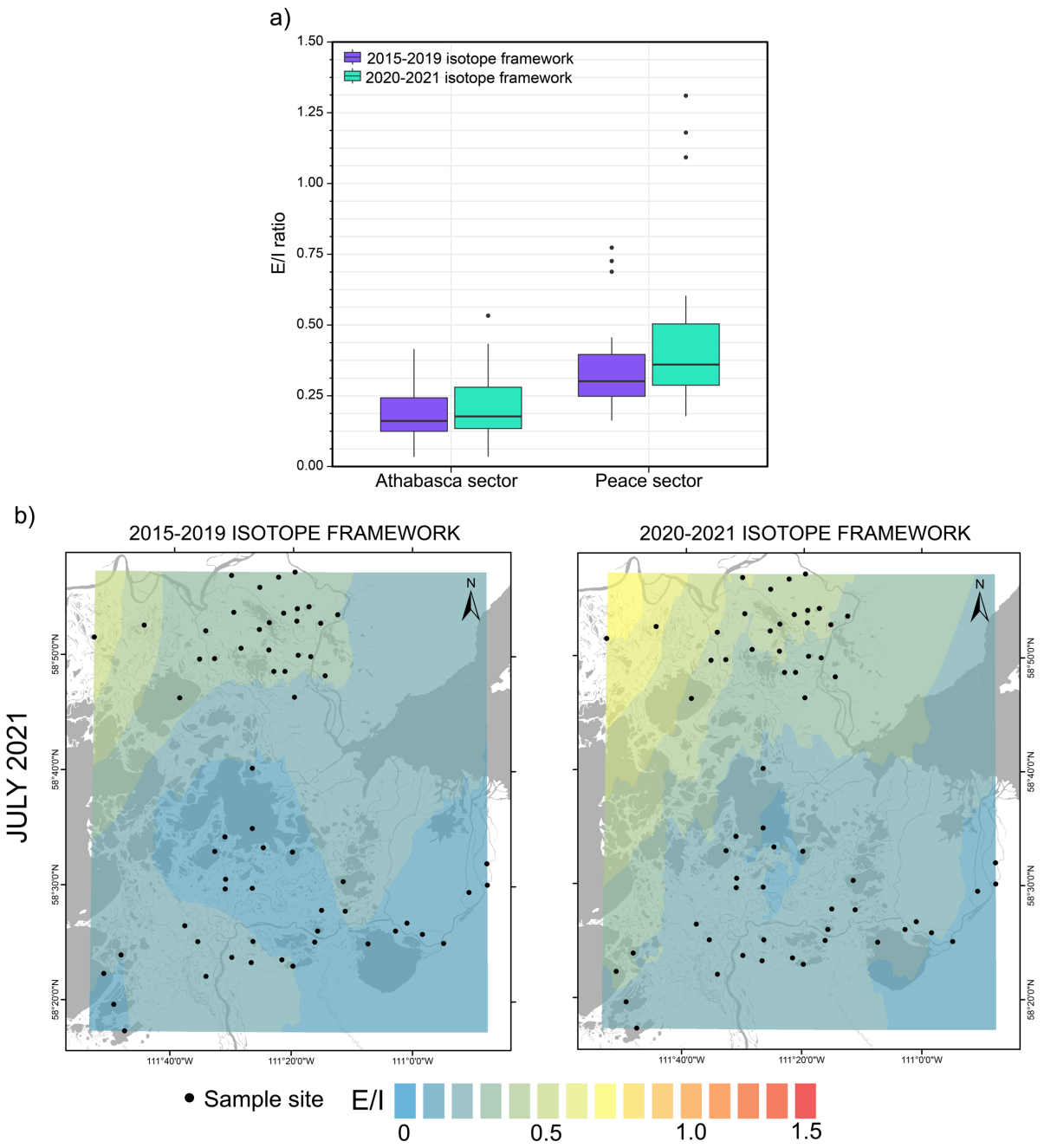


Figure 2.6: The distribution of evaporation-to-inflow (E/I) ratios derived from lake water isotope compositions from the Peace-Athabasca Delta (PAD) in July 2021.**a)** boxplots comparing the distribution of E/I ratios computed using the 2015-2019 isotope framework (purple boxplots) and 2020-2021 isotope framework (teal boxplots) for lakes in the Athabasca sector and Peace sector. **b)** isoscapes displaying spatial interpolation of E/I ratios calculated using the 2015-2019 isotope framework as presented in Remmer et al. (2020a) (left panel) and the 2020-2021 isotope framework (right panel). Warm-toned colours represent higher E/I ratios and cool-toned colours represent lower E/I ratios based on a scale from 0-1.5.



Figure 2.7: Aerial photograph of PAD 33 (May 27, 2023) displaying visible evidence of water-level drawdown.

2.4 Conclusions and Recommendations

After nearly two decades of sampling PAD 18, an index lake used for isotope mass-balance calculations for lakes across the hydrologically dynamic Peace-Athabasca Delta, an unprecedented shift in water isotope composition was observed in 2020-2021. Through re-evaluation of the isotope framework, supported by independent calculation of δ_{SSL} values (Equation 2), we demonstrate that a ~5% increase in relative humidity during 2020-2021 is the primary cause for isotopically depleted values at PAD 18 during 2020-2021. Comparison of annual independently-derived δ_{SSL} values (Equation 2) to estimates of δ_{SSL} based on measured water isotope compositions at PAD 18 during the monitoring periods of 2000-2006 and 2014-2019 further demonstrate that the index lake method is preferable for tracking δ_{SSL} because the approach

naturally integrates the influence of shifting local atmospheric conditions including relative humidity, temperature and δ_{As}.

Accurately characterizing and tracking the influence of evaporation from lakes in the PAD is critical, as a petition to enlist WBNP as a UNESCO World Heritage Site in Danger was driven, in part, by concerns about lake-level decline (MCFN, 2014). In response to the petition and recommendations from UNESCO (WHC/ICUN, 2017), a federal Action Plan was developed to "detect cumulative effects on the PAD and to generate information that informs land-use management and regulatory decision making" (WBNP, 2019; p.79). As Parks Canada Agency collaborates with federal, provincial, territorial, and Indigenous governments to lead execution of an aquatic ecosystem monitoring program within the Action Plan, we advocate for continued use of water isotope tracers to capture the influence of hydrological processes on lake water balances and status and trends in freshwater availability in the PAD, as demonstrated and advocated for in Remmer et al. (2020a) and Neary et al. (2023). From our long-term repeated sampling, we have confirmed that PAD 18 continues to serve as a useful and sensitive index lake to constrain isotope mass-balance calculations of lakes in the PAD. In recognition of the important value of PAD 18, we highly recommend continued measurement for water isotope composition to allow for straightforward evaluation in the context of the long-term record displayed in Figure 2.4, and to ensure ongoing parameterization of the isotope framework remains representative of the prevailing atmospheric conditions. Continued assessment of annual meteorological conditions will also inform re-evaluation of the isotope framework as shifts from long-term conditions, particularly in relative humidity, can result in changes to the predicted LEL, thereby affecting interpretation of lake water isotope data (Brock et al., 2008; Gibson et al., 2016; Sun et al., 2021; Wang et al., 2023). Consistent with recommendations for an isotope-based aquatic ecosystem monitoring program in Vuntut National Park, Yukon (Tondu et al., 2013), monitoring of an evaporation pan in Fort Chipewyan can further validate that PAD 18 remains at hydrologic and isotopic steady-state for a terminal basin and to assist with defining framework parameters during years of atypical atmospheric conditions. Furthermore, we recommend lake-level monitoring via the use of water-depth loggers deployed at a consistent station at the centre of PAD 18 for the duration of the ice-free season to obtain data to ensure the assumption of hydrologic steady-state is satisfied. Aside from the initial, yet critical, evaporation pan experiment in 2003, these two supplementary aspects

were subsequently absent from this study, which presented some limitations and therefore are considered priorities to support ongoing water isotope monitoring in the region. Knowledge generated from these results offer pivotal guidance for agencies in the event that they apply isotope-based techniques towards the fulfilment of the Canadian federal government's Action Plan for WBNP. As several studies have projected, atmospheric conditions will continue to become variable in the future as a consequence of global warming (Prowse et al., 2009; Aygün et al., 2019; IPCC, 2021; Zaitchik et al., 2023) and inter-annual and multi-annual shifts in meteorological conditions will require close scrutiny of isotope framework parameters to accurately inform about lake hydrologic conditions at the PAD and other water-rich landscapes.

2.5 References

Allison, G.B., Brown, R.M., Fritz, P., 1979a. Estimation of the isotopic composition of lake evaporate. J. *Hydrol.*, 42, 109-127. https://doi.org/10.1016/0022-1694(79)90009-X.

Allison, G.B., Brown, R.M., Fritz, P., 1979b. Evaluation of water balance parameters from isotopic measurements in evaporation pans, in: Isotopes in lake studies. *International Atomic Energy Agency*, Vienna.

Aygün, O., Kinnard, C., Campeau, S., 2019. Impacts of climate change on the hydrology of northern midlatitude cold regions. *Prog. Phys. Geo.: Earth Environ.*, 44, 338-375. https://doi.org/10.1177/0309133319878123.

Bowen, G.J., 2016. The Online Isotopes in Precipitation Calculator, version 2.2. Accessible at http://www.waterisotopes.org.

Bowen, G.J., Revenaugh, J., 2003. Interpolating the isotopic composition of modern meteoric precipitation. *Water Resour. Res.*, 39. https://doi.org/10.1029/2003WR002086.

Brock, B.E., Wolfe, B.B., Edwards, T.W.D., 2008. Spatial and temporal perspectives on spring break-up flooding in the Slave River Delta, NWT. *Hydrol. Processes*, 22, 4058-4072. https://doi.org/10.1002/hyp.7008.

Brock, B.E., Wolfe, B.B., Edwards, T.W.D., 2007. Characterizing the hydrology of shallow floodplain lakes in the Slave River Delta, NWT, Canada, using water isotope tracers. *Arct. Antarct. Alp. Res.*, 39, 388-401. https://doi.org/10.1657/1523-0430(06-026)[BROCK]2.0.CO;2.

Brooks, J.R., Gibson, J.J., Jean Birks, S., Weber, M.H., Rodecap, K.D., Stoddard, J.L., 2014. Stable isotope estimates of evaporation: Inflow and water residence time for lakes across the United States as a tool for national lake water quality assessments. *Limnol. Oceanogr.*, 59, 2150-2165. https://doi.org/10.4319/lo.2014.59.6.2150.

Clark, I.D., Fritz, P., 1997. Environmental Isotopes in Hydrogeology, 1st ed, Environmental Isotopes in Hydrogeology. *CRC Press*. https://doi.org/10.1201/9781482242911.

Chasmer, L., Hopkinson, C., 2017. Threshold loss of discontinuous permafrost and landscape evolution. *Global Change Biol.,* 23, 2672-2686. https://doi.org/10.1111/gcb.13537.

Coplen, T.B., 1996. New guidelines for reporting stable hydrogen, carbon, and oxygen isotope-ratio data. *Geochim Cosmochim Acta*, 60, 3359-3360. https://doi.org/10.1016/0016-7037(96)00263-3.

Craig, H., 1961. Isotopic variations in meteoric waters. *Science*, 133, 1702-1703. https://doi.org/10.1126/science.133.3465.1702.

Craig, H., Gordon, L.I., 1965. Deuterium and oxygen 18 variations in the ocean and the marine atmosphere, in: Stable Isotopes in Oceanographic Studies and Paleotemperatures, E Tongiorgi (ed). *Laboratorio di Geologia Nucleare*, Pisa, Italy.

Cui, J., Tian, L., Biggs, T.W., Wen, R., 2017. Deuterium-excess determination of evaporation to inflow ratios of an alpine lake: Implications for water balance and modeling. *Hydrol. Processes*, 31, 1034-1046. https://doi.org/10.1002/hyp.11085.

Dansgaard, W., 1964. Stable isotopes in precipitation. *Tellus*, 16, 436-468.

Dinçer, T., 1968. The Use of Oxygen 18 and Deuterium Concentrations in the Water Balance of Lakes. *Water Resour. Res.*, 4, 1289-1306. https://doi.org/10.1029/WR004i006p01289.

Edwards, T.W.D., Wolfe, B.B., Gibson, J.J., Hammarlund, D., 2007. Use of water isotope tracers in high latitude hydrology and paleohydrology, in: Long-Term Environmental Change in Arctic and Antarctic Lakes. *Springer*, Dordrecht. https://doi.org/10.1007/978-1-4020-2126-8_7.

Falcone, M.D., 2007. Assessing hydrological processes controlling the water balance of lakes in the PAD, Canada using water isotope tracers. MSc. Thesis University of Waterloo.

Gat, J.R., 1996. Oxygen and hydrogen isotopes in the hydrologic cycle. *Annu. Rev. Earth Planet. Sci.*, 24, 225-262. https://doi.org/10.1146/annurev.earth.24.1.225.

Gat, J.R., 1995. Stable Isotopes of Fresh and Saline Lakes, in: Physics and Chemistry of Lakes. *Springer*, Berlin. https://doi.org/10.1007/978-3-642-85132-2_5.

Gat, J.R., Levy, Y., 1978. Isotope hydrology of inland sabkhas in the Bardawil area, Sinai. *Limnol. Oceanogr.*, 23, 841-850. https://doi.org/10.4319/lo.1978.23.5.0841.

Gibson, J.J., 2002. A new conceptual model for predicting isotopic enrichment of lakes in seasonal climates. *PAGES news*., 10, 10-11. https://doi.org/10.22498/pages.10.2.10.

Gibson, J.J., Birks, S.J., Yi, Y., 2016. Stable isotope mass balance of lakes: A contemporary perspective. *Quat. Sci. Rev.*, 131, 316-328. https://doi.org/10.1016/j.quascirev.2015.04.013.

Gibson, J.J., Eby, P., Birks, S.J., Twitchell, C., Gray, C., Kariyeva, J., 2022. Isotope-based water balance assessment of open water wetlands across Alberta: Regional trends with emphasis on the oil sands region. *J. Hydrol.: Reg. Stud.*, 40, 101036. https://doi.org/10.1016/j.ejrh.2022.101036.

Gibson, J.J., Edwards, T.W.D., 2002. Regional water balance trends and evaporation-transpiration partitioning from a stable isotope survey of lakes in northern Canada. *Glob. Biogeochem. Cycles*, 16, 10-1-10-14. https://doi.org/10.1029/2001gb001839.

Gibson, J.J., Edwards, T.W.D., Prowse, T.D., 1999. Pan-derived isotopic composition of atmospheric water vapour and its variability in northern Canada. *J. Hydrol.*, 217, 55-74. https://doi.org/10.1016/S0022-1694(99)00015-3.

Gibson, J.J., Prepas, E.E., McEachern, P., 2002. Quantitative comparison of lake throughflow, residency, and catchment runoff using stable isotopes: Modelling and results from a regional survey of Boreal lakes. *J. Hydrol.*, 262, 128-144. https://doi.org/10.1016/S0022-1694(02)00022-7.

Gibson, J.J., Reid, R., 2014. Water balance along a chain of tundra lakes: A 20-year isotopic perspective. *J. Hydrol.*, 519, 2148-2164. https://doi.org/10.1016/j.jhydrol.2014.10.011.

Gonfiantini, R., 1986. Environmental Isotopes in Lake Studies, in: Fritz, P., Clark, J.-C. (Eds.), Handbook of Environmental Isotope Geochemistry. *Elsevier Science*. https://doi.org/10.1016/b978-0-444-42225-5.50008-5.

Horita, J., Wesolowski, D.J., 1994. Liquid-vapor fractionation of oxygen and hydrogen isotopes of water from the freezing to the critical temperature. *Geochim Cosmochim Acta*, 58, 3425-3437. https://doi.org/10.1016/0016-7037(94)90096-5.

IAEA, 1981. Stable isotope hydrology. Deuterium and oxygen-18 in the water cycle. Technical reports series no.201, *Earth-Science Reviews*. Vienna. https://doi.org/10.1016/0012-8252(83)90069-7.

IAEA/WMO, 2015. Global Network of Isotopes in Precipitation. The GNIP Database. Accessible at: https://nucleus.iaea.org/wiser.

Intergovernmental Panel of Climate Change (IPCC), 2021. Climate Change 2021: The Physical Sciences Basis Contribution of Working Group I to the Sixth Assessment Report of the Intergovernmental Panel on Climate Change. *Cambridge University Press*, Cambridge. https://doi.org/10.1017/9781009157896.

Kebede, S., Ayenew, T., Umer, M., 2001. Application of isotope and water balance approaches for the study of the hydrogeological regime of the Bishoftu crater lakes, Ethiopia. *Ethiop. J. Sci*, 24, 151-166. https://doi.org/10.4314/sinet.v24i2.18183.

Kebede, S., Travi, Y., Rozanski, K., 2009. The $\delta^{18}O$ and $\delta^{2}H$ enrichment of Ethiopian lakes. *J. Hydrol.*, 365, 173-182. https://doi.org/10.1016/j.jhydrol.2008.11.027.

Kershaw, G.G.L., Wolfe, B.B., English, M.C., 2022. Characterizing seasonal differences in hydrological flow paths and source water contributions to alpine tundra streamflow. *Hydrol. Processes*, 36. https://doi.org/10.1002/hyp.14775.

MacDonald, L.A., Turner, K.W., McDonald, I., Kay, M.L., Hall, R.I., Wolfe, B.B., 2021. Isotopic evidence of increasing water abundance and lake hydrological change in Old Crow Flats,

Yukon, Canada. *Environ. Res. Lett.*, 16, 124024. https://doi.org/10.1088/1748-9326/ac3533.

MacDonald, L.A., Wolfe, B.B., Turner, K.W., Anderson, L., Arp, C.D., Birks, S.J., Bouchard, F., Edwards, T.W.D., Farquharson, N., Hall, R.I., McDonald, I., Narancic, B., Ouimet, C., Pienitz, R., Tondu, J., White, H., 2017. A synthesis of thermokarst lake water balance in high-latitude regions of North America from isotope tracers. *Arct. Sci.*, 3, 118-149. https://doi.org/10.1139/as-2016-0019.

Mikisew Cree First Nation (MCFN), 2014. Petition to the World Heritage Committee requesting inclusion of Wood Buffalo National Park on the list of World Heritage in danger. Accessible at https://cpawsnab.org/wp-content/uploads/2018/03/Mikisew_Petition_respecting_UNESCO_Site_256_-_December_8_2014.pdf.

Neary, L.K., Remmer, C.R., Krist, J., Wolfe, B.B., Hall, R.I., 2021. A new lake classification scheme for the Peace-Athabasca Delta (Canada) characterizes hydrological processes that cause lake-level variation. *J. Hydrol.: Reg. Stud.*, 38, 100948. https://doi.org/10.1016/j.ejrh.2021.100948.

Neary, L.K., Remmer, C.R., Owca, T.J., Girard, C.A.M., Kay, M. L., Wiklund, J.A., Imran, A., Hall, R.I., Wolfe, B.B., 2023. A framework for integrated monitoring of status and trends in water balance, water chemistry and contaminant enrichment for lakes across a northern dynamic freshwater delta. EarthArXiv (preprint) https://doi.org/10.31223/X5MH4P.

Prowse, T.D., Conly, F.M., 1998. Effects of climatic variability and flow regulation on ice-jam flooding of a northern delta. *Hyrol. Processes*, 12, 1589-1610. https://doi.org/10.1002/(SICI)1099-1085(199808/09)12:10/11<1589::AID-HYP683>3.0.CO;2-G.

Prowse, T.D., Furgal, C., Wrona, F.T., Reist, J.D., 2009. Implications of climate change for northern Canada: freshwater, marine, and terrestrial ecosystems. *Ambio*, 38, 282-289. https://www.jstor.org/stable/25515856.

Remmer, C.R., Klemt, W.H., Wolfe, B.B., Hall, R.I., 2018. Inconsequential effects of flooding in 2014 on lakes in the Peace-Athabasca Delta (Canada) due to long-term drying. *Limnol. Oceanogr.*, 63, 1502-1518. https://doi.org/10.1002/lno.10787.

Remmer, C.R., Neary, L.K., Kay, M.L., Wolfe, B.B., Hall, R.I., 2020a. Multi-year isoscapes of lake water balances across a dynamic northern freshwater delta. *Environ. Res. Lett.*, 15, 104066. https://doi.org/10.1088/1748-9326/abb267.

Remmer, C.R., Owca, T., Neary, L., Wiklund, J.A., Kay, M., Wolfe, B.B., Hall, R.I., 2020b. Delineating extent and magnitude of river flooding to lakes across a northern delta using water isotope tracers. *Hydrol. Processes*, 34, 303-320. https://doi.org/10.1002/hyp.13585.

Rozanski, K., Araguás-Araguás, L., Gonfiantini, R., 1993. Isotopic Patterns in Modern Global Precipitation, in: Swart, P.K., Lohmann, K.C., Mckenzie, J., Savin, S. (Eds.), Climate Change in Continental Isotopic Records. *American Geophysical Union.* https://doi.org/10.1029/gm078p0001.

St. Amour, N.A., Gibson, J.J., Edwards, T.W.D., Prowse, T.D., Pietroniro, A., 2005. Isotopic time-series partitioning of streamflow components in wetland-dominated catchments, lower Liard River basin, Northwest Territories, Canada. *Hydrol. Processes*, 19, 3357-3381. https://doi.org/10.1002/hyp.5975.

Sun, Z., Zhu, G., Zhang, Z., Xu, Y., Yong, L., Wan, Q., Ma, H., Sang, L., Liu, Y., 2021. Identifying surface water evaporation loss of inland river basin based on evaporation enrichment model. *Hydrol. Processes*, 35. https://doi.org/10.1002/hyp.14093.

Thornthwaite, C.W., 1948. An Approach toward a Rational Classification of Climate. *Geogr. Rev.*, 38, 55-94. https://doi.org/10.2307/210739.

Timoney, K.P., 2013. The Peace-Athabasca Delta: Portrait of a dynamic ecosystem, The Peace-Athabasca Delta: Portrait of a Dynamic Ecosystem. *The University of Alberta Press*, Edmonton.

Tondu, J.M.E., Turner, K.W., Wolfe, B.B., Hall, R.I., Edwards, T.W.D., McDonald, I., 2013. Using water isotope tracers to develop the hydrological component of a long-term aquatic ecosystem monitoring program for a northern lake-rich landscape. *Arct. Antarct. Alp. Res.*, 45, 594-614. https://doi.org/10.1657/1938-4246-45.4.594.

Turner, K.W., Wolfe, B.B., Edwards, T.W.D., 2010. Characterizing the role of hydrological processes on lake water balances in the Old Crow Flats, Yukon Territory, Canada, using water isotope tracers. *J. Hydrol.*, 386, 103-117. https://doi.org/10.1016/j.jhydrol.2010.03.012.

Turner, K.W., Wolfe, B.B., Edwards, T.W.D., Lantz, T.C., Hall, R.I., Larocque, G., 2014. Controls on water balance of shallow thermokarst lakes and their relations with catchment characteristics: a multi-year, landscape-scale assessment based on water isotope tracers and remote sensing in Old Crow Flats, Yukon (Canada). *Global Change Biol.*, 20, 1585-1603. https://doi.org/10.1111/gcb.12465.

Wan, C., Gibson, J.J., Peters, D.L., 2020. Isotopic constraints on water balance of tundra lakes and watersheds affected by permafrost degradation, Mackenzie Delta region, Northwest Territories, Canada. *Sci. Total Environ.*, 731, 139176. https://doi.org/10.1016/j.scitotenv.2020.139176.

Wang, Y., Du, R., Cao, X., Yu, H., Xu, Y., Yu, Y., Peng, J., 2023. Evaporation dominates the loss of plateau lake in Southwest China using water isotope balance assessment. *Sci. Total Environ.,* 873, 162415. https://doi.org/10.1016/j.scitotenv.2023.162415.

Welhan, J.A., Fritz, P., 1977. Evaporation pan isotopic behavior as an index of isotopic evaporation conditions. *Geochim Cosmochim Acta*, 41, 682-686. https://doi.org/10.1016/0016-7037(77)90306-4.

WHC/IUCN, 2017. Reactive monitoring mission to Wood Buffalo National Park, Canada; mission report March 2017. *United Nations Educational, Scientific and Cultural Organization.* https://whc.unesco.org/en/documents/156893.

WHC/IUCN, 2022. Reactive monitoring mission to Wood Buffalo National Park, Canada; mission report August 2022. *United Nations Educational, Scientific and Cultural Organization.* https://whc.unesco.org/en/documents/200340.

Wilcox, E.J., Wolfe, B.B., Marsh, P., 2022. Assessing the influence of lake and watershed attributes on snowmelt bypass at thermokarst lakes. *Hydrol. Earth Syst. Sci.*, 26. https://doi.org/10.5194/hess-26-6185-2022.

Wolfe, B. B., Hall, R. I., Edwards, T. W. D., Johnston, J. W., 2012. Developing temporal hydroecological perspectives to inform stewardship of a northern floodplain landscape subject to multiple stressors: paleolimnological investigations of the Peace–Athabasca Delta. *Environ. Rev.*, 20, 191-210. https://doi.org/10.1139/a2012-008.

Wolfe, B.B., Hall, R.I., Edwards, T.W.D., Vardy, S.R., Falcone, M.D., Sjunneskog, C., Sylvestre, F., McGowan, S., Leavitt, P.R., van Driel, P., 2008. Hydroecological responses of the Athabasca Delta, Canada, to changes in river flow and climate during the 20th century. *Ecohydrology*, 1, 131-148. https://doi.org/10.1002/eco.13.

Wolfe, B.B., Karst-Riddoch, T.L., Hall, R.I., Edwards, T.W.D., English, M.C., Palmini, R., McGowan, S., Leavitt, P.R., Vardy, S.R., 2007. Classification of hydrological regimes of northern floodplain basins (Peace-Athabasca Delta, Canada) from analysis of stable isotopes ($\delta^{18}O$, $\delta^{2}H$) and water chemistry. *Hydrol. Processes*, 21, 151-168. https://doi.org/10.1002/hyp.6229.

Wolfe, B.B., Karst-Riddoch, T.L., Vardy, S.R., Falcone, M.D., Hall, R.I., Edwards, T.W.D., 2005. Impacts of climate and river flooding on the hydro-ecology of a floodplain basin, Peace-Athabasca Delta, Canada since A.D. 1700. *Quat. Res.*, 64, 147-162. https://doi.org/10.1016/j.yqres.2005.05.001.

Wood Buffalo National Park (WBNP), 2019. World Heritage Site Action Plan. *Parks Canada*. https://parks.canada.ca/pn-np/nt/woodbuffalo/info/action.

Yi, Y., Brock, B.E., Falcone, M.D., Wolfe, B.B., Edwards, T.W.D., 2008. A coupled isotope tracer method to characterize input water to lakes. *J. Hydrol.*, 350, 1-13. https://doi.org/10.1016/j.jhydrol.2007.11.008.

Zaitchik, B.F., Rodell, M., Biasutti, M., Seneviratne, S.I., 2023. Wetting and drying trends under climate change. *Nat. Water*, 1, 502-513. https://doi.org/10.1038/s44221-023-00073-w.

Chapter 3 | Overlooked and underrated: Snowmelt runoff rivals influence of river floodwaters on lake-level rise at a cold region freshwater delta

3.1 Introduction

Shallow water bodies are typically abundant in cold regions, where they provide important habitat for wildlife and support socio-economic and cultural sustainability of communities (Lehner and Döll, 2004; Schindler and Smol, 2006; Rautio et al., 2011; Smol, 2016; Medeiros et al., 2017). Across broad swaths of northwestern North America where landscapes are not prone to river flooding, snowmelt runoff is well-recognized as an influential source of freshwater for maintaining lake water balances, because snowfall constitutes 40-80% of total annual precipitation (Woo, 1980; Woo et al., 1981; Roulet and Woo, 1988; Rouse et al., 1997) and annual evaporation often exceeds precipitation (Rovansek et al., 1996; Bowling et al., 2003; Mielko and Woo, 2006; Schindler and Smol, 2006). During two consecutive springs at a small lake in the High Arctic (Northwest Territories, Canada), for instance, snowmelt runoff was observed to raise water levels by 0.5 m and 1.1 m (Woo, 1980). Using remote sensing data, snowmelt input was estimated to have increased maximum surface water extent of ponds and wetlands by 175-338% relative to mid-summer in the Putuligayuk River watershed of northern Alaska (Bowling et al., 2003). A study at Old Crow Flats (Yukon, Canada) and Hudson Bay Lowlands (Manitoba, Canada) identified that shallow lakes in low-relief catchments with sparse tundra vegetation are vulnerable to desiccation under conditions of low snowmelt runoff (Bouchard et al., 2013). In the Northern Great Plains, snowfall constitutes only about one-third of total annual precipitation yet contributes more than 80% of annual surface runoff to waterbodies and groundwater (Shjeflo, 1968; Gray et al., 1970; Granger et al., 1984; Little et al., 2007). Annual water levels in the Prairie Potholes region typically peak during the freshet when frozen soils, relatively cold air temperatures, and high humidity combine to reduce infiltration and evaporation and effectively deliver snowmelt via surface runoff (Conly and van der Kamp, 2001; van der Kamp et al., 2003). Snowmelt runoff is important for some waterfowl (e.g., mallards), as increase of water levels in spring enhances breeding activities (Krapu et al., 1983) and food supply (Swanson et al., 1985). It is well known that climate change threatens the persistence of shallow waterbodies by reducing the thickness, water content, duration and spatial distribution of snow cover (Barnett et al., 2005; Adam et al., 2009; Prowse et al. 2006a, 2009; Musselman et al., 2017).

Despite recognition of snowmelt as important for maintaining water levels in cold regions, research on shallow lakes in floodplains of northwestern North America has, understandably, focused mainly on fluvial processes because changes to the flood regime strongly influence lake water balances (Prowse et al., 2006a,b, 2009, 2011; Peters et al., 2015; Wrona et al., 2016). Hydrological studies in the Mackenzie River Delta and Slave River Delta in the Northwest Territories of Canada, for example, have historically focused on understanding the role of ice-jam induced river flooding on lake water balances (Marsh and Lesack, 1996; Goulding et al., 2009a,b; Brock et al., 2008, 2010; Beltaos et al., 2013; Zhang et al., 2017) and their relations with river discharge characteristics (Bigras, 1990; Brock et al., 2008, 2009; Marsh et al., 2009). These hydrological themes have also been studied intensely at the Peace-Athabasca Delta (PAD; Figure 3.1a), a lake-rich floodplain in northeastern Alberta that drains the headwaters of the Mackenzie River Basin. The PAD is designated as a Ramsar Wetland of International Importance and 80% of it is protected within Wood Buffalo National Park (WBNP), where it contributes importantly to the park's UNESCO World Heritage status (Timoney, 2013). Widespread flooding of the PAD typically occurs during the freshet when ice-jams form at a time of high river discharge (PADPG, 1973; PADTS, 1996; Prowse and Conly, 2002; Peters et al., 2006b). Previous scientific studies have claimed that ice-jam flooding is the primary, or sometimes, the only mechanism responsible for replenishing the delta's perched basins (i.e., restricted- and closed-drainage lakes and wetlands; Pietroniro et al., 1999) which are abundant across the slightly more elevated areas of the relatively flat fluvio-deltaic terrain (Prowse and Lalonde, 1996; Prowse and Conly, 1998, 2002; Wolfe et al., 2005; Peters et al., 2006a,b; MCFN, 2014; Beltaos and Bonsal, 2021; Beltaos, 2023). Reduction in the frequency and magnitude of ice-jam floods, variably associated with climate change (Wolfe et al., 2006, 2012, 2020; Beltaos and Bonsal, 2021; Lamontagne et al., 2021; Kay et al., 2024) and upstream hydroelectric regulation of Peace River flow (PADPG, 1973; Beltaos, 2014, 2018), has coincided with drawdown of lake levels across the delta (MCFN, 2014; IEC, 2018; WHC/IUCN, 2017, 2022). Growing concern for lake drying contributed to a petition by the Mikisew Cree First Nation (MCFN) to UNESCO to enlist WBNP as 'World Heritage in Danger' (MCFN, 2014), which prompted national (IEC, 2018) and international investigations (WHC/IUCN, 2017, 2022) and development of a federal Action Plan for WBNP (WBNP, 2019). The most recent international investigation found most threats identified in the petition remain valid, "in particular as a result of

changes to the hydrology of the PAD exacerbated by the impacts of climate change and the impacts of the industrial developments adjacent to the property" (WHC/IUCN, 2022, p. 63).

While much focus at the PAD has been on consequences of changes to the flood regime, far less scientific attention has been paid to the importance of snowmelt input on the water balance of shallow lakes. Thick snowpack and rapid generation of snowmelt runoff in upstream regions of the Peace and Athabasca river watersheds are well recognized as conditions that generate high river flows and ice-jam flooding (Beltaos et al., 2006; Peters and Prowse, 2006; Prowse et al., 2006a; Romolo et al., 2006; Jasek, 2019; Lamontagne et al., 2021; Emmer et al., 2021; Nafziger et al., 2021), but the role of snowmelt runoff within the delta on lake water balance and water-levels remains poorly characterized. Prowse et al. (1996), for example, considered the importance of snowmelt runoff, but only in relation to contributions to Peace River flow from the Smoky River, a key upstream 'trigger tributary', for generation of river discharge that triggers and enhances ice-jam flooding at the PAD. A water-balance model applied to perched lakes by Peters et al. (2006a) initially excluded snowmelt runoff as it was assumed to be a minor input source due to the delta's low topographic relief and typically small lake catchments. They acknowledged, however, that modelling of water levels could be improved by incorporating snowmelt runoff, especially in the northeastern region of the PAD where greater relief may generate more substantial snowmelt runoff. More recently, a study by Remmer et al. (2020a) recognized snowmelt as a contributor to lake-water balances and used water isotope tracers to delineate the spatial extent of floodwaters and estimate the proportion of input from floodwater and precipitation (snowmelt and rainfall) to flooded lakes after widespread ice-jam flooding in 2018. However, when reporting results of a 5-year-long study that demonstrated substantial spatial and temporal variability of lake water balances across the PAD, Remmer et al. (2020b) provide only brief mention of the role of snowmelt.

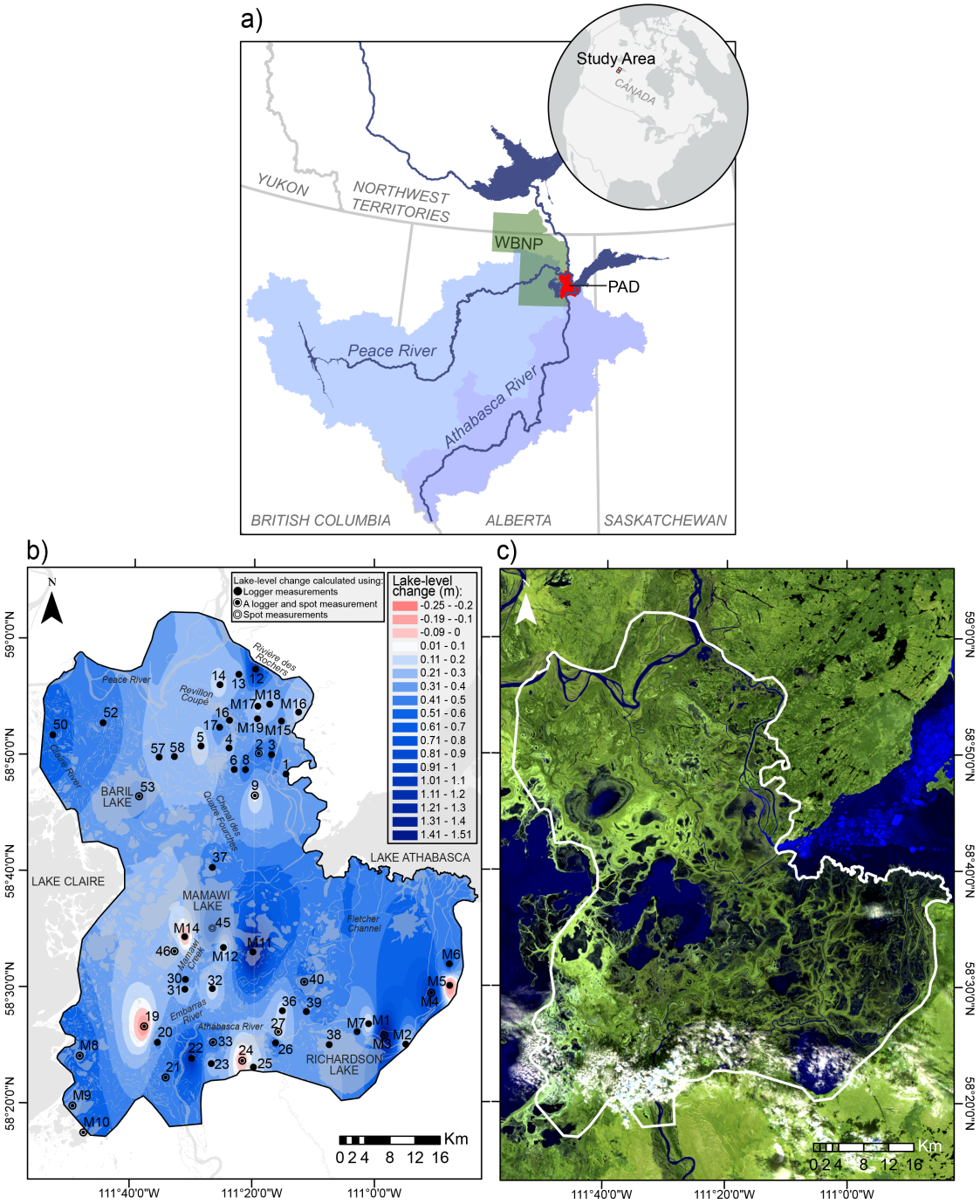


Figure 3.1: Maps displaying **a)** location of the Peace-Athabasca Delta (PAD) within Wood Buffalo National Park (WBNP) in northern Alberta, Canada, and the watersheds of the Peace (light blue) and Athabasca (light purple) rivers; **b)** spatial interpolation (by inverse distance weighting; Moran's I = -0.15, p = 0.15) of the magnitude of lake-level change (m) between September 2019 and May 2020 for 58 lakes where measurements were obtained using water-depth loggers and/or spot depth measurements; **c)** water extent (dark blue) in spring 2020 based on false colour satellite imagery (Sentinel-2) obtained on May 24 (from https://apps.sentinel-hub.com/eo-browser/).

Following widespread ice-jam flooding of lakes in spring of 2020, opportunity emerged to elucidate the relative contributions of snowmelt and floodwater to lake-level rise in the PAD. Routine examination of hourly water-depth measurements and remotely sensed data revealed that lake levels rose across much of the delta during the freshet, including in areas that were not flooded (Figure 3.1b,c; Desrochers et al., 2023; Neary et al., 2024). Flyover observations identified that ice-jams along the Athabasca River triggered extensive flooding in the central to eastern portions of the Athabasca sector (Timoney, 2020; Nafziger et al., 2021). Along the Peace River, ice jams formed upstream of the PAD, which delayed delivery of elevated discharge until after the river ice had decayed thermally and prevented widespread flooding of perched lakes in the Peace sector (Timoney, 2020; Beltaos and Carter, 2021; Emmer et al., 2021; Lamontagne et al., 2021). Notably, observations of marked lake-level rise at many of the non-flooded lakes prompted us to investigate if input of snowmelt was an important contributor to lake-level rise, given that higher-than-normal snowpack occurred across the Peace and Athabasca river basins during March and April 2020 (Emmer et al., 2021; Nafziger et al., 2021).

Here, our goal is to quantify the contribution of snowmelt input to lake-level rise in the PAD during spring 2020 and compare it to the contribution from river floodwater. We combine information obtained from measurements of water isotope composition and lake depth at more than 50 well-dispersed lakes that span the delta's broad hydrological gradients to 1) identify the lakes that did and did not receive input of river floodwater, and 2) quantify the magnitude of lake-level rise attributable to input of snowmelt and floodwater. We determined the importance of snowmelt input by comparing the lake-level rise at non-flooded lakes due to input of snowmelt versus the lake-level rise at flooded lakes due to floodwater, and the lake-level rise at flooded lakes due to input of snowmelt versus floodwater. To partition the roles of snowmelt versus Peace or Athabasca river floodwaters on water-level rise at the flooded lakes, we applied two binary mixing models to estimates of input water isotope compositions. We also use geospatial analyses to identify landscape features within the delta that contribute to spatial variation in lake-level rise attributable to input of snowmelt and floodwater. Using meteorological records, we assess how typical the snow water equivalent and melt rate in spring of 2020 have been relative to the past 61 years (since 1963) for which meteorological records exist. Findings challenge the long-held scientific notion that ice-jam floods are the sole mechanism capable of replenishing perched basins

at the PAD and perhaps in other cold region floodplains, but also suggest that declining snowmelt influence has contributed to reduction in freshwater abundance across the PAD.

3.2 Methods

3.2.1 Study Area

The PAD is located in the Prairie-Boreal transition region of the Boreal Plains ecozone and within the Slave River Lowlands ecoregion, a northern extension of the Great Plains (Ecological Stratification Working Group, 1995). The ecoregion is described as having a subhumid mid-Boreal climate where long, cold winters are followed by short, cool summers (Ecological Stratification Working Group, 1995). Based on the 1981-2010 climate normals at Fort Chipewyan, Alberta (Climate Station ID: 3072658), located at the eastern margin of the PAD, mean annual air temperature is -1.5 °C and annual precipitation is 365.7 mm. Estimated annual evaporation is about 450 mm, which typically exceeds annual precipitation (Prowse and Demuth, 1996). The delta is considered an extralimital occurrence of prairie-wetland, as the soils (mainly imperfectly to poorly drained Regosols and Gleysols) and vegetation are characteristic of the Prairie and Hemiboreal regions rather than Boreal regions (Timoney, 2002, 2013).

The PAD is among the world's largest inland freshwater deltas (~6000 km^2) and is fed primally by the Athabasca and Peace rivers (Peters et al., 2006a; Timoney, 2013). The low-lying fluvio-deltaic terrain supports an abundance of productive shallow lakes and wetlands (Timoney, 2013; Figure 3.1, 3.2). Two distinct sectors with varying topography and vegetation cover have been recognized (Figure 3.2). The Peace sector, here defined as areas north of Jemis Lake ('PAD 37'; Figure 3.1, 3.2), is a relic delta with numerous bedrock inliers and greater topographic relief (>225 masl) that receives Peace River floodwaters when episodic ice-jams cause southward flow reversals into distributary channels and promote flooding of perched lakes (NRBS, 1996; Timoney, 2002; Peters, 2006a; Wolfe et al., 2007; Neary et al., 2024). Dense coniferous forest and shrub vegetation occur across northeastern areas of the Peace sector, where the bedrock inliers are located, and extensive northwestern areas where flooding has declined in recent decades (Figure 3.2b; Timoney, 2013; Kay et al., 2024). The Athabasca River flows through the lower relief Athabasca sector (the area south of Jemis Lake), where it maintains an active delta characterized

by frequent river flooding during spring ice-jam flood events and high discharge episodes during the open-water season (Wolfe et al., 2008; Peters, 2013; Remmer et al., 2020b; Neary et al., 2021a, 2024). Unlike the Peace sector, few bedrock inliers occur in the Athabasca sector. The flat terrain of the Athabasca sector supports sparser terrestrial vegetation, where trees are limited largely to narrow river levees and a slightly elevated area in the south-central area east of Lake Claire (Figure 3.2b). Shrubs and trees are almost completely absent from the low elevation, low-relief terrain that occupies much of the central portion of the PAD where large open-drainage lakes occur.

Perched lake water levels tend to draw down during the open-water season (May – September) due to evaporation, or they remain stable if input from precipitation to the lake and local catchment offsets losses by evaporation (Neary et al., 2021a). In the Athabasca sector, high river discharge during the open-water season can cause sharp rise or gradual rise of lake levels due to direct input from river floodwaters or input from adjacent open-drainage lakes when their water levels overtop their sills, respectively (Neary et al., 2021a). Groundwater influence on lake water balance is considered negligible across much of the PAD because of the low hydraulic conductivity of the underlying flood-deposited fine-grained sediment, discontinuous permafrost, and low horizontal gradients between lakes (Nielsen, 1972; Prowse et al., 1996; Wolfe et al., 2007).

3.2.2 Meteorological conditions prior to and during the 2020 freshet

Mean monthly air temperatures for March, April, and May of 2020 at Fort Chipewyan, Alberta (Climate Station ID: 3072659) were >1 standard deviation below the 1981-2010 climate normal (Figure 3.3a). The maximum snow water equivalent (SWE; 80.4 mm), attained on April 22 was more than 10 mm higher than the median for the long-term daily SWE based on modelling of measurements at 10 adjacent townships during 1991-2020 obtained from the Alberta Climate Information Service (https://www.acis.alberta.ca/acis/; Figure 3.3b). During the snowfall period (October 1, 2019 – April 15, 2020), strong winds (≥ 20 km/h) were predominantly from the west (WSW to NW) (Figure 3.3c). Snowmelt was rapid in 2020, with an average melt rate of 10.1 mm/day during an 8-day span when the snow cover completely melted.

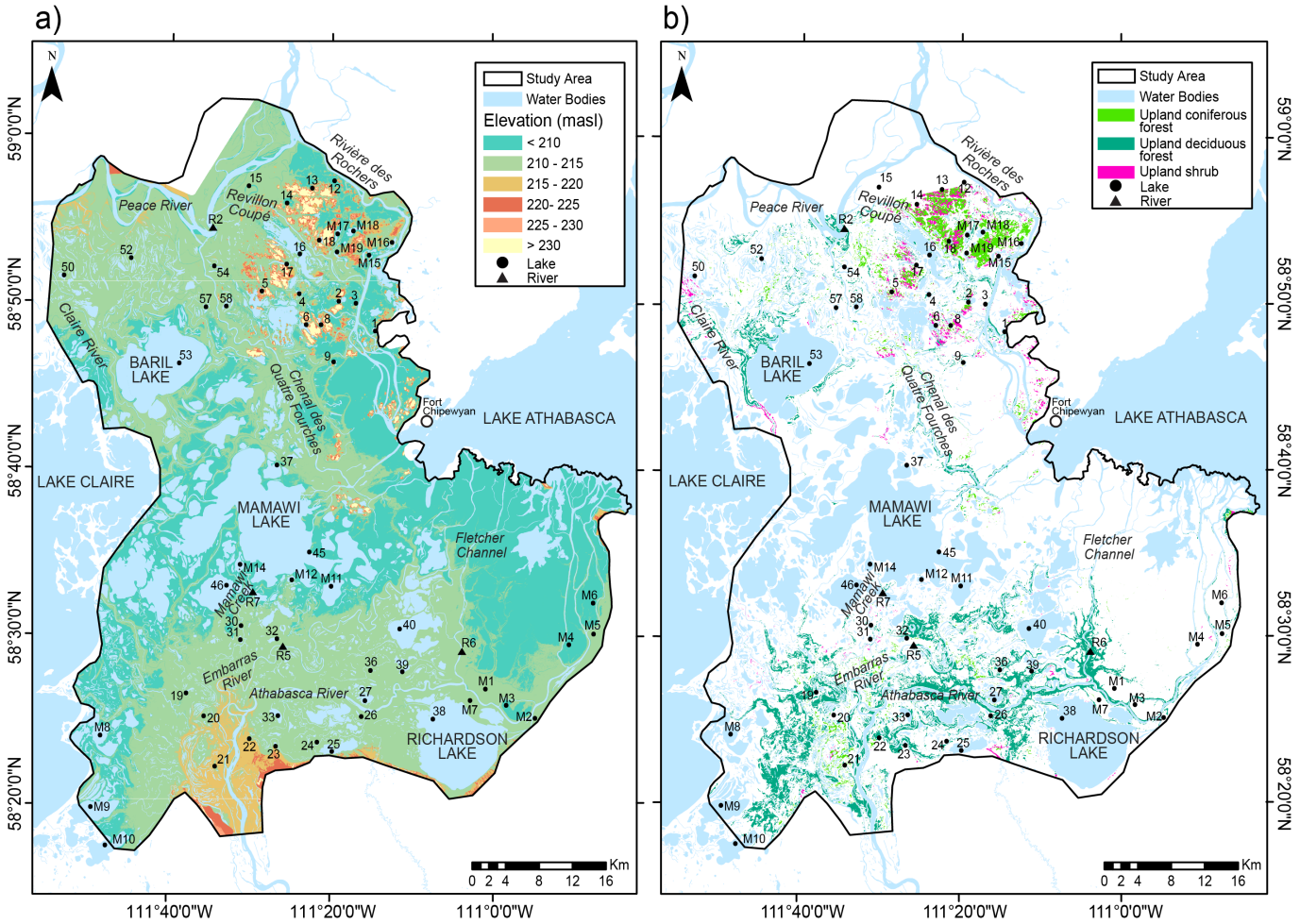


Figure 3.2: Maps displaying **a)** variation of ground elevation (masl) and **b)** vegetation cover across the PAD. Panels a) and b) show the locations of the 59 lakes (black circles) and 4 river sites (black triangles) sampled for water isotope composition in May 2020. Water-depth loggers were deployed at these lakes in May through September of 2019 and 2020. High-resolution digital elevation model data (4-m resolution) were sourced from Environment and Climate Change Canada and are accessible at https://open.canada.ca/data/en/dataset/03568324-1a8b-4c00-8650-f5c35f6e0bff. Vegetation data from circa 2017 were sourced from French et al. (2022) and are accessible at https://daac.ornl.gov/.

The spring 2020 isotherm date, which is strongly correlated with the date of ice break-up on shallow lakes (Duguay et al., 2006), was estimated to be April 23 using methods of Bonsal and Prowse (2003). Our field sampling on May 26-28 occurred one month later. A total of 59.0 mm of rainfall was measured between the spring isotherm date of April 23 and the last date of spring sampling on May 28, 2020. Also, 27.4 mm of rainfall were recorded between September 12, 2019, when the water-depth loggers were removed, and October 18, 2019, when temperatures dropped below 0°C and ice-cover likely formed. Thus, a total of 86.4 mm of rainfall may have contributed to lake-level rise in spring of 2020 although, as presented below, the water isotope data indicate snowmelt was the main source of precipitation to enter the lakes.

3.2.3 Field work and laboratory analyses

Water samples were collected by WBNP employees on May 26-28, 2020 from a set of 59 lakes and 4 river sites spanning the Peace sector (26 lakes, 1 river site) and Athabasca sector (33 lakes, 3 river sites) for analysis of oxygen and hydrogen isotope composition, which subsequently were used to identify which lakes flooded and did not flood, and to quantify the input sources. Samples were collected mid-lake or mid-channel at ~10 cm below the water surface from a helicopter with fixed floats and stored in 30 ml high-density polyethylene bottles. Water isotope compositions of the lake and river samples were analyzed at the University of Waterloo – Environmental Isotope Laboratory (UW – EIL) by Off-Axis Integrated Cavity Output Spectroscopy (O-AICOS) via a Los Gatos Research Triple Liquid Water Isotope Analyzer (LGR T-LWIA 45-EP). Isotope compositions are reported as δ-values, representing deviations in per mil (‰) from Vienna Standard Mean Ocean Water (VSMOW), such that $\delta_{sample} = [(R_{sample}/R_{VSMOW}) - 1] \times 10^3$ where R is the $^{18}O/^{16}O$ or $^{2}H/^{1}H$ ratio in the sample and VSMOW, on a scale normalized to values of Standard Light Antarctic Precipitation (-55.5‰ for $\delta^{18}O$; -428‰ for $\delta^{2}H$; Coplen, 1996). Analytical uncertainties are ± 0.2 ‰ for $\delta^{18}O$ and ± 0.8 ‰ for $\delta^{2}H$.

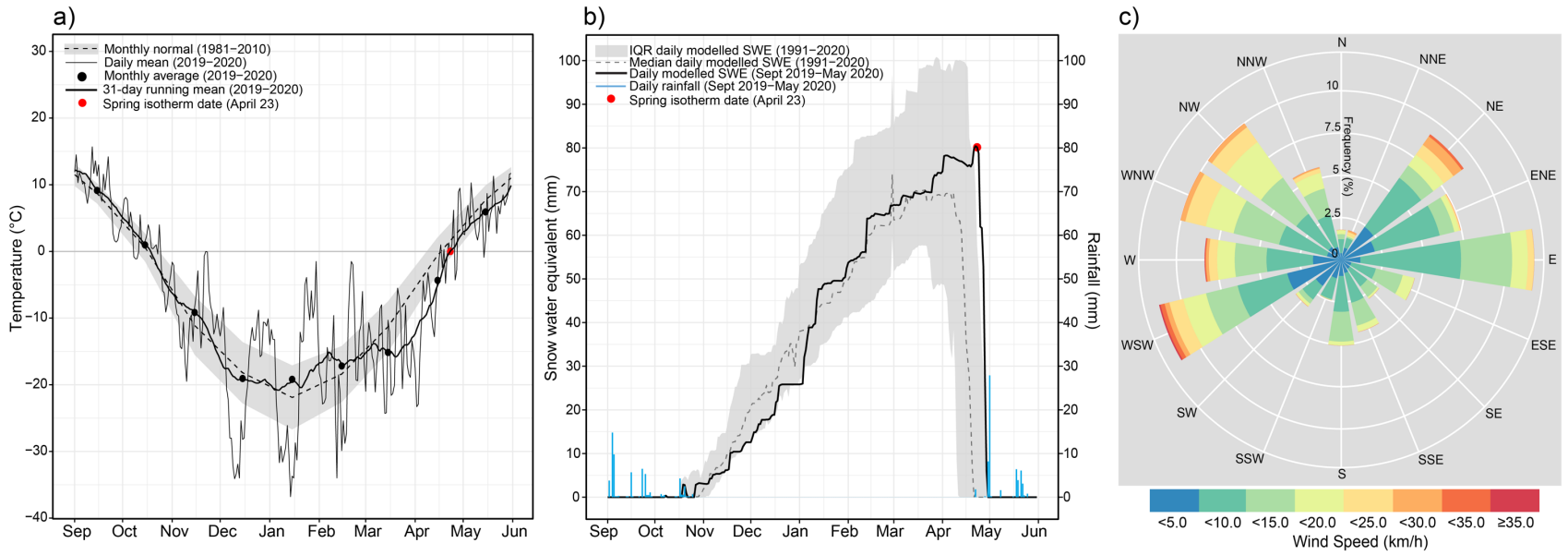


Figure 3.3: Graphs showing temporal variation of meteorological variables between fall of 2019 and spring of 2020. **a)** Air temperature (°C) expressed as daily (thin black line) and monthly means (black circles) recorded at station "Fort Chipewyan RCS" at the Fort Chipewyan airport, Alberta, Canada (Climate ID: 3072659) compared to Climate Normal (1981-2010) for the 31-day running mean (thick black line) and monthly mean (dashed line) and associated variability (1 standard deviation unit; grey band) at station "Fort Chipewyan A" near the airport (Climate ID: 3072658). Spring isotherm date (red circle) is the date when the 31-day running mean is above 0°C. **b)** Daily modelled snow water equivalent (SWE; mm; black line) and daily rainfall (mm; vertical blue bars) between September 1, 2019 and May 31, 2020 compared to the median (dashed line) and interquartile range (grey band) of long-term daily modelled SWE for 1991-2020, with the spring isotherm date (red circle). Daily rainfall data represent precipitation when average daily mean air temperature exceeded 0°C at Fort Chipewyan airport (Climate ID: 3072659). Daily SWE data are averaged from ten townships (T110R07W4, T110R08W4, T112R05W4, T112R07W4, T112R08W4, T112R10W4, T113R05W4, T113R10W4, T115R07W4, T115R08W4) and sourced from Alberta's AgroClimatic Information Service (https://www.alberta.ca/acis-find-historic-climate-data). **c)** Wind rose plot indicating wind direction and speed patterns at 10-m height recorded during the estimated snowfall period (October 1, 2019 – April 15, 2020), at Fort Chipewyan airport (Climate ID: 3072659). The wind rose plot was extracted from Alberta's AgroClimatic Information Service (https://www.acis.alberta.ca/acis/wind-rose.jsp). Temperature and SWE plots were created using the package 'ggplot2' in RStudio (version 2023.03.0+386) using packages lubridate (v.1.9.1; Grolemund and Wickham, 2011), zoo (v.1.8-11; Zeileis and Grothendieck, 2005), and ggplot2 (v.3.4.4; Wickham, 2016).

Specific conductivity (μS/cm) and turbidity (NTU) were measured *in situ* at lakes during spring of 2020 using a handheld multiparameter meter (YSI ProDSS). These measurements provided additional information, beyond the water isotope compositions, to identify if river floodwaters had entered the lakes. Unfortunately, these measurements were not collected from the river sites in May 2020, so we used river values obtained in May 2018, shortly after previous widespread ice-jam flooding occurred (Remmer et al., 2020a).

Water-depth loggers (Onset HOBO pressure transducers; Model U20-001-01, 4-m range, 0.3-cm accuracy) were deployed at a central deep-water area of the 59 lakes between May 13-15 and September 12-14 of 2019, and between May 26-28 and September 15-16 of 2020. The geographic coordinates were recorded using a handheld GPS (Garmin GPSMAP 60CSx) to ensure that the paired depth measurements at each lake were recorded at the same location. The loggers were set to record hourly water pressure (psi) and temperature (°C) and attached at the bottom of a line connecting an anchor (rock filled sock) to a wooden float. During both years, a single logger was also deployed in the air at the field house or WBNP office in Fort Chipewyan to measure variation in local atmospheric pressure and air temperature, and to convert the pressure readings (psi) at the lakes to water depth (m) using the Barometric Compensation Assistant in the HOBOware Pro software program (version 3.7.23). Spot depth measurements were also recorded *in situ* using a hand-held sonar or tape measure, which were used if a logger was not retrieved in September 2019 or 2020. The difference in lake depth between September 12, 2019 (last date of measurement before the 2020 freshet) and May 28, 2020 (last date of deployment after the 2020 freshet) is used to quantify the magnitude and direction of lake-level change after the freshet and ice-jam flooding had occurred in 2020.

3.2.4 Data analyses

3.2.4.1 Analysis of water isotope composition

Lake water isotope compositions are typically interpreted in '$\delta^{18}O$-$\delta^{2}H$ space' (i.e., cross-plots) in reference to an isotope framework consisting of linear relations and key parameters. Regional isotope composition of precipitation is captured by the Local Meteoric Water Line (LMWL), which serves as a function of isotope compositions of local input sources (i.e., snowmelt,

rainfall, river floodwaters) supplied to surface waters (Edwards et al., 2004). Surface waters within a region undergoing evaporation will deviate from the LMWL and cluster along a Local Evaporation Line (LEL), which is controlled by primarily relative humidity, temperature, and the isotope composition of atmospheric moisture (δ_A; Edwards et al., 2004). Key isotope parameters along the LEL include the average annual isotope composition of precipitation (δ_P), the isotope composition of a terminal basin at hydrological steady state, where evaporation equals inflow (δ_{SSL}), and the theoretical limiting isotope composition of a desiccating water body (δ^*). The predicted LEL for 2020 at the PAD is defined by $\delta^2H = 4.3\delta^{18}O - 62.85$ (Imran et al., 2024 [Chapter 2]). Displacement of lake water isotope data along the LEL can provide information about the degree of evaporation, whereas the offset above or below the LEL can reflect mixing with other input sources such as rainfall or snowmelt, respectively, and/or river floodwaters.

3.2.4.2 Identification of flooded lakes

Following protocols developed at the PAD by Remmer et al. (2020a,b), the flood status (flooded vs. non-flooded) of each lake sampled in May 2020 was determined by comparing the isotope compositions and *in situ* measurements of specific conductivity (µS/cm) and turbidity (NTU) in lake water with those in river water, supplemented by field observations (Appendix 2 Table A2.1). Lakes were designated as flooded if 1) the lake water isotope composition was similar to or overlapped with river water isotope compositions in May 2020 (Peace River: $\delta^{18}O$ = -18.82‰, δ^2H = -145.02‰; Athabasca River: $\delta^{18}O$ = -17.84‰, δ^2H = -138.21‰), 2) specific conductivity measurements in May 2020 were close to the range of river values recorded in spring 2018 (Peace sector rivers: 164.5 – 176.5 µS/cm; Athabasca sector rivers: 179.5 – 188.5 µS/cm; Remmer et al., 2020a), and 3) observations recorded in field notes during sampling in May 2020 are consistent with evidence of recent floodwater input (i.e., lake water colour resembled the nearest river, water was turbid with suspended river sediment, lake margins were flooded) or supported by high *in situ* turbidity measurements and daily flyover observations during the spring ice-breakup (Timoney, 2020). For 1), the isotope composition of the Athabasca River was estimated using the isotope compositions of its distributary channels (Embarras River, Mamawi Creek, Fletcher Channel) because the Athabasca River was not sampled in May 2020.

3.2.4.3 Quantifying the proportion of input from snowmelt and river floodwater to the flooded lakes

For the lakes classified as flooded in 2020, two binary mixing models, first developed by Remmer et al. (2020a), were employed to partition the proportion of input from snowmelt and Peace or Athabasca river floodwater (Figure 3.4). For this, we estimated the isotope composition of input water (δ_I) using the coupled isotope tracer approach of Yi et al. (2008), which assumes water isotope compositions of all lakes that experience similar atmospheric conditions and, in the absence of water replenishment from input sources, will undergo evaporation and converge at δ^* (i.e., the maximum isotope composition of a lake approaching desiccation). The estimated δ_I value for each flooded lake was constrained to one of two Meteoric Water Line segments (MWLs) (i.e., snow – Peace River; snow – Athabasca River), following Remmer et al. (2020a). The position of δ_I on one of the two MWLs was determined by the intersection of a lake-specific evaporation line extending between the isotope of composition of the lake water (δ_L) and the isotope composition of the evaporated vapour (δ_E). δ_E was determined for each flooded lake using the following equation (Craig and Gordon, 1965) and isotope framework parameters reported in Imran et al. (2024 [Chapter 2]; also see Appendix 2 Table A2.2):

$$\delta_E = [(\delta_L - \varepsilon^*)/\alpha^* - h\delta_{As} - \varepsilon_K]/(1 - h + \varepsilon_K) \quad (1)$$

The snow end-member isotope composition ($\delta^{18}O$ = -26.02‰, δ^2H = -199.0%) on the MWL segments is estimated based on modelled data from the Online Isotopes in Precipitation Calculator (OIPC; Bowen and Revenaugh, 2003; IAEA/WMO, 2015; Bowen, 2016), as reported in Remmer et al. (2020a), and the river end-members are based on the measured isotope composition of the Peace River ($\delta^{18}O$ = -18.82‰, δ^2H = -145.02‰) and estimated isotope composition of the Athabasca River ($\delta^{18}O$ = -17.84‰, δ^2H = -138.21‰), as reported above. For flooded lakes, the percent snow input was calculated using binary mixing model equations for the Peace sector,

$$\%\ snow\ input = \frac{\delta_I - \delta_{Peace\ River}}{\delta_{snow} - \delta_{Peace\ River}} \quad (2)$$

or the Athabasca sector,

$$\% \; snow \; input = \frac{\delta_I - \delta_{Athabasca\ River}}{\delta_{snow} - \delta_{Athabasca\ River}} \quad (3)$$

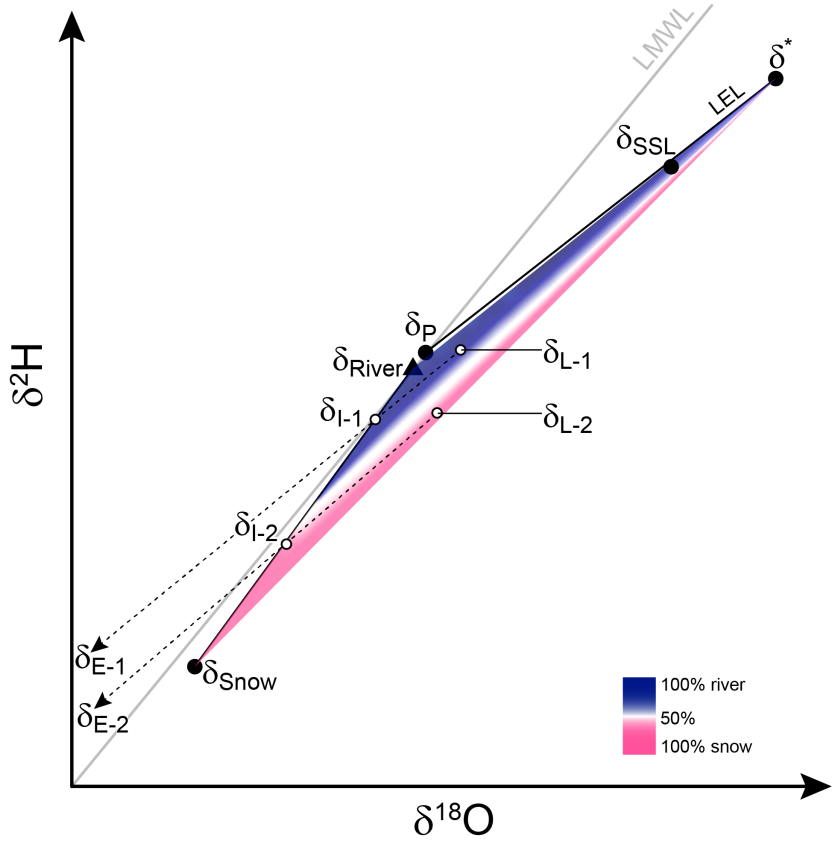


Figure 3.4: Schematic $\delta^{18}O$-$\delta^{2}H$ diagram identifying key reference lines and isotope parameters used in isotope mass-balance studies alongside isotope compositions of two hypothetical lakes; one that received primarily river floodwaters ($\delta_{L\text{-}1}$) and one that received primarily snowmelt ($\delta_{L\text{-}2}$). The three linear relations displayed are: 1) the Local Meteoric Water Line (LMWL), which represents the region-specific distribution of the isotope composition of precipitation (rain, snow), 2) the Local Evaporation Line (LEL), which represents the evaporative trajectory of lake surface water (δ_L) fed by waters of mean annual isotope composition of precipitation (δ_P), and 3) a river – snow Meteoric Water Line segment between the isotope composition of river water (δ_{River}) and snow (δ_{Snow}), which defines the potential range of the isotope composition of input water (δ_I) for lakes fed by mixtures of river water and snowmelt, as determined by the intersection of a lake-specific evaporation line between the isotope composition of evaporated vapour (δ_E) and δ_L, based on Remmer et al. (2020a) and the coupled-isotope tracer approach of Yi et al. (2008). Shaded regions in the polygon represent zones where δ_I will primarily reflect inputs of river floodwaters (blue), snowmelt (pink), or a 50% mixture (white) based on the position of δ_L in $\delta^{18}O$-$\delta^{2}H$ space. Key reference parameters used in isotope mass-balance studies include δ_{SSL}, which represents the special case of a terminal (i.e., closed-drainage) basin in isotopic and hydrologic steady-state (evaporation = inflow) fed by δ_P, and δ^* which represents the theoretical limiting isotope composition of a desiccating water body.

3.2.4.4 Determination of lake-level change

The water-depth measurements recorded by the data loggers, and on occasion the spot depth measurements with a hand-held sonar or tape measure, were used to determine the magnitude and direction of lake-level change between fall of 2019 and spring of 2020. Paired measurements from the water-depth loggers are available from 40 of the 56 study lakes where loggers were deployed (n = 51 in 2019, 44 in 2020). For the 16 lakes where paired depth-logger measurements were not available, we used the spot depth measurements collected at the time of water isotope sampling to estimate the lake-level change. Analysis of spot depth measurements at PAD 45 (Mamawi Lake), where water-depth loggers were not retrieved in 2019 and 2020, provided confidence in the methodology because the change in water depth computed using the spot measurements (0.70 m) corresponded well with the change (0.69 m) recorded at the Water Survey of Canada's Mamawi Lake Channel at Old Dog Camp hydrometric station (Station ID: 07KF003) during the same time interval.

As summarized in Appendix 2 Table A2.3, water isotope composition and water depth measurements were obtained at all 59 of the study lakes. One lake, PAD 18, was excluded from analysis of lake-level change because it serves as a 'index lake' for estimating a key parameter for modelling of water balance metrics at the other PAD lakes using water isotope composition (δ_{SSL}; Imran et al., 2024 [Chapter 2]). Also, due to its higher elevation atop a bedrock inlier, well above the reach of floodwaters, PAD 18 does not serve as a lake that is representative of floodwater or snowmelt input to the fluvio-deltaic lakes in the PAD. Two oxbow lakes (PAD 15, PAD 54) were also excluded from analysis of lake-level change, because they are relatively deep and narrow former river channels with marked depth variation across their basins where minor discrepancy in the location of depth-logger deployment in 2019 vs 2020 introduced too much uncertainty in estimated lake-level change. Analyses of the contributions from snowmelt and floodwater input to lake-level rise were performed on a subset of 52 of the remaining 56 lakes, because lake-levels declined at four of the lakes (PAD 19, PAD 24, M5, M14). The four lakes where lake-levels declined were not used to quantify the influence of snowmelt and floodwater on lake-level rise, but they were used to generate maps showing the spatial distribution of lake-level change.

3.2.4.5 Estimating the lake-level rise due to input of snowmelt versus floodwater

For the lakes identified as flooded in spring 2020, we used the calculated input proportions of snowmelt and river floodwater following methods described in section 3.2.4.3 to partition the amount of lake-level rise attributable to these two input water sources. Bar charts and boxplots were used to visualize the distribution of the data using RStudio (v.2023.03.0+386) and the ggplot2 (v.3.4.4) package (Wickham, 2016). Mann-Whitney U tests were conducted to determine if the magnitude of lake-level rise in non-flooded lakes from snowmelt input differs from the lake-level rise in flooded lakes from floodwater input, and if lake-level rise from snowmelt input differs between non-flooded lakes and flooded lakes. A paired-samples Wilcoxon signed ranks test was used to determine if the magnitude of lake-level rise attributable to floodwater differs from that due to snowmelt in flooded lakes. Due to insufficient sample size of non-flooded and flooded lakes in each sector, non-flooded and flooded lakes from both sectors were grouped to increase statistical power. All statistical tests were conducted using SPSS Statistics version 29.0.2.0.

3.2.4.6 Geospatial analyses

Maps were generated to display spatial interpolation of the proportion of input from river floodwaters to lakes across the PAD, as well as the total lake-level change and the lake-level rise attributable to input of snowmelt and floodwater. We used inverse distance weighting because it offers a more conservative approach for interpolating between measured values than the multiquadric radial basis function used by Remmer et al. (2020a) to depict the extent and magnitude of floodwater input to lakes in spring of 2018. An assumption of inverse distance weighting is that the weight of measured values on neighboring points diminishes as distance increases, which aligns with the expectation that proportion of river floodwater decreases with increasing distance from distributary channels (Remmer et al., 2020a). Spatial autocorrelation was determined using Moran's *I* coefficient (Anselin, 1995) where values indicative of clustering range from -1 (strong clustering of dissimilar values) to 1 (strong clustering of similar values). We acknowledge spatial autocorrelation was not significant ($p>0.05$) for some analyses, however, spatial interpolations were used to explore the general spatial patterns of flooding extent and lake-level change. Spatial analyses were conducted using ArcGIS Pro (v.2.7.0).

3.3 Results

3.3.1 Flood status of lakes in 2020

Based on lake water isotope compositions that fall below the river isotope compositions, which are indicative of recent inputs of river floodwaters and snowmelt, and supported by field observations and *in situ* measurements, 50% (29 of 58) of the lakes sampled were designated as flooded in spring 2020 (Figure 3.5a, Appendix 2 Table A2.1). In the Peace sector, 6 of the 25 lakes (24.0%) were identified to have flooded, where $\delta^{18}O$ ranged from -19.66‰ to -18.33‰ and $\delta^{2}H$ ranged from -156.89‰ to -149.83‰. In the more flood-prone Athabasca sector, 23 of the 33 lakes (69.7%) were identified to have flooded, where $\delta^{18}O$ ranged from -19.30‰ to -17.96‰ and $\delta^{2}H$ ranged from -145.36‰ to -154.27‰.

In both sectors, water in the non-flooded lakes was more isotopically enriched than the flooded lakes, due to absence of input of isotopically depleted river floodwaters, and their position below the LEL indicates input was predominantly from snowmelt (Figure 3.5a). In the Peace sector, 19 lakes were identified as not flooded, where $\delta^{18}O$ ranged from -17.76‰ to -13.42‰ and $\delta^{2}H$ ranged from -150.55‰ to -124.14‰ (Appendix 2 Table A2.1). In the Athabasca sector, 10 lakes were considered non-flooded, where $\delta^{18}O$ ranged from -19.19‰ to -14.92‰ and $\delta^{2}H$ ranged from -151.65‰ to -129.93‰ (Appendix 2 Table A2.1). Although some of the non-flooded lakes have isotope compositions similar that of flooded lakes, YSI measurements (i.e., low conductivity and turbidity values) and field observations (i.e., water clarity) were used to support their designations (Appendix 2 Table A2.1). These include PAD 27, M2, and M5 in the Athabasca sector whose water isotope compositions cluster with flooded lakes (Figure 3.5a), but were considered non-flooded because they had values of specific conductivity and turbidity that were lower than river water and the water was clear at the time of sampling in May 2020. The isotopically depleted values in M2 and M5 likely result from input of snowmelt from adjacent elevated sand dunes within their catchment, as also noted by Remmer et al. (2020b) and Neary et al. (2024).

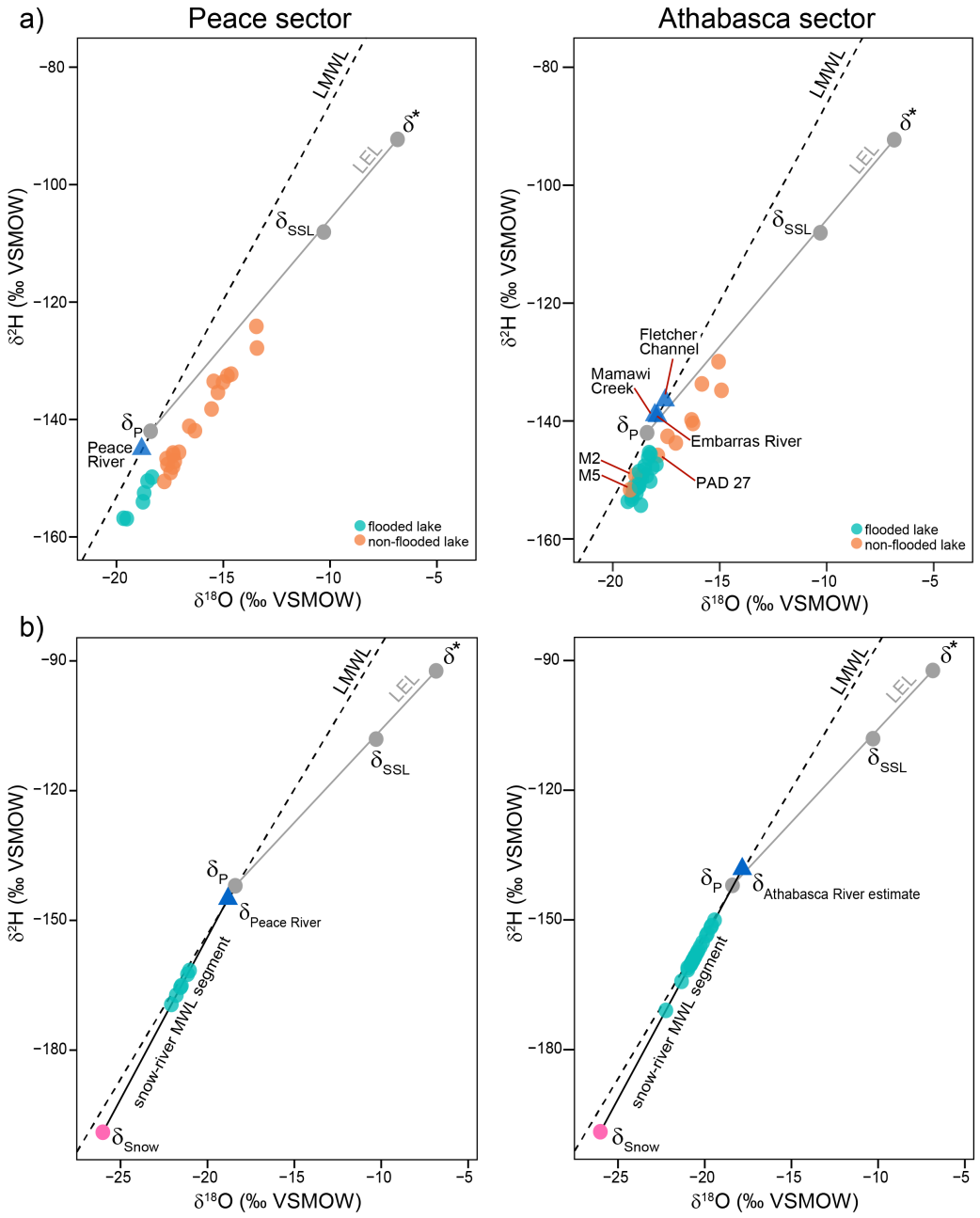


Figure 3.5: Isotope compositions of 58 lakes, 1 index lake (PAD 18 which approximates δ_{SSL}; Imran et al., 2024 [Chapter 2]), and 4 river sites sampled in May 2020 plotted in reference to the predicted LEL based on meteorological conditions during 2020-2021, as reported in Imran et al. (2024 [Chapter 2]). **a)** Top panels show isotope compositions of flooded lakes (blue circles), non-flooded lakes (orange circles), and rivers (blue triangles) in the Peace sector (left panel) and Athabasca sector (right panel). **b)** Bottom panels display the estimated isotope compositions of input water (δ_I) of flooded lakes on snow-river Meteoric Water Line segments between the isotope composition of snow (pink circle) and the respective river (blue triangle) for the Peace sector (left panel) and Athabasca sector (right panel). The isotope composition of the Athabasca River is estimated from its distributary channels (Embarras River, Mamawi Creek, Fletcher Channel).

Lakes in the Peace sector display greater evaporative isotopic enrichment than lakes in the Athabasca sector given the broader distribution of lake water isotope compositions along the LEL. However, the perpendicular distances of lake water isotope compositions below the LEL are slightly greater for Peace sector lakes (average distance = -1.81) than those in the Athabasca sector (average distance = -1.47) suggesting greater dilution by isotopically depleted snowmelt for the former.

3.3.2 Quantifying the proportion of input from floodwaters and snowmelt to the lakes that flooded in spring 2020

The average proportions of snowmelt and river floodwater input to the flooded lakes, generated by applying equations 1 and 2 to the estimated isotope composition of input waters (δ_I; Figure 3.5b), are comparable in the Peace (snowmelt input average = 37%; river input average = 63%, n = 6) and Athabasca sectors (snowmelt input average = 32%; river input average = 68%, n = 23) (Appendix 2 Table A2.4). These estimates are based on the water isotope composition of snow ($\delta^{18}O$ = -26.02‰, $\delta^{2}H$ = -199.0‰) derived from a global model (OIPC; Bowen and Revenaugh, 2003; IAEA/WMO, 2015; Bowen, 2016) because there were no direct measurements to characterize the isotope composition of snow within or near to the delta in 2020. We recognize that sampling of snow for analysis of water isotope composition may improve estimates of the proportion of input attributable to snowmelt runoff generated by the mixing model. Using the average isotope composition of three snow samples collected in March 2019 ($\delta^{18}O$ = -24.38‰, $\delta^{2}H$ = -185.71‰), computations suggest that the proportion of snowmelt input may be underestimated by the modelled snowmelt end-member composition by ~23% in the flooded lakes in the Peace sector and by ~20% in the flooded lakes in Athabasca sector. These values indicate that use of the global modelled value may have resulted in conservative estimates of the input proportions of snowmelt in spring of 2020.

Geospatial interpolation of the proportion of river input to flooded lakes reveals that extensive flooding occurred across the Athabasca sector in 2020, with similarities and differences in extent and magnitude from the last major ice-jam flood in 2018 (Figure 3.6). Widespread flooding of the Athabasca sector in 2020 was also reported in Neary et al. (2024) but here we provide estimates

of the proportion of input from river floodwater. Also, the spatial distribution of floodwaters depicted in Figure 3.6 agrees well with the limit of flooding captured by satellite imagery (Figure 3.1c), which lends confidence in the isotopic measurements and methodology used to infer and delineate river input proportions. In the Peace sector, the flooded lakes are located near the Rivière des Rochers (PAD 12), Revillon Coupé (PAD 15), and Chenal des Quatre Fourches (PAD 54). Flooded lakes farther inland received river floodwaters via Chilloney's Creek (PAD 8) and a distributary channel of the Rivière des Rochers (M17 and M18). The greatest contribution of river floodwaters (72 – 80%) was supplied by Mamawi Creek to the central region in the Athabasca sector (PAD 30, 31, 45, 46, M12, M14). Flooding of the central region during spring 2018 was also highlighted by Remmer et al. (2020a) and is attributed to the Embarras Breakthrough, a natural avulsion that occurred in 1982 and diverts substantial flow from the Athabasca and Embarras rivers towards the central portion of the delta via Cree and Mamawi creeks (Wolfe et al., 2008; Kay et al., 2019; Wang et al., 2023). The flood extent in 2020 spanned from a few kilometers west of the Embarras River (e.g., PAD 46) to the eastern terminus of the Athabasca River (e.g., M3, M4, M6), a region that did not flood in 2018 and is generally identified as less flood-prone since the Embarras Breakthrough (Kay et al., 2019, 2024). Although the flooded area was larger in 2020, the proportion of input from river floodwaters was lower in 2020 (46 – 80%) than in 2018 (60 – 98%; Remmer et al., 2020a), likely due to greater input from snowmelt in 2020.

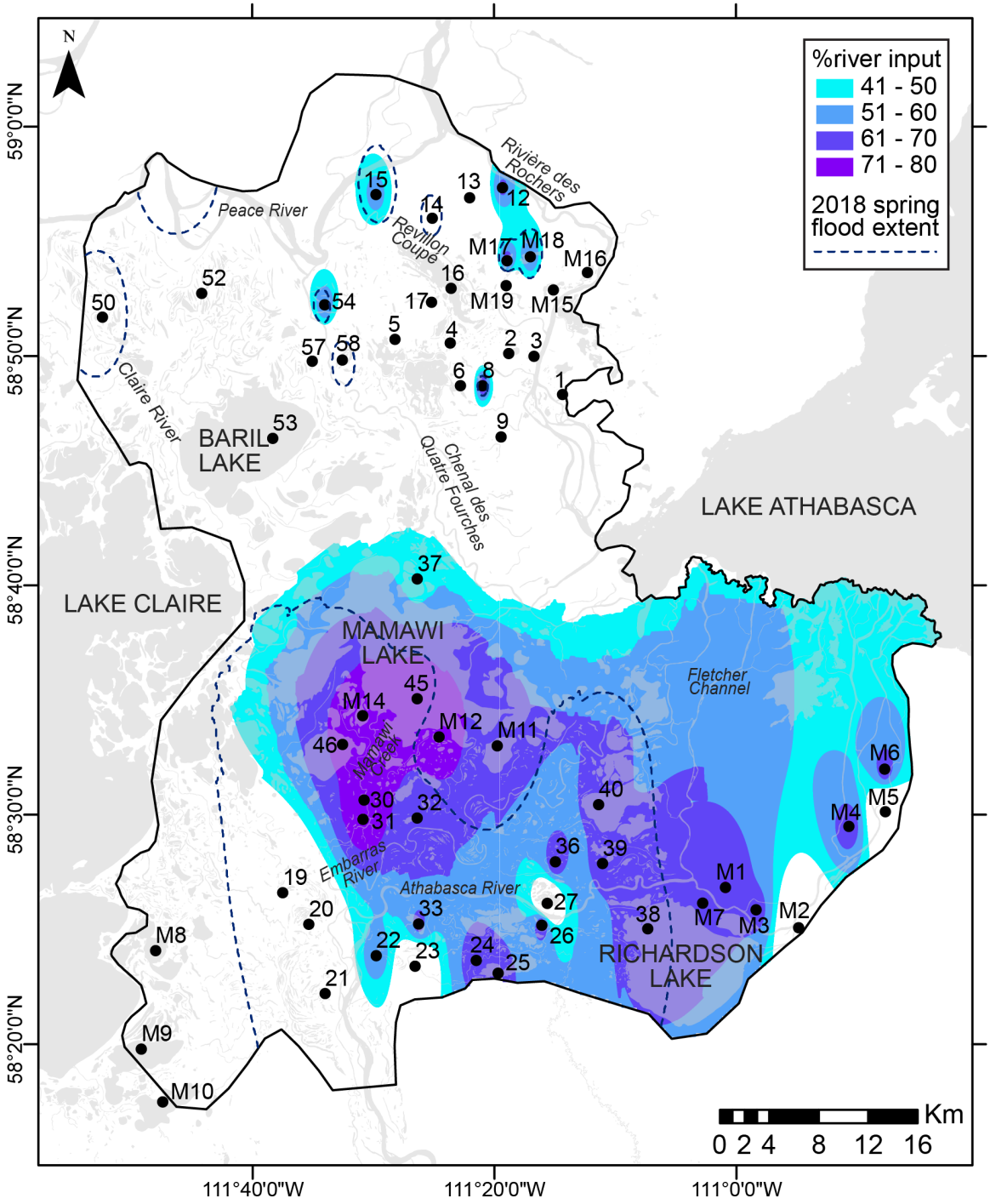


Figure 3.6: Map showing geospatial interpolation (by inverse distance weighting) of isotope-inferred percent river floodwater input to flooded lakes in spring 2020 (Moran's $I = 0.40$, $p<0.01$) compared to the spring 2018 flood extent (dashed line) in the Peace-Athabasca Delta. Spring 2018 flood extent is from Remmer et al. (2020a), with modifications that include constraining the interpolation to within the study area extent and using inverse distance weighting.

3.3.3 Comparison of lake-level rise by input from snowmelt versus river floodwaters in 2020

Water levels rose at 52 of the 56 lakes where paired water depth measurements were obtained in September 2019 and May 2020. This includes all 23 lakes sampled in the Peace sector, and 29 lakes sampled in the Athabasca sector (Appendix 2 Table A2.5, Figure 3.7a). Lake-level rise ranged 0.02 - 1.51 m, with the greatest rise occurring in four of the flooded lakes in the Athabasca sector and one flooded lake in the Peace sector that received substantial contributions from floodwater and snowmelt. Lake-level rise was also substantial at several of the non-flooded lakes and exceeded the rise at many of the flooded lakes. This feature is especially noticeable in the Peace sector where the rise at 12 of the 19 non-flooded lakes exceeded the rise that occurred in half of the flooded lakes, and where the rise at 9 of them exceeded the median total lake-level rise (0.31 m). Also, the lake-level rise recorded at half (4 of 8) the non-flooded lakes in the Athabasca sector exceeded the median lake-level rise for all the lakes in that sector (0.42 m).

At the scale of the entire delta, the lake-level rise attributed to snowmelt at the non-flooded lakes (median = 0.32 m, interquartile range [IQR] = 0.21 – 0.46 m) rivalled the rise due to floodwater at the flooded lakes (median = 0.26 m, IQR = 0.14 – 0.40 m; Appendix 2 Table A2.6, Figure 3.7b), and the distributions are indistinguishable based on a Mann-Whitney U test ($U = 312$, $p = 0.640$, $n = 27, 25$). The rise attributed to snowmelt, however, was significantly greater at the non-flooded lakes than the flooded lakes (median = 0.15 m, IQR = 0.05 - 0.22 m; Mann-Whitney U test; $U = 176$, $p = 0.015$, $n = 25, 27$). At the flooded lakes, snowmelt contributed 37% of the total rise at the flooded lakes, where the median rise due to input of floodwater (median = 0.26 m) is significantly higher than that due to snowmelt (median = 0.15 m) (Wilcoxon signed-ranks test; $Z = -4.292$, $p < 0.001$, $n = 1, 24, 0$). Boxplots in Figure 3.7b reveal that the distribution of lake-level rise among the three categories (snowmelt input to non-flooded lakes, snowmelt input to flooded lakes, floodwater input to flooded lakes) is consistent across both sectors of the PAD.

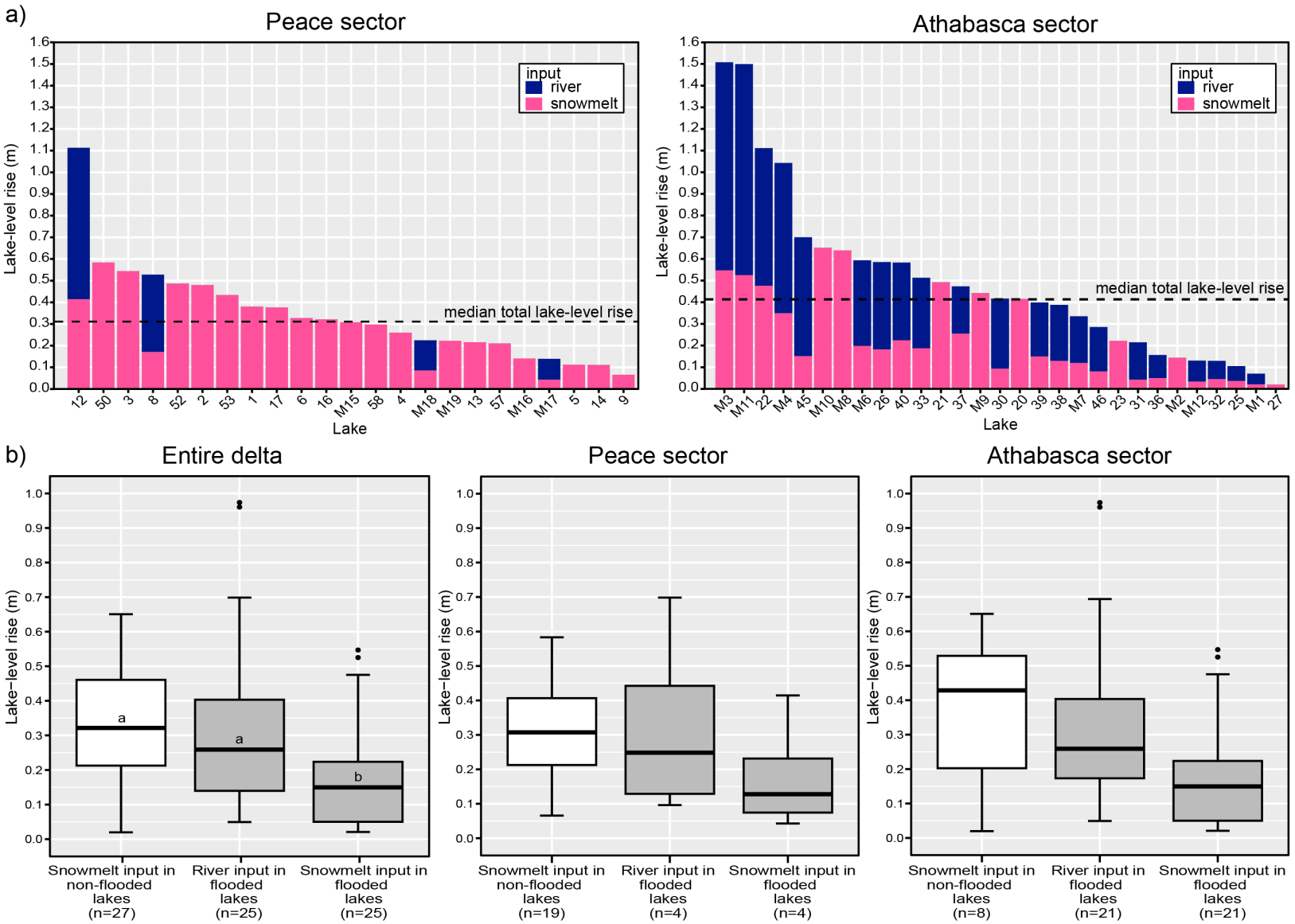

a)
Peace sector
Athabasca sector
Lake-level rise (m)
input
river
snowmelt
median total lake-level rise
Lake
12 50 3 8 52 2 53 1 17 6 16 M15 58 4 M18 M19 13 57 M16 M17 5 14 9
M3 M11 22 M4 45 M10 M8 M6 26 40 33 21 37 M9 30 20 39 38 M7 46 23 31 36 M2 M12 32 25 M1 27
b)
Entire delta
Peace sector
Athabasca sector
Lake−level rise (m)
a
a
b
Snowmelt input in non-flooded lakes (n=27)
River input in flooded lakes (n=25)
Snowmelt input in flooded lakes (n=25)
Snowmelt input in non-flooded lakes (n=19)
River input in flooded lakes (n=4)
Snowmelt input in flooded lakes (n=4)
Snowmelt input in non-flooded lakes (n=8)
River input in flooded lakes (n=21)
Snowmelt input in flooded lakes (n=21)

Figure 3.7: Distribution of lake-level rise at 52 lakes in spring 2020 in the Peace-Athabasca Delta. **a)** Bar plots showing the rise in lake level between September 2019 and May 2020 and the amount attributable to snowmelt (pink) and river floodwater (blue) in the (left panel) Peace sector (n=23) and (right panel) Athabasca sector (n=29). Lakes are arranged in descending order by total lake-level rise. Medians for the total lake-level rise (dashed line) are displayed for the Peace sector (0.31 m) and Athabasca sector (0.41 m). **b)** Boxplots showing the distribution of lake-level rise in (left panel) lakes across both sectors attributable to snowmelt input in non-flooded lakes (n=27), river floodwaters in flooded lakes (n=25), and snowmelt input in flooded lakes (n=25), (middle panel) the lakes in the Peace sector attributable to snowmelt input in non-flooded lakes (n=19), river floodwaters in flooded lakes (n=4), and snowmelt input in flooded lakes (n=4), and (right panel) the lakes in the Athabasca sector attributable to snowmelt input in non-flooded lakes (n=8), river floodwaters in flooded lakes (n=21), snowmelt input in flooded lakes (n=21). Mann-Whitney U tests (snowmelt input in non-flooded lakes vs river input in flooded lakes; snowmelt input in non-flooded lakes vs flooded lakes) and a paired-samples Wilcoxon signed ranks test (river input vs snowmelt input in flooded lakes) were conducted on the entire set of study lakes across both sectors (differences are identified by the letters in the left panel).

Lake-level rise was pervasive across the delta after the ice-jam flooding in 2020 (Figure 3.8a), but the contributions of snowmelt and floodwater to lake-level rise were not uniform (Figure 3.8b,c). The contribution of snowmelt was highest along the western margins of the Peace sector, where topographic relief is slightly greater and trees and shrubs are dense, and the western margins of the Athabasca sector adjacent to large open-drainage Lake Claire (Figure 3.8b). Lake-level rise due to snowmelt input is also relatively high in eastern portions of the Peace sector, where bedrock inliers increase topographic relief and support dense forest vegetation, and an elevated area at the southern margin of the Athabasca sector (the area around PAD 20-22) that supports dense forest vegetation (Figure 3.2, 8b). Notably, snowmelt contributed very little to the rise of lake levels across a broad central swath in the Athabasca sector where the terrain is flat and sparsely vegetated. The contribution of floodwater to lake-level rise was typically greatest in areas of the delta where the contribution by snowmelt was lowest (Figure 3.8c). This includes broad areas of the central and eastern Athabasca sector adjacent to the rivers and open-drainage Mamawi Lake, and the terminus region of the Athabasca River. It also includes four lakes in low elevations areas of the Peace sector connected (PAD 8) or adjacent (PAD 12, M18) to rivers. Of the total 56 lakes where we obtained measurements of change in lake depth, drawdown occurred at only four of them (PAD 19, 24, M5, M14). Drawdown at these lakes may have occurred because they did not receive substantial input from snowmelt and floodwater, or alternatively, the depth loggers may have been deployed at different locations in 2019 and 2020. Neary et al. (2021a) identified substantial lake-level rise caused by open-water flooding in 2019 at PAD 24 and M14, which may have filled these basins to brim full at the time of flooding in spring of 2020. Additional inputs of snowmelt and floodwater to these lakes in spring of 2020, therefore, may not have further raised their water levels.

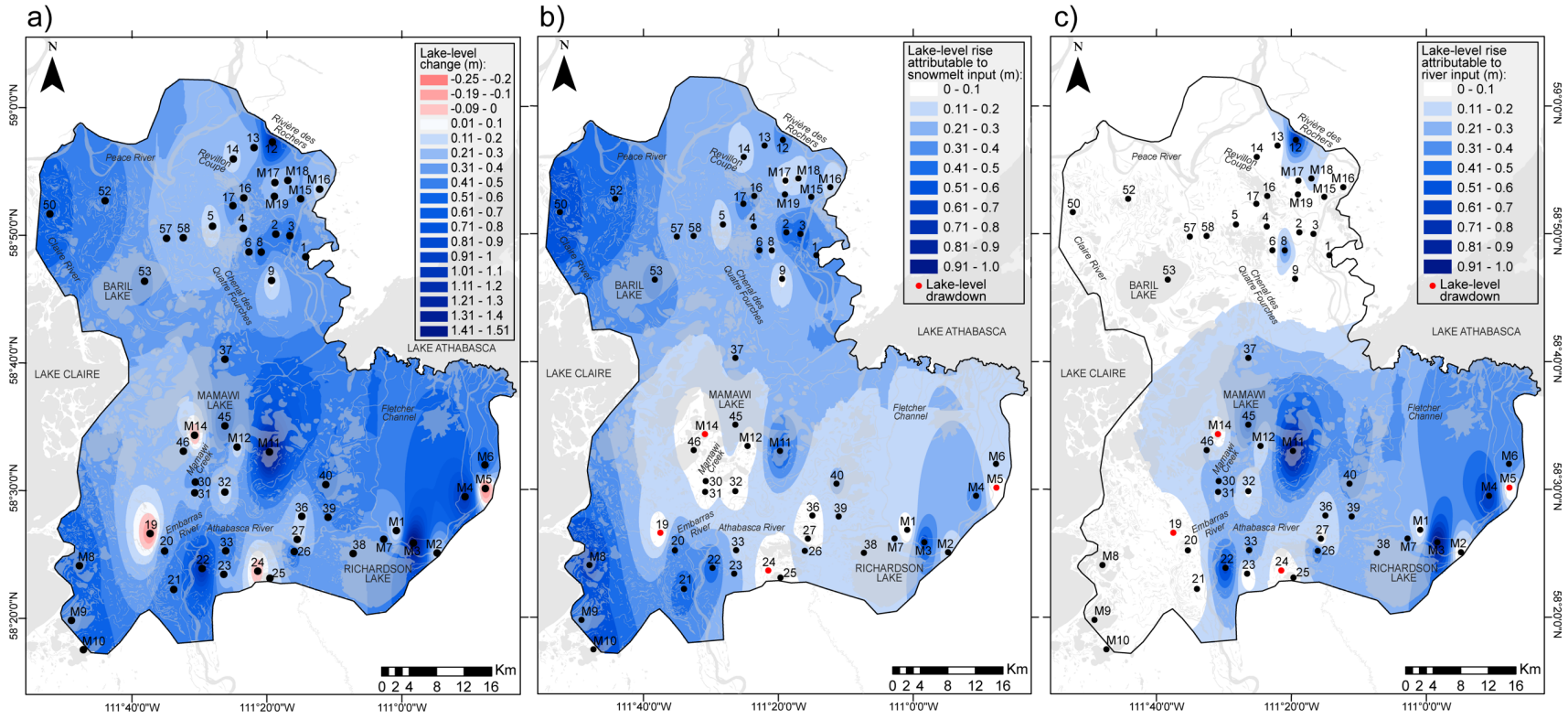


Figure 3.8: Maps showing spatial interpolation (by inverse distance weighting) of the **a)** magnitude of lake-level change (m) between September 2019 and May 2020 (Moran's I = -0.15, p = 0.15) for lakes where measurements were obtained using water-depth loggers and/or spot depth measurements lake-level rise (m); lake-level rise (m) in spring 2020 attributable to input of **b)** snowmelt (Moran's I = 0.31, p<0.01) and **c)** river floodwater (Moran's I = 0.04, p = 0.54). Lakes where water level declined were assigned a value of zero for spatial interpolations in panels in b) and c) and are indicated as red circles.

3.4 Discussion

Snowmelt has long been recognized as an important source of input water for maintaining water balance of shallow lakes in cold regions of northwestern North America where climates are arid to sub-humid and river floodwaters are not a factor (Shjeflo, 1968; Gray et al., 1970; Granger et al., 1984; Woo, 1980; Woo et al., 1981; Granger et al., 1984; Roulet and Woo, 1988; Rouse et al., 1997). Recognition of the importance of snowmelt on lake water balance, however, has been largely overlooked in floodplains, such as the PAD, because concern for alteration of river flood regimes by industrial activities and climate change has focused much of the scientific attention on assessing the importance of input from floodwaters (Prowse and Lalonde, 1996; Prowse and Conly, 2002; Beltaos et al., 2006, 2023; Peters and Prowse, 2006, Prowse et al., 2006a). Widespread flooding, however, typically occurs during the freshet when regional climatic conditions generate substantial runoff from rapid melt of thick snowpack that elevates river discharge at a time when river ice is strong at the delta (Beltaos et al., 2006; Romolo et al., 2006; Jasek, 2019; Lamontagne et al., 2021). These climatic conditions are also likely to generate substantial input of snowmelt runoff to both flooded and non-flooded lakes within the delta, which may also contribute importantly to maintenance of water levels. Here, using measurements of water isotope composition and water depth, we demonstrate that in 2020, when widespread ice-jam flooding occurred in the PAD, the rise of water levels in non-flooded perched basins due to snowmelt (median = 0.32 m) rivalled the rise in flooded lakes by floodwaters (median = 0.26 m; Figure 3.7). The contribution from snowmelt is considerable given it exceeds the magnitude of water-level drawdown that occurred during open water seasons of 2018 and 2019 (median = 0.17 m and 0.16 m, respectively) based on values reported for non-flooded lakes by Neary et al. (2021). On this basis, we suggest the widespread, often unsubstantiated, claims that ice-jam flooding is the primary, or only, mechanism capable of protecting the delta's perched lakes from desiccation (Prowse and Lalonde, 1996; Prowse and Conly, 1998, 2002; Peters et al., 2006a,b; Beltaos and Bonsal, 2021; Beltaos, 2023) need revision to better recognize the important potential contribution made by snowmelt. In support of this, a 7-year study in the PAD by Neary et al. (2024) revealed more widespread occurrence of negative perched lake water balances in summer and fall of 2015-2017, when snowpack depth was below the long-term (1968-1984) average, and broader

distribution of positive water balances in 2018-2021 when snowpack depth was at or above the long-term average.

Contributions of snowmelt and floodwater to lake-level rise were not uniformly distributed across the delta after ice-jam flooding in spring of 2020. Snowmelt contributed most substantially to lake-level rise in the slightly more elevated areas of the delta where topographic relief and density of trees and shrubs are greatest (e.g., northwestern and eastern portions of the Peace sector, a smaller south-central area in the Athabasca sector), and in areas adjacent to the eastern margins of the large open-drainage lakes Claire, Mamawi, and Richardson (Figure 3.8). In contrast, floodwaters contributed most substantially to lake-level rise in largely non-overlapping areas where the terrain is lower-lying and sparsely vegetated, and where wind-driven erosion and sublimation reduce the accumulation of snow. These include restricted-drainage lakes adjacent to distributary channels and open-drainage Lake Mamawi, which are amongst the areas most prone to flooding (Kay et al., 2024; Neary et al. 2024). A result is that lake-level rise was pervasive across the delta because snowmelt contributed in areas beyond the reach of river floodwaters. The smaller contribution of snowmelt to the rise of flooded lakes versus non-flooded lakes suggests the prevailing strong winds from the west re-distributed snow away from the lower lying, flat, sparsely vegetated flood-prone areas of the delta and towards the more elevated, less flood-prone areas with denser forests. Forest vegetation is well known to entrap and retain wind-distributed snow (McFadden et al., 2001; Sturm et al., 2001; Essery and Pomeroy, 2004; Boon, 2009; Marsh et al., 2010; Varhola et al., 2010; Woo et al., 2012), although forest cover can, under some conditions, also reduce snow accumulation due to canopy interception and sublimation (Pomeroy and Gray, 1995). Due to these differences, restricted-drainage lakes, the perched basins that occupy slightly lower elevations, may be more vulnerable to drawdown during years of below-average snowfall and minimal ice-jam flooding than higher elevation closed-drainage lakes. At the closed-drainage lakes, forest vegetation and greater topographic relief is likely to continue to entrap and store snow blown in from adjacent sparsely vegetated areas of the delta, which may sustain input from snowmelt runoff during years of below-average snowfall. These differences may, however, be negated during the summer and fall because restricted-drainage lakes are more likely to receive input of floodwaters during the open-water season and water balance of closed-drainage lakes is more strongly affected by evaporation (Neary et al., 2021, 2024).

The contribution of snowmelt to lake-level rise in spring of 2020 may have been augmented by above average antecedent precipitation in 2019 (Remmer et al., 2020b; Neary et al., 2024). Soils in the PAD are dominated by imperfectly to poorly drained Regosols and Gleysols (Timoney, 2013) and may have been nearly to fully saturated prior to the freshet in 2020. Soils close to saturation have reduced storage capacity, and, thus, greater ability to deliver snowmelt runoff to lakes (Harms and Chanasyk, 1998; Fang and Pomeroy, 2007; He et al., 2015). Also, peak snow water equivalent (SWE) was above-average and delayed in 2020 (Figure 3.3b), which may have increased the magnitude of lake-level rise by snowmelt runoff when coupled with a rapid melt (e.g., Barnhart et al., 2016; Musselman et al., 2017). Meteorological conditions in 2020 generated the second highest water levels on record (highest since 1935) in Lake Athabasca and the open-drainage lakes within the delta (Desrochers et al., 2023; Neary et al., 2024), thus we explored long-term meteorological records available since 1963 to assess how representative the freshet of 2020 is relative to previous decades (Figure 3.9). Estimates of the peak SWE and melt rate, reveal that comparable contribution of snowmelt runoff to lake-level rise likely occurred quite regularly between the early 1960s and late 1980s (based on 2020 peak snow water equivalent = 80.4 mm and melt rate = 10.1 mm/day), but these thresholds have been exceeded just once since 1987. That single exceedance occurred in 2018 when substantial ice-jam flooding also occurred in the PAD (Remmer et al., 2020a). Since the late 1980s, peak SWE and melt rate have declined substantially, and peak SWE has occurred earlier (often by a month or more). As captured by Generalized Additive Model (GAM) trendlines, peak SWE began to decline in the late 1980s and the melt rate has declined since the early 1980s. These changes align with shifts in synoptic meteorological conditions that have raised winter air temperatures and reduced winter precipitation and snowpack volume within broad regions of the Peace River watershed (Moore & McKendry, 1996; Keller, 1997). Notably, decline in peak SWE and melt rate also coincide with widespread decline of the surface water extent (Figure 3.9) and drawdown of the delta's ecologically important shallow perched lakes, which, to date, have largely been attributed to reduced incidence of major ice-jam floods (Prowse and Lalonde, 1996; Prowse and Conly, 1998, 2002; Beltaos and Bonsal, 2021; Beltaos, 2023). Thus, reduction in snowmelt runoff may also have contributed to the drawdown of perched lake water levels during at least the past three decades.

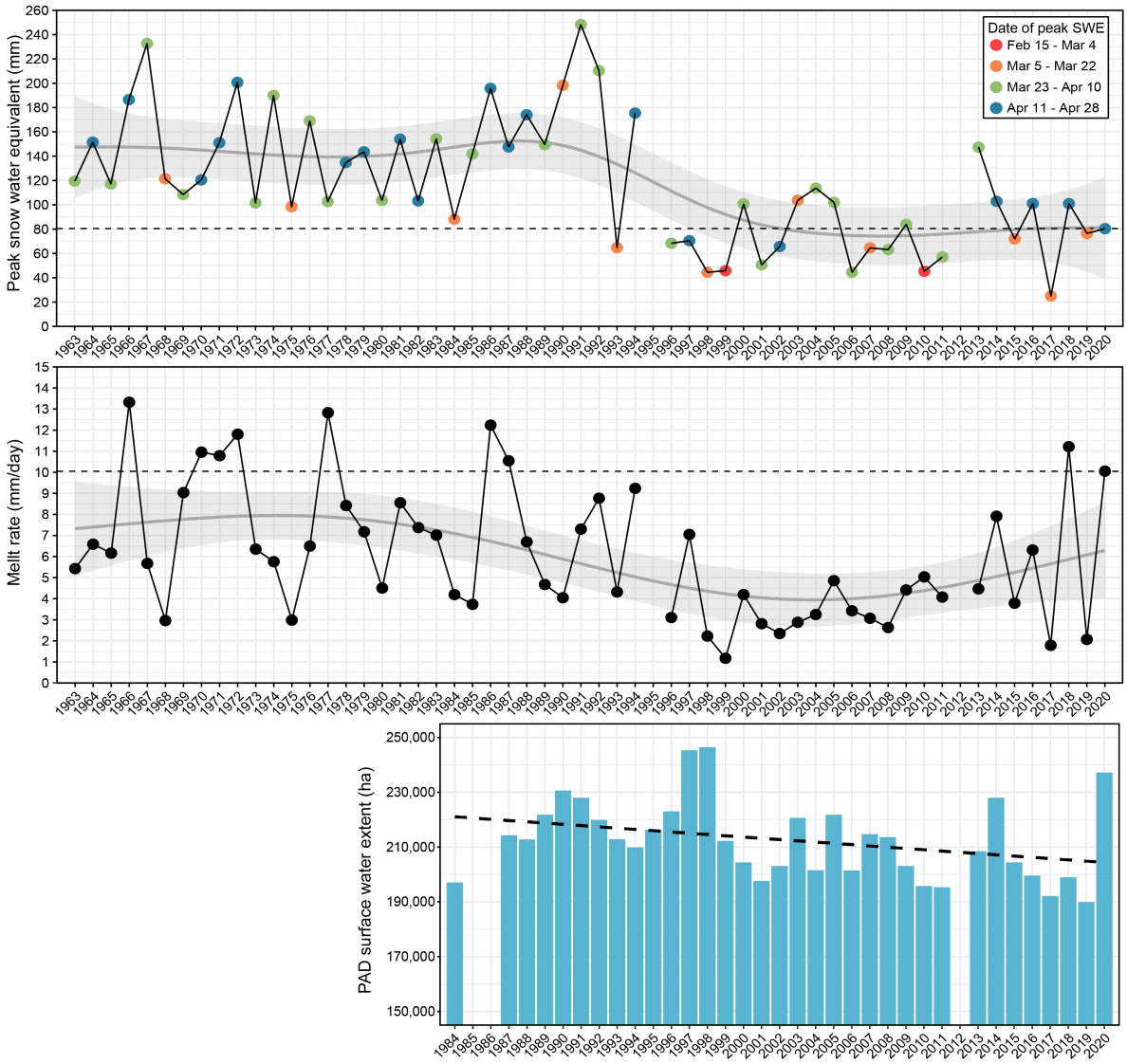


Figure 3.9: Long-term trends captured with generalized additive models (GAMs; grey line; shaded region represents 95% confidence interval) of peak snow water equivalent (SWE) values between Feb 15 – April 28 (top panel) and rate of melt (mm/day; i.e., total number of days for peak SWE to reach zero; middle panel) from 1963 – 2020. Daily SWE data are averaged from ten townships (T110R07W4, T110R08W4, T112R05W4, T112R07W4, T112R08W4, T112R10W4, T113R05W4, T113R10W4, T115R07W4, T115R08W4) and sourced from Alberta's AgroClimatic Information Service (https://www.alberta.ca/acis-find-historic-climate-data). Bottom panel shows temporal variation of surface water extent (ha) in the Peace-Athabasca Delta from 1984 – 2020, as reported in WBNP (2022), based on Global Surface Water (LANDSAT Satellite 30 m resolution) derived from May or June images (dashed line shows the simple linear regression). Data for bottom panel were provided by Parks Canada and presented as shown in WBNP (2022).

3.5 Implications and recommendations

As climate change and industrialization continue to threaten the security of freshwater supply, mitigative actions may be required to minimize drawdown of the delta's lakes. Installation of a weir on a channel that conveys outflow from Lake Claire and Mamawi Lake to Lake Athabasca and the Peace River is currently being contemplated by the WBNP Action Plan (WBNP, 2019) to raise levels in the open-water network and adjacent restricted-drainage lakes. This weir may serve well to retain influence of snowmelt runoff on water levels in some lakes within central areas of the delta but, as identified by Kay et al. (2024), it will also result in undesirable sediment accumulation as a consequence of the Embarras Breakthrough, a natural river avulsion that now delivers massive volumes of water and sediment towards the proposed weir via Mamawi Creek and Mamawi Lake (Wang et al., 2023; Smith et al. 2023). Strategic releases of water from the W.A.C. Bennett Dam to the Peace River are also being considered within the WBNP Action Plan for years when meteorological conditions are conducive for formation of ice-jams on the Peace River at the PAD and risk of damage is low to communities and infrastructure between the dam and delta (WBNP, 2019). If successful, this will increase the role of floodwater input in maintaining water levels of perched basins within the reach of the floodwaters. Based on evidence from this study, winters that are conducive to ice-jam flooding in the PAD also lead to lake-level rise from substantial input of snowmelt, which may sustain water levels in lakes not reached by the induced flooding. Continued seasonal collection and analysis of water samples for isotope composition and hourly lake depth measurements, as also advocated for by Neary et al. (2024), will be important to assess the success of these mitigative actions. This combination of measurements can, for example, be used to decipher the relative importance of floodwaters enhanced by strategic flow releases versus snowmelt runoff on lake levels, as is critical to inform a risk-benefit analysis.

Snowpack can potentially be augmented artificially via use snow fences and snow-making machinery. Snow fences are known to effectively accumulate snowpack in flat terrain and increase streamflow (Brown, 1983; Martinelli, 1973), and they have been used to augment water supply to small villages in Alaska (Slaughter et al., 1975; McFadden and Collins, 1978). In a study by Steufer and Kane (2016), snowmelt runoff generated using snow fences allowed longer retention of water during the open-water season and increased the lake volume by 21-29%. Thus, installation of snow

fences in the PAD may enhance delivery of snowmelt runoff to lakes of cultural importance, but, of course, they will prevent delivery of snow to lakes positioned further downwind. Use of snow-making machinery from river water also has potential to augment water levels in non-flooded lakes that are significant for traditional land use by increasing input of snowmelt runoff. Project design and cost-benefit studies would be needed to determine the feasibility of these methodologies and optimize their application in the PAD. Consultation with Indigenous communities, careful consideration of the limitations of the methodologies, ecological implications, and modelling of the influence of snowmelt on lake water balances are all required before implementing such strategies in the PAD. For example, areas of the delta where lakes are most prone to drawdown are located at considerable distance from rivers and expansive areas with sparse vegetation, which may limit the feasibility and success of these possible mitigative actions.

3.6 References

Adam, J.C., Hamlet, A.F., Lettenmaier, D.P., 2009. Implications of global climate change for snowmelt hydrology in the twenty-first century. *Hydrol. Processes*, 23, 962-972. https://doi.org/10.1002/hyp.7201.

Anselin, L., 1995. Local Indicators of Spatial Association—LISA. *Geogr. Anal.*, 27, 93-115. https://doi.org/10.1111/j.1538-4632.1995.tb00338.x.

Barnett, T.P., Adam, J.C., Lettenmaier, D.P., 2005. Potential impacts of a warming climate on water availability in snow-dominated regions. *Nature*. 438, 303–309. https://doi.org/10.1038/nature04141.

Barnhart, T.B., Molotch, N.P., Livneh, B., Harpold, A.A., Knowles, J.F., & Schneider, D., 2016. Snowmelt rate dictates streamflow. *Geophys. Res. Lett.*, 43, 8006-8016. https://doi.org/10.1002/2016GL069690.

Beltaos, S., 2013. Hydrodynamic and climatic drivers of ice breakup in the lower Mackenzie River. *Cold Reg. Sci. Technol.* 95, 39-52. https://doi.org/10.1016/j.coldregions.2013.08.004.

Beltaos, S., 2014. Comparing the impacts of regulation and climate on ice-jam flooding of the Peace-Athabasca Delta. *Cold Reg. Sci. Technol.*, 108, 49-58. https://doi.org/10.1016/j.coldregions.2014.08.006.

Beltaos, S., 2018. Frequency of ice-jam flooding of Peace-Athabasca Delta. *Can. J. Civ. Eng.,* 45, 71-75. https://doi.org/10.1139/cjce-2017-0434.

Beltaos, S., 2023. The drying Peace–Athabasca Delta, Canada: Review and synthesis of cryo-hydrologic controls and projections to future climatic conditions. *Sustainability*, 15, 2103. https://doi.org/10.3390/su15032103.

Beltaos, S., Bonsal, B., 2021. Climate change impacts on Peace River ice thickness and implications to ice-jam flooding of Peace-Athabasca Delta, Canada. *Cold Reg. Sci. Technol.*, 186, 103279. https://doi.org/10.1016/j.coldregions.2021.103279.

Beltaos, S., Carter, T., 2021. Minor 2020 ice jamming in lower Peace River despite extreme breakup flows: assessment of hydroclimatic controls. CGU HS Committee on River Ice Processes and the Environment 21st Workshop on the Hydraulics of Ice Covered Rivers. Accessible at https://cripe.ca/publications/proceedings/workshop-21

Beltaos, S., Prowse, T., Bonsal, B., MacKay, R., Romolo, L., Pietroniro, A., Toth, B., 2006. Climatic effects on ice-jam flooding of the Peace-Athabasca Delta. *Hydrol. Processes*, 20, 4031-4050. https://doi.org/10.1002/hyp.6418.

Bonsal, B.R., Prowse, T.D., 2003. Trends and variability in spring and autumn 0°C-isotherm dates over Canada. *Clim. Change*, 57, 341-358. https://doi.org/10.1023/A:1022810531237.

Bigras, S.C., 1990. Hydrological regime of lakes in the Mackenzie delta, Northwest Territories, Canada. Arct. *Alp. Res.*, 22, 163-174. https://doi.org/10.2307/1551301.

Boon, S., 2009. Snow ablation energy balance in a dead forest stand. *Hydrol. Processes*., 23, 2600-2610. https://doi.org/10.1002/hyp.7246.

Bouchard, F., Turner, K.W., MacDonald, L.A., Deakin, C., White, H., Farquharson, N., Medeiros, A.S., Wolfe, B.B., Hall, R.I., Pienitz, R., Edwards, T.W.D., 2013. Vulnerability of shallow subarctic lakes to evaporate and desiccate when snowmelt runoff is low. *Geophys. Res. Lett.*, 40, 6112-6117. https://doi.org/10.1002/2013GL058635.

Bowen, G.J., 2016. The Online Isotopes in Precipitation Calculator, version 2.2. Accessible at http://www.waterisotopes.org.

Bowen, G.J., Revenaugh, J., 2003. Interpolating the isotopic composition of modern meteoric precipitation. *Water Resour Res.*, 39. https://doi.org/10.1029/2003WR002086.

Bowling, L.C., Kane, D.L., Gieck, R.E., Hinzman, L.D., Lettenmaier, D.P., 2003. The role of surface storage in a low-gradient Arctic watershed. *Water Resour. Res.*, 39. https://doi.org/10.1029/2002WR001466.

Brock, B.E., Martin, M.E., Mongeon, C.L., Sokal, M.A., Wesche, S.D., Armitage, D., Wolfe, B.B., Hall, R.I. and Edwards, T.W.D., 2010. Flood frequency variability during the past 80 years in the Slave River Delta, NWT, as determined from multi-proxy paleolimnological analysis. *Can. Water Resour. J.*, 35, 281-300. https://doi.org/10.4296/cwrj3503281.

Brock, B.E., Wolfe, B.B., Edwards, T.W.D., 2008. Spatial and temporal perspectives on spring break-up flooding in the Slave River Delta, NWT. *Hydrol. Processes*, 22, 4058-4072. https://doi.org/10.1002/hyp.7008.

Brock, B.E., Yi, Y., Clogg-Wright, K.P., Edwards, T.W.D., Wolfe, B.B., 2009. Multi-year landscape-scale assessment of lakewater balances in the Slave River Delta, NWT, using water isotope tracers. *J. Hydrol.*, 379, 81-91. https://doi.org/10.1016/j.jhydrol.2009.09.046.

Brown, R.H., 1983. Snow fences: then and now. *J. Cult. Geogr.*, 4, 87-98. https://doi.org/10.1080/08873638309478585.

Bush, E., Lemmen, D.S., 2019. Canada's Changing Climate Report; Government of Canada. Accessible at https://changingclimate.ca/CCCR2019/.

Conly, F. M., van der Kamp, G. (2001). Monitoring the hydrology of Canadian prairie wetlands to detect the effects of climate change and land use changes. *Environ. Monit. Assess.*, 67, 195-215. https://doi.org/10.1023/A:1006486607040.

Coplen, T.B., 1996. New guidelines for reporting stable hydrogen, carbon, and oxygen isotope-ratio data. *Geochim. Cosmochim. Acta*, 60, 3359-3360. https://doi.org/10.1016/0016-7037(96)00263-3.

Craig, H., Gordon, L.I., 1965. Deuterium and oxygen 18 variations in the ocean and the marine atmosphere, in: Tongiorgi, E. (Ed.), Stable Isotopes in Oceanographic Studies and Paleotemperatures, *Laboratorio di Geologia Nucleare*, Pisa, Italy.

Demuth, M.N., Keller, R., 2006. An Assessment of the Mass Balance of Peyto Glacier (1966–1995) and its Relation to Recent and Past-century Climatic Variability, in: Demuth, M.N., Munro, D.S., Young, G.J. (Eds.), Peyto Glacier - One Century of Science, NHRI Science Report No. 8, 83-132.

Desrochers, N.M., Peters, D.L., Siles, G., Cauvier Charest, E., Trudel, M., Leconte, R., 2023. A remote sensing view of the 2020 extreme lake-expansion flood event into the Peace–Athabasca Delta floodplain—implications for the future SWOT mission. *Remote Sens.*, 15, 1278. https://doi.org/10.3390/rs15051278

Dibike, Y., Eum, H.I., Prowse, T., 2018. Modelling the Athabasca watershed snow response to a changing climate. *J. Hydrol.: Reg. Stud.*, 15, 134-148. https://doi.org/10.1016/j.ejrh.2018.01.003.

Duguay, C.R., Prowse, T.D., Bonsal, B.R., Brown, R.D., Lacroix, M.P., Ménard, P., 2006. Recent trends in Canadian lake ice cover. *Hydrol. Processes*, 20, 781-801. https://doi.org/10.1002/hyp.6131.

Ecological Stratification Working Group, 1995. A National Ecological Framework for Canada. Agriculture and Agri-Food Canada, Research Branch, Centre for Land and Biological Resources Research and Environment Canada, State of the Environment Directorate, Ecozone Analysis Branch, Ottawa/Hull. Report and national map at 1:7500 000 scale.

Edwards, T.W.D., Wolfe, B.B., Gibson, J.J., Hammarlund, D., 2007. Use of water isotope tracers in high latitude hydrology and paleohydrology, in: Long-Term Environmental Change in Arctic and Antarctic Lakes. *Springer*, Dordrecht. https://doi.org/10.1007/978-1-4020-2126-8_7.

Emmer, S., Kovachis, N., Nafziger, J., 2021. A Tale of Two Basins: The 2020 river ice breakup in northern Alberta, part II: The Peace River. CGU HS Committee on River Ice Processes and the Environment 21st Workshop on the Hydraulics of Ice Covered Rivers. Accessible at https://cripe.ca/publications/proceedings/workshop-21.

Essery, R., Pomeroy, J.W., 2004. Vegetation and topographic control of wind-blown snow distributions in distributed and aggregated simulations for an Arctic tundra basin. *J. Hydrometeorol.*, 5, 735-744. https://doi.org/10.1175/1525-7541(2004)005%3C0735:VATCOW%3E2.0.CO;2.

Fang, X., Pomeroy, J.W., 2007. Snowmelt runoff sensitivity analysis to drought on the Canadian prairies. *Hydrol. Processes*, 21, 2594-2609. https://doi.org/10.1002/hyp.6796.

French, N.H.F., Graham, J.A., Vander Bilt, D.J.L., Jenkins, L.K., Battaglia, M.J., Bourgeau-Chavez, L.L., 2022. ABoVE: wetland type, Slave River and Peace-Athabasca Deltas, Canada, 2007 and 2017. ORNL DAAC. https://doi.org/https://doi.org/10.3334/ORNLDAAC/1947.

Ge, Y., Gong, G., 2009. North American Snow Depth and Climate Teleconnection Patterns. *J. Clim*., 22, 217-233. https://doi.org/10.1175/2008JCLI2124.1.

Goulding, H.L., Prowse, T.D., Bonsal, B., 2009a. Hydroclimatic controls on the occurrence of break-up and ice-jam flooding in the Mackenzie Delta, NWT, Canada. *J. Hydrol.*, 379, 251-267. https://doi.org/10.1016/j.jhydrol.2009.10.006.

Goulding, H.L., Prowse, T.D., Beltaos, S., 2009b. Spatial and temporal patterns of break-up and ice-jam flooding in the Mackenzie Delta, NWT. *Hydrol. Processes*, 23, 2654-2670. https://doi.org/10.1002/hyp.7251.

Granger, R.J., Gray, D.M., Dyck, G.E., 1984. Snowmelt infiltration to frozen Prairie soils. *Can. J. Earth Sci.*, 21, 669-677. https://doi.org/10.1139/e84-073.

Gray, D.M., Norum, D.I., Dyck, G.E., 1970. Densities of prairie snowpacks. 38th Annual Western Snow Conference Proceedings, 39, 24-30.

Grolemund, G., Wickham, H., 2011. Dates and times made easy with lubridate. *J. Stat. Softw.*, 40, 1-25. https://doi.org/10.18637/jss.v040.i03.

Harms, T.E., Chanasyk, D.S., 1998. Variability of Snowmelt Runoff and Soil Moisture Recharge. *Hydrol. Res*., 29, 179-198. https://doi.org/10.2166/nh.1998.0010.

He, H., Dyck, M.F., Si, B.I., Zhang, T., Lv, J., Wang, J., 2015. Soil freezing–thawing characteristics and snowmelt infiltration in Cryalfs of Alberta, Canada. *Geoderma Reg.*, 5, 198-208. https://doi.org/10.1016/j.geodrs.2015.08.001.

IAEA/WMO, 2015. Global Network of Isotopes in Precipitation. The GNIP Database. Accessible at: https://nucleus.iaea.org/wiser.

Independent Environment Consultants (IEC), 2018. Strategic environmental assessment of Wood Buffalo National Park World Heritage Site. Volume 1, Milestone 3 – Final SEA Report. Independent Environmental Consultants (IEC). Accessible at: http://parkscanadahistory.com/publications/woodbuffalo/#documents.

Imran, A., Neary, L.K., Falcone, M.D., Wolfe, B.B., Hall, R.I., 2024. Value of long-term isotope monitoring of an index lake for tracking changes in lake water balances across a northern

freshwater landscape. *J. Hydrol.: Reg. Stud.*, 53, 101765. https://doi.org/10.1016/j.ejrh.2024.101765.

Jasek, M., 2019. An emerging picture of Peace River break-up types that influence ice jam flooding of the Peace-Athabasca Delta part 1: The 2018 Peace River break-up. CGU HS Committee on River Ice Processes and the Environment 20th Workshop on the Hydraulics of Ice Covered Rivers. Accessible at: https://cripe.ca/publications/proceedings/workshop-20.

Jasek, M., Lamontagne, J.R., Smith, J.D. 2021. Analysis of climatic and riverine factors influencing Peace River ice jam flood frequency in the Peace-Athabasca Delta: From history to future climate implications. Proceedings of the 21st Workshop on the Hydraulics of Ice Covered Rivers. Saskatoon, SK, Canada. Accessible at: https://cripe.ca/publications/proceedings/workshop-21.

Jiang S., Zhu, C., Hu, Z., Jiang, N., Zheng, F., 2023. Triple-dip La Niña in 2020–23: understanding the role of the annual cycle in tropical Pacific SST. *Environ. Res. Lett*., 18, 084002. https://doi.org/10.1088/1748-9326/ace274.

Kay, M.L., MacDonald, L.A., Wiklund, J.A., Girard, C.A., Wolfe, B.B., Hall, R.I., 2024. 'Paleofloodscapes': Application of sediment source fingerprinting to track flood regime change over space and time at the Peace-Athabasca Delta, Canada. *Sci. Total Environ.*, 912, 169538. https://doi.org/10.1016/j.scitotenv.2023.169538.

Kay, M.L., Wiklund, J.A., Remmer, C.R., Neary, L.K., Brown, K., Ghosh, A., MacDonald, E., Thomson, K., Vucic, J.M., Wesenberg, K., Hall, R.I., Wolfe, B.B., 2019. Bi-directional hydrological changes in perched basins of the Athabasca Delta (Canada) in recent decades caused by natural processes. *Environ. Res. Commun.*, 1, 081001. https://doi.org/10.1088/2515-7620/ab37e7.

Keller, R., 1997. Variability in Spring Snowpack and Winter Atmospheric Circulation Pattern Frequencies in the Peace River Basin. MSc. Thesis, University of Saskatchewan.

Krapu, G., Klett, A., Dennis, J., 1983. The effect of variable spring water conditions on mallard reproduction. *The Auk: Ornithol. Adv.*, 100, 689-698. https://doi.org/10.1093/auk/100.3.689.

Lamontagne, J.R., Jasek, M., Smith, J.D., 2021. Coupling physical understanding and statistical modeling to estimate ice jam flood frequency in the northern Peace-Athabasca Delta under climate change. *Cold Reg. Sci. Technol.,* 192, 103383. https://doi.org/10.1016/j.coldregions.2021.103383.

Lehner, B., Döll, P., 2004. Development and validation of a global database of lakes, reservoirs and wetlands. *J. Hydrol*., 296, 1-22. https://doi.org/10.1016/j.jhydrol.2004.03.028.

Little, J.L., Nolan, S.C., Casson, J.P., Olson, B.M., 2007. Relationships between soil and runoff phosphorus in small Alberta watersheds. *J. Environ. Qual.*, 36, 1289-1300. https://doi.org/10.2134/jeq2006.0502.

Marsh, P., Bartlett, P., MacKay, M., Pohl, S., Lantz T., 2010. Snowmelt energetics at a shrub tundra site in the western Canadian Arctic. *Hydrol. Processes*, 24, 3603-3620. https://doi.org/10.1002/hyp.7786.

Marsh, P., Lesack, L.F., 1996. The hydrologic regime of perched lakes in the Mackenzie Delta: potential responses to climate change. *Limnol. Oceanogr.,* 41, 849-856. https://doi.org/10.4319/lo.1996.41.5.0849.

Marsh, P., Lesack, L., Hicks, F., Roberts, A., Hopkinson, C., Solomon, S., Forbes, D.L., Russell, M., Haywood, H., 2009. Hydrology of the Mackenzie Delta: off-channel water storage and delta interaction with the Beaufort Sea. In Proceedings, 17th International Northern Research Basins Symposium and Workshop, Iqaluit-Pangnirtung-Kuujjuaq, August, 12, 217-226.

Martinelli, M., 1973. Snow-fence experiments in alpine areas. *J. Glaciol*., 12, 291-303. https://doi.org/10.3189/S002214300003210X.

McFadden, J.P., Liston, G.E., Sturm, M., Pielke, R. A., Chapin, F.S., 2001. Interactions of shrubs and snow in arctic tundra: measurements and models. Proceedings of a symposium held during the Sixth IAHS Scientific Assembly at Maastricht, The Netherlands, July 2001. IAHS Publication no. 270, 317-325.

McFadden, J.P., T.T., Collins, C.M., 1978. Fresh water supply for a village surrounded by salt water: Point Hope, Alaska. US Army Cold Regions Research and Engineering Laboratory, CRREL Special Report, 78-7.

Medeiros, A. S., Wood, P., Wesche, S. D., Bakaic, M., Peters, J.F., 2017. Water security for northern peoples: review of threats to Arctic freshwater systems in Nunavut, Canada. *Reg. Environ. Change*, 17, 635-647. https://doi.org/10.1007/s10113-016-1084-2.

Mikisew Cree First Nation (MCFN), 2014. Petition to the World Heritage Committee Requesting Inclusion of Wood Buffalo National Park on the List of World Heritage in Danger. Accessible at https://cpawsnab.org/wp-content/uploads/2018/03/Mikisew_Petition_respecting_UNESCO_Site_256_-_December_8_2014.pdf.

Mielko, C., Woo, M.K., 2006. Snowmelt runoff processes in a headwater lake and its catchment, subarctic Canadian Shield. *Hydrol. Processes.*, 20, 987-1000. https://doi.org/10.1002/hyp.6117.

Moore, R.D., McKendry, I.G., 1996. Spring snowpack anomaly patterns and winter climatic variability, British Columbia, Canada. *Water Resour. Res.*, 32, 623-632.

https://doi.org/10.1029/95WR03640.

Musselman, K.N., Clark, M.P., Liu, C., Ikeda, K., Rasmussen, R., 2017. Slower snowmelt in a warmer world. *Nat. Clim. Change*, 7, 214-219. https://doi.org/10.1038/nclimate3225.

Nafziger, J., Kovachis, N., Emmer, S., 2021. A Tale of Two Basins: The 2020 river ice breakup in northern Alberta, part I: The Athabasca River. CGU HS Committee on River Ice Processes and the Environment 21st Workshop on the Hydraulics of Ice Covered Rivers. Accessible at https://cripe.ca/publications/proceedings/workshop-21.

Neary, L.K., Remmer, C.R., Krist, J., Wolfe, B.B., Hall, R.I., 2021a. A new lake classification scheme for the Peace-Athabasca Delta (Canada) characterizes hydrological processes that cause lake-level variation. *J. Hydrol.: Reg. Stud.*, 38, 100948. https://doi.org/10.1016/j.ejrh.2021.100948.

Neary, L.K., Remmer, C.R., Owca, T.J., Girard, C.A.M., Kay, M.L., Wiklund, J.A., Imran, A., Hall, R.I., Wolfe, B.B., 2024. Synthesis of a hydrological, water chemistry and contaminants research program in the Peace-Athabasca Delta (Canada) to inform long-term monitoring of shallow lakes. *Environ. Rev.* 32, 688-706. https://doi.org/10.1139/er-2024-0041.

Neary, L.K., Wolfe, B.B., Hall, R.I., 2021b. Hourly lake level data across the Peace-Athabasca Delta (Canada) in 2018 and 2019. Borealis, V1. https://doi.org/https://doi.org/10.5683/SP2/D5TVYG.

Newton, B.W., Farjad, B., Orwin, J.F., 2021. Spatial and temporal shifts in historic and future temperature and precipitation patterns related to snow accumulation and melt regimes in Alberta, Canada. *Water*, 13, 1013. https://doi.org/10.3390/w13081013.

Nielsen, G., 1972. Groundwater Investigation, Peace-Athabasca Delta, Section J. In: Peace-Athabasca Delta Project, Technical reports and appendices: Volume 1: hydrological investigations.

NRBS (Northern River Basins Study), 1996. *Northern Rivers Basins Study—Report to the Ministries*. Alberta Environmental Protection: Edmonton, Alberta. Accessible at: https://www.ceaa.gc.ca/050/documents_staticpost/63919/96375/3-1996-Northern_River_Basins_Study-Report_to_the_Ministers.pdf.

PADPG, 1973. Peace-Athabasca Delta Project, Technical reports and appendices, Volume 1: Hydrological Investigations, Volume 2: Ecological Investigations. Peace-Athabasca Delta Project Group, Delta Implementation Committee, Governments of Alberta, Saskatchewan and Canada.

PADTS, 1996. Final report. Peace-Athabasca Delta Technical Studies, Fort Chipewyan, Alberta, Canada.

Peters, D.L., 2013. Multi-scale hydroclimatic controls on the duration of water in perched wetlands of a cold regions delta, Northwestern Canada. Environment Canada, Saskatoon, Saskatchewan, Canada.

Peters, D.L., Caissie, D., Monk, W.A., Rood, S.B., St-Hilaire, A., 2015. An ecological perspective on floods in Canada. *Can. Water Resour. J.*, 41, 288-306. https://doi.org/10.1080/07011784.2015.1070694.

Peters, D.L., Prowse, T.D., 2006. Generation of streamflow to seasonal high waters in a freshwater delta, northwestern Canada. *Hydrol. Processes*, 20, 4173-4196. https://doi.org/10.1002/hyp.6425.

Peters, D.L., Prowse, T.D., Marsh, P., Lafleur, P.M., Buttle, J.M., 2006a. Persistence of water within perched basins of the Peace-Athabasca Delta, Northern Canada. *Wetlands Ecol. Manage.*, 14, 221-243. https://doi.org/10.1007/s11273-005-1114-1.

Peters, D.L., Prowse, T.D., Pietroniro, A., Leconte, R., 2006b. Flood hydrology of the Peace-Athabasca Delta, northern Canada. *Hydrol. Processes*, 20, 4073-4096. https://doi.org/10.1002/hyp.6420.

Pietroniro, A., Prowse, T., Peters, D.L., 1999. Hydrologic assessment of an inland freshwater delta using multi-temporal satellite remote sensing. *Hydrol. Processes*, 13, 2483-2498. https://doi.org/10.1002/(SICI)1099-1085(199911)13:16%3C2483::AID-HYP934%3E3.0.CO;2-9.

Pomeroy, J.W., Gray, D.M., 1995. Snowcover accumulation, relocation and management. National Hydrology Research Institute, Science Report No. 7. Environment Canada, Saskatoon, Saskatchewan.

Prowse, T.D., Alfredsen, K., Beltaos, S., Bonsal, B.R., Bowden, W.B., Duguay, C.R., Korhola, A., McNamara, J., Vincent, W.F., Vuglinsky, V., Walter Anthony, K.M., 2011. Effects of changes in arctic lake and river ice. *AMBIO*, 40, 63-74. https://doi.org/10.1007/s13280-011-0217-6.

Prowse, T.D., Conly, F.M., 1998. Effects of climatic variability and flow regulation on ice-jam flooding of a northern delta. *Hydrol. Processes*, 12, 1589-1610. https://doi.org/10.1002/(SICI)1099-1085(199808/09)12:10/11<1589::AID-HYP683>3.0.CO;2-G.

Prowse, T.D., Conly, F.M., 2002. A review of hydroecological results of the Northern River Basins Study, Canada. Part 2. Peace-Athabasca Delta. *River Res. Appl.*, 18, 447-460. https://doi.org/10.1002/rra.682.

Prowse, T.D., Demuth, M.N., 1996. Using ice to flood the Peace–Athabasca delta, Canada. *Regul. Rivers: Res. Manage.*, 12, 447-457. https://doi.org/10.1002/(SICI)1099-1646(199607)12:4/5%3C447::AID-RRR404%3E3.0.CO;2-Y.

Prowse, T.D., Furgal, C., Melling, H., Smith, S.L., 2009. Implications of climate change for northern Canada: The physical environment. *AMBIO*, 38, 266-271. https://doi.org/10.1579/0044-7447-38.5.266.

Prowse, T.D., Lalonde, V., 1996. Open-water and ice-jam flooding of a northern delta. *Hydrol. Res.*, 27, 85-100. https://doi.org/10.2166/nh.1996.0021.

Prowse, T.D., Peters, D.L., Marsh, P., 1996. Modelling the Water Balance of the Peace-Athabasca Delta Perched Basins. Peace-Athabasca Delta Technical Studies Report. Fort Smith, Northwest Territories.

Prowse, T.D., Wrona, F.J., Reist, J.D., Gibson, J.J., Hobbie, J.E., Lévesque, L.M., Vincent, W.F., 2006a. Climate change effects on hydroecology of Arctic freshwater ecosystems. *AMBIO*, 35, 347-358. https://doi.org/10.1579/0044-7447(2006)35[347:CCEOHO]2.0.CO;2.

Prowse, T.D., Wrona, F.J., Reist, J.D., Hobbie, J.E., Lévesque, L.M., Vincent, W.F., 2006b. General features of the Arctic relevant to climate change in freshwater ecosystems. *AMBIO*, 35, 330-338. https://doi.org/10.1579/0044-7447(2006)35[330:GFOTAR]2.0.CO;2.

Rautio, M., Dufresne, F., Laurion, I., Bonilla, S., Vincent, W.F., Christoffersen, K.S., 2011. Shallow freshwater ecosystems of the circumpolar Arctic. *Écoscience*, 18, 204-222. https://doi.org/10.2980/18-3-3463.

Remmer, C.R., Owca, T., Neary, L., Wiklund, J.A., Kay, M., Wolfe, B.B., Hall, R.I., 2020a. Delineating extent and magnitude of river flooding to lakes across a northern delta using water isotope tracers. *Hydrol. Processes*, 34, 303–320. https://doi.org/10.1002/hyp.13585.

Remmer, C.R., Neary, L.K., Kay, M.L., Wolfe, B.B., Hall, R.I., 2020b. Multi-year isoscapes of lake water balances across a dynamic northern freshwater delta. *Environ. Res. Lett.*, 15, 104066. https://doi.org/10.1088/1748-9326/abb267.

Romolo, L., Prowse, T.D., Blair, D., Bonsal, B.R., Martz, L.W., 2006. The synoptic climate controls on hydrology in the upper reaches of the Peace River Basin. Part I: snow accumulation. *Hydrol. Processes,* 20, 4097-4111. https://doi.org/10.1002/hyp.6421.

Rood S.B., Strupple, G.W., Gill, K.M., 2015. Century-long records reveal slight, ecoregion-localized changes in Athabasca River flows. *Hydrol. Processes*, 29, 805-816. https://doi.org/10.1002/hyp.10194.

Roulet, N. T., Woo, M.K., 1986. Wetland and lake evaporation in the Low Arctic. *Arct. Alp. Res.*, 18, 195-200. https://doi.org/10.2307/1551129.

Roulet, N.T., Woo, M.K., 1988. Runoff generation in a low Arctic drainage basin. *J. Hydrol.*,101, 213-226. https://doi.org/10.1016/0022-1694(88)90036-4.

Rouse, W.R., Douglas, M.S.V., Hecky, R.E., Hershey, A.E., Kling, G.W., Lesack, L., Marsh, P., McDonald, M., Nicholson, B.J., Roulet, N.T., Smol, J.P., 1997. Effects of climate change on the freshwaters of arctic and subarctic North America. *Hydrol. Processes*, 11, 873-902. https://doi.org/10.1002/(SICI)1099-1085(19970630)11:8<873::AID-HYP510>3.0.CO;2-6.

Rovansek, R.J., Hinzman, L.D., Kane, D.L., 1996. Hydrology of a tundra wetland complex on the Alaskan Arctic Coastal Plain, USA. *Arct. Alp. Res.*, 28, 311-317. https://doi.org/10.2307/1552110.

Schindler, D.W., Smol, J.P., 2006. Cumulative effects of climate warming and other human activities on freshwaters of Arctic and subarctic North America. *AMBIO*, 35, 160-168. https://doi.org/10.1579/0044-7447(2006)35[160:CEOCWA]2.0.CO;2.

Shjeflo, J.B., 1968. Evapotranspiration and water budget of prairie potholes in North Dakota. US Geological Survey Professional Paper. https://doi.org/10.3133/pp585B.

Slaughter, C.W., Mellor, M., Sellmann, P.V., Brown, J., Brown, L., 1975. Accumulating snow to augment the fresh water supply at Barrow, Alaska. US Army Cold Regions Research and Engineering Laboratory, CRREL Special Report, 217.

Smith, L.C., Fayne, J.V., Wang, B., Kyzivat, E.D., Gleason, C J., Harlan, M.E., Langhorst, T., Feng, D., Pavelsky, T.M., Peters, D.L., 2023. Peace-Athabasca Delta water surface elevations and slopes mapped from AirSWOT Ka-band InSAR. *Remote Sens. Lett.*, 14, 1238–1250. https://doi.org/10.1080/2150704X.2023.2280464.

Smol, J.P., 2016. Arctic and Sub-Arctic shallow lakes in a multiple-stressor world: a paleoecological perspective. *Hydrobiologia*, 778, 253-272. https://doi.org/10.1007/s10750-015-2543-3.

Stewart, I.T., Cayan, D.R., Dettinger, M.D., 2004. Changes in snowmelt runoff timing in western North America under abusiness as usual'climate change scenario. *Clim Change,* 62, 217-232. https://doi.org/10.1023/B:CLIM.0000013702.22656.e8.

Stuefer, S.L., Kane, D.L., 2016. Snow retention for increased water supply of shallow Arctic lakes. *Cold Reg. Sci. Technol.*, 123, 32-43. https://doi.org/10.1016/j.coldregions.2015.11.011.

St. Jacques, J.M., Sauchyn, D.J., Zhao, Y., 2010. Northern Rocky Mountain streamflow records: Global warming trends, human impacts or natural variability?. *Geophys. Res. Lett.*, 37. https://doi.org/10.1029/2009GL042045.

Sturm, M., Holmgren, J., McFadden, J.P., Liston, G.E., Chapin, F.S., Racine, C., 2001. Snow–Shrub Interactions in Arctic Tundra: A Hypothesis with Climatic Implications. *J. Clim.*, 14, 336-344. https://doi.org/10.1175/1520-0442(2001)014%3C0336:SSIIAT%3E2.0.CO;2.

Swanson, G. A., Meyer, M. I., Adomaitis, V. A., 1985. Foods consumed by breeding mallards on wetlands of south-central North Dakota. J. *Wildl. Manage.,* 49, 197-203. https://doi.org/10.2307/3801871.

Timoney, K., 2002. A dying delta? A case study of a wetland paradigm. *Wetlands*, 22, 282-300. https://doi.org/10.1672/0277-5212(2002)022[0282:ADDACS]2.0.CO;2.

Timoney, K.P., 2009. Three centuries of change in the Peace–Athabasca Delta, Canada. *Clim. Change*, 93, 485-515. https://doi.org/10.1007/s10584-008-9536-4.

Timoney, K.P., 2013. *The Peace-Athabasca Delta: Portrait of a dynamic ecosystem, The Peace-Athabasca Delta: Portrait of a Dynamic Ecosystem*. The University of Alberta Press, Edmonton, Alberta.

Timoney, K.P., 2020. Observations of recent flooding along the lower Peace and Athabasca Rivers and the Peace-Athabasca Delta. Report for BC Hydro, Burnaby, BC.

Turner, K.W., Wolfe, B.B., Edwards, T.W.D., 2010. Characterizing the role of hydrological processes on lake water balances in the Old Crow Flats, Yukon Territory, Canada, using water isotope tracers. *J. Hydrol*., 386, 103-117. https://doi.org/10.1016/j.jhydrol.2010.03.012.

Turner, K.W., Wolfe, B.B., Edwards, T.W.D., Lantz, T.C., Hall, R.I., Larocque, G., 2014. Controls on water balance of shallow thermokarst lakes and their relations with catchment characteristics: a multi-year, landscape-scale assessment based on water isotope tracers and remote sensing in Old Crow Flats, Yukon (Canada). *Global Change Biol.*, 20, 1585-1603. https://doi.org/10.1111/gcb.12465.

van der Kamp, G., Hayashi, M., Gallén, D., 2003. Comparing the hydrology of grassed and cultivated catchments in the semi-arid Canadian prairies. *Hydrol. Processes*, 17, 559-575. https://doi.org/10.1002/hyp.1157.

Varhola, A., Coops, N.C., Weiler, M., Moore, R.D., 2010. Forest canopy effects on snow accumulation and ablation: An integrative review of empirical results. *J. Hydrol*., 392, 219-233. https://doi.org/10.1016/j.jhydrol.2010.08.009.

Wang, B., Smith, L.C., Gleason, C., Kyzivat, E.D., Fayne, J.V., Harlan, M.E., Langhorst, T., Feng, D., Eidam, E., Munoz, S., Davis, J., Peters, D.L., 2023. Athabasca River Avulsion Underway in the Peace-Athabasca Delta, Canada. *Water Resour. Res.*, 59, e2022WR034114. https://doi.org/10.1029/2022WR034114.

WHC/IUCN, 2017. Reactive monitoring mission to Wood Buffalo National Park; mission report, March 2017. Accessible at http://whc.unesco.org/en/documents/156893.

WHC/IUCN, 2022. Reactive monitoring mission to Wood Buffalo National Park; mission report, August 2022. Accessible at https://whc.unesco.org/en/documents/200340.

Whitfield, P.H., Moore, R.D., Fleming, S.W., Zawadzki, A., 2010. Pacific Decadal Oscillation and the hydroclimatology of western Canada – Review and Prospects. *Can. Water Resour. J.*, 35, 1-28. https://doi.org/10.4296/cwrj3501001.

Wickham, H., 2016. ggplot2: Elegant Graphics for Data Analysis., Media. Springer-Verlag New York.

Wolfe, B.B., Hall, R.I., Edwards, T.W.D., Johnston, J.W., 2012. Developing temporal hydroecological perspectives to inform stewardship of a northern floodplain landscape subject to multiple stressors: paleolimnological investigations of the Peace–Athabasca Delta. *Environ. Rev.*, 20, 191-210. https://doi.org/10.1139/a2012-008.

Wolfe, B.B., Hall, R.I., Edwards, T.W.D., Vardy, S.R., Falcone, M.D., Sjunneskog, C., Sylvestre, F., McGowan, S., Leavitt, P.R., van Driel, P., 2008. Hydroecological responses of the Athabasca Delta, Canada, to changes in river flow and climate during the 20th century. *Ecohydrology*, 1, 131-148. https://doi.org/10.1002/eco.13.

Wolfe, B.B., Hall, R.I., Last, W.M., Edwards, T.W.D., English, M.C., Karst-Riddoch, T.L., Paterson, A., Palmini, R., 2006. Reconstruction of multi-century flood histories from oxbow lake sediments, Peace-Athabasca Delta, Canada. *Hydrol. Processes*, 20, 4131-4153. https://doi.org/10.1002/hyp.6423.

Wolfe, B.B., Hall, R.I., Wiklund, J.A., Kay, M.L., 2020. Past variation in Lower Peace River ice-jam flood frequency. *Environ. Rev.*, 28, 209-217. https://doi.org/10.1139/er-2019-0047.

Wolfe, B.B., Karst-Riddoch, T.L., Hall, R.I., Edwards, T.W.D., English, M.C., Palmini, R., McGowan, S., Leavitt, P.R., Vardy, S.R., 2007. Classification of hydrological regimes of northern floodplain basins (Peace-Athabasca Delta, Canada) from analysis of stable isotopes ($\delta^{18}O$, $\delta^{2}H$) and water chemistry. *Hydrol. Process.*, 21, 151-168. https://doi.org/10.1002/hyp.6229.

Wolfe, B.B., Karst-Riddoch, T.L., Vardy, S.R., Falcone, M.D., Hall, R.I., Edwards, T.W.D., 2005. Impacts of climate and river flooding on the hydro-ecology of a floodplain basin, Peace-Athabasca Delta, Canada since A.D. 1700. *Quat. Res.*, 64, 147-162. https://doi.org/10.1016/j.yqres.2005.05.001.

Woo, M.K., 1980. Hydrology of a small lake in the Canadian High Arctic. *Arct. Alp. Res.*, 12, 227-235. https://doi.org/10.2307/1550519.

Woo, M.K., 2012. Snow Cover. In: Permafrost Hydrology. Springer, Berlin, Heidelberg. https://doi.org/10.1007/978-3-642-23462-0_4.

Woo, M.K., Heron, R., Steer, P., 1981. Catchment hydrology of a High Arctic lake. *Cold Reg. Sci.* Technol., 5, 29-41. https://doi.org/10.1016/0165-232X(81)90038-0.

Woo, M.K., Thorne, R., 2008. Analysis of cold season streamflow response to variability of climate in north-western North America. *Hydrol. Res.*, 39, 257-265. https://doi.org/10.2166/nh.2008.102.

Wood Buffalo National Park (WBNP), 2019. World Heritage Site Action Plan. *Parks Canada*. Accessible at https://www.pc.gc.ca/en/pn-np/nt/woodbuffalo/info/action.

Wood Buffalo National Park (WBNP), 2022. Report on the State of Conservation of Wood Buffalo National Park World Heritage Site (Canada) property ID 256 in response to: World Heritage Committee decision 44 COM 7B.190. *Parks Canada*. Accessible at https://whc.unesco.org/en/documents/191641.

Wrona, F.J., Johansson, M., Culp, J.M., Jenkins, A., Mård, J., Myers-Smith, I.H., Prowse, T.D., Vincent, W.F., Wookey, P.A., 2016. Transitions in Arctic ecosystems: Ecological implications of a changing hydrological regime. *J. Geophys. Res. G: Biogeosci.*, 121, 650-674. https://doi.org/10.1002/2015JG003133.

Yi, Y., Brock, B.E., Falcone, M.D., Wolfe, B.B., Edwards, T.W.D., 2008. A coupled isotope tracer method to characterize input water to lakes. *J. Hydrol.*, 350, 1-13. https://doi.org/10.1016/j.jhydrol.2007.11.008.

Zeileis, A., Grothendieck, G., 2005. Zoo: S3 infrastructure for regular and irregular time series. *J. Stat. Softw.*, 14, 1-27. https://doi.org/10.18637/jss.v014.i06.

Zhang, F., Mosaffa, M., Chu, T., Lindenschmidt, K.E., 2017. Using remote sensing data to *parameterize* ice jam modeling for a northern inland delta. *Water*, 9, 306. https://doi.org/10.3390/w9050306.

Chapter 4 | Conclusions and Recommendations

At the Peace-Athabasca Delta (PAD; northeastern Alberta), the need for effective aquatic ecosystem monitoring has long been motivated by concerns stemming from decline of lake levels by multiple potential stressors, predominantly natural resource development and climate change (PADPG, 1973; PADIC, 1987; PADTS, 1996; Timoney, 2013). Implementing an effective monitoring program relies upon research to generate comprehensive and advanced understanding of the key processes operating at a range of spatial and temporal scales (Franklin et al., 1999; Lindenmayer et al., 2022). The ranges may span days at a specific location to several decades across the entire landscape. Obtaining measurements across these scales of space and time can be difficult because the PAD is large (~6000 km^2), remote, and hydrologically complex (Timoney, 2013; Neary et al., 2024). In light of these challenges and the pressing need for a monitoring program, a 7-year research project was conducted between 2015 and 2021 at 63 lakes and 9 river sites to improve knowledge of the hydrological processes that regulate the water balance and depth variation of lakes across the PAD and inform the design of an aquatic ecosystem monitoring program aimed at tracking hydrological changes and their causative processes (Neary et al., 2024). Commonly, scientific research guides the development and operation of monitoring programs, as demonstrated at the PAD by Neary et al. (2024) and other northern lake-rich landscapes by Tondu et al. (2013) and MacDonald et al. (2021). Investment in systematic, repeated measurements over many years may also, on occasion, capture changes caused by unanticipated phenomena which may be sufficiently important to warrant further scientific investigation (Franklin et al., 1999; Wintle et al., 2010). This thesis reports on research that was triggered by observations, made during the last two years of the 7-year research project at the PAD, which provided opportunities to address research questions that were not among the original objectives when the project was launched. Observations included 1) during 2020-2021, water isotope composition decreased below the long-term range of variation at an index lake (PAD 18) used for isotope mass-balance modeling of lakes in the PAD, and 2) in spring of 2020, water levels rose at lakes beyond the reach of ice-jam induced floodwaters. These observations raised questions concerning parameterization of the isotope mass-balance model used to assess water balance of lakes in the PAD and the importance of snowmelt on lake water balances.

In Chapter 2, titled "Value of long-term isotope monitoring of an index lake for tracking changes in lake water balances across a northern freshwater landscape", I explored if the sudden, persistent decline of water isotope composition in the index lake PAD 18 during 2020-2021 (average: $\delta^{18}O$ = -10.30 ± 0.41‰, $\delta^{2}H$ = -108.29 ± 1.80‰; d-excess = -25.93 ± 1.71‰) from consistently higher water composition measured during 2000-2006 and 2014-2019 ($\delta^{18}O$ = -9.15 ± 0.42‰, $\delta^{2}H$ = -103.92 ± 1.76‰; d-excess = -30.56 ± 2.88‰) could be accounted for by the 4.6% increase in open-water season relative humidity and, if so, what effect this has on water balance modelling of lakes in the PAD. For the past two decades, PAD 18 served as an important benchmark (δ_{SSL}; i.e., isotope composition of a terminal basin where evaporation = inflow) for constraining estimates of the isotope composition of input waters and isotope mass-balance modelling of lakes across the landscape (Yi et al., 2008; Remmer et al., 2020a,b). An independent calculation of δ_{SSL} using formulation by Gonfiantini (1986) and flux-weighted air temperature and relative humidity data from 2020-2021 ($\delta^{18}O$ = -10.26‰; $\delta^{2}H$ = -107.99‰) was determined to be equivalent to the average measured isotope composition of PAD 18 during 2020-2021. Results revealed the lake water isotope composition re-equilibrated with the atmosphere following the 4.6% rise of relative humidity. The use of the lower isotope composition of PAD 18 resulted in improved parameterization of the isotope mass-balance model for evaluating water balances in the PAD for 2020-2021. Comparison of isotope-inferred evaporation-to-inflow (E/I) ratios at 61 lakes in the PAD in July 2021 using the 2020-2021 isotope framework versus the previous 2015-2019 isotope framework revealed minor differences between the two frameworks when E/I ratios are low (mean E/I ratio = 0.18 and 0.21 for the 2015–2019 and 2020–2021 isotope frameworks, respectively). The difference, however, becomes meaningful at higher E/I ratios (mean E/I ratio = 0.34 and 0.43 for the 2015–2019 and 2020–2021 isotope frameworks, respectively). Given that lake-level drawdown remains a major concern at the PAD (MCFN, 2014), continued sampling of PAD 18 for water isotope composition and assessment of meteorological conditions is recommended to inform ongoing evaluation of the isotope framework used for isotope mass-balance modelling of lake water balances in the PAD.

In Chapter 3, titled "Overlooked and underrated: Snowmelt runoff rivals influence of river floodwaters on lake-level rise at a cold region freshwater delta", I explored the influence of snowmelt runoff on lake levels in perched lakes of the PAD. Extensive flooding occurred during

spring of 2020 (Timoney, 2020; Desrochers et al., 2023), but examination of water-depth measurements revealed that water levels rose in almost all the 59 lakes where repeated measurements had been obtained since 2018, including most of the lakes that did not receive input of floodwaters. At the PAD, lake-level drawdown has been widely attributed to alteration of the Peace River's ice-jam flood regime (Beltaos et al., 2006; Peters and Prowse, 2006; Lamontagne et al., 2021; Beltaos, 2023), but there has been little to no assessment of the contributions from snowmelt to lake levels within the delta. Measurements of water isotope and water depth were combined to evaluate and partition the contributions from snowmelt and floodwaters to lake-level rise. Meteorological data show maximum snow water equivalent (SWE) was higher (80.4 mm) than the long-term median (70.4 mm) and a rapid melt (10.1 mm/day) occurred prior to sampling in May 2020. Results identify the median lake-level rise from snowmelt input at non-flooded lakes (0.32 m) is comparable to the median lake-level rise from river floodwaters at flooded lakes (0.26 m; Mann-Whitney U Test, $U = 312$, $p = 0.640$, $n = 27, 25$). Geospatial analysis revealed that lake-level rise by snowmelt was greatest in regions where greater topographic relief and denser vegetation entrap wind-distributed snow from adjacent flat, sparsely vegetated terrain, whereas rise due to floodwater input was greatest in the lower relief flood-prone areas, particularly in the Athabasca sector. Exploration of long-term meteorological records since 1963 revealed that comparable values of peak snow water equivalent and melt rate as in 2020 were prevalent between the early 1960s and late 1980s but have occurred only once since 1987. A meteorological shift to thinner snowpack appears to have contributed substantially to the drawdown of shallow perched lakes in the delta since the late 1980s, which counters a long- and widely-held paradigm that lakes in the delta have drawn down due to a decline in the frequency of ice-jam flooding (Beltaos et al., 2006; Peters and Prowse, 2006, Peters et al., 2006; Beltaos, 2023). Mitigative actions to counter trends towards thinner snowpack, may include installation of artificial snow fences and use of snow-making machinery to augment snowmelt runoff to selected lakes at high risk of desiccation and cultural importance, but they require rigorous assessment of their feasibility and risk-benefit ratio. To improve estimates of snowmelt input proportions using the isotope-based binary mixing model, snow samples should be collected for analysis of water isotope composition to use as an end member. The approaches used at the PAD to elucidate the role of snowmelt runoff on lake levels and water balance over space and time are also applicable at other northern floodplains

downstream of the PAD, such as the Slave River and Mackenzie River deltas where, similarly, river dynamics are the primary focus (Marsh and Lesack, 1996; Brock et al., 2008).

The knowledge and recommendations provided in this thesis come at a critical time when UNESCO is contemplating enlisting Wood Buffalo National Park (WBNP) as 'World Heritage in Danger' (WHC/IUCN, 2022). In response to a petition by the Mikisew Cree First Nation (MCFN, 2014), which expressed concerns about declining water abundance in the PAD, a UNESCO monitoring mission provided 17 recommendations to guide stewardship and management of WBNP (WHC/IUCN, 2017). Based on these recommendations, a federal Action Plan was developed to implement specific actions aimed at protecting the 'Outstanding Universal Value' of WBNP (WBNP, 2019, 2022). One of the goals of the Action Plan is "to enhance monitoring and to improve the assessment of current and future water quantity conditions in the Peace and Athabasca River Basins" (WBNP, 2019; pg. 48). For the PAD, however, this requires a depth of understanding of the hydrological processes affecting lake water balances and water levels. In this thesis, knowledge has been improved to enhance monitoring about the influence of changes in relative humidity on isotope-based modelling of lake water balances and the influence of snowmelt runoff on lake depth. The research in Chapter 3 communicated the first integration of water isotope composition and water depth measurements in lakes across the PAD, which enabled the ability to partition the lake-level rise to two distinct input water sources (snowmelt and river floodwater). Integration of these measurements may be very valuable for assessing the success of strategic releases of water from the W.A.C Bennett Dam to induce ice-jam floods, which has been identified as a mitigative action as part of the federal Action Plan (WBNP, 2019) to maintain water levels of the delta's perched basins. When releases occur, it will be important to delineate the extent of floodwaters in the delta and quantify the effects of snowmelt runoff versus floodwaters on lake-level change. Application of isotope-based methods, however, require careful evaluation of the values of key parameters used in isotope mass-balance models, as these can be sensitive to changes in relative humidity, as presented in Chapter 2. As demonstrated by the research reported in this thesis and advocated by Wintle et al. (2010), continued monitoring and building on long-term datasets has value for continued evaluation that can lead to rapid corroboration of emerging hypotheses and detection of the unexpected.

References (Chapters 1 and 4)

Anderson, L., Birks, J., Rover, J., Guldager, N., 2013. Controls on recent Alaskan lake changes identified from water isotopes and remote sensing. *Geophys. Res. Lett.*, 40, 3413-3418. https://doi.org/10.1002/grl.50672.

Arctic Monitoring and Assessment Programme (AMAP), 2021. AMAP Arctic Climate Change Update 2021: Key Trends and Impacts. Arctic Monitoring and Assessment Programme (AMAP), Tromsø, Norway. Accessible at https://www.amap.no/publications.

Athabasca Chipewyan First Nation (ACFN), 2021. A History of Wood Buffalo National Park's Relations with the Denésuline Final Report. Accessible at http://acfn.woodbuffaloexpulsion.ca/.

Beltaos, S., 2014. Comparing the impacts of regulation and climate on ice-jam flooding of the Peace-Athabasca Delta. *Cold Reg. Sci. Technol.*, 108, 49-58. https://doi.org/10.1016/j.coldregions.2014.08.006.

Beltaos, S., 2023. The drying Peace–Athabasca Delta, Canada: Review and synthesis of cryo-hydrologic controls and projections to future climatic conditions. *Sustainability*, 15, 2103. https://doi.org/10.3390/su15032103.

Beltaos, S., Prowse, T., Bonsal, B., MacKay, R., Romolo, L., Pietroniro, A., Toth, B., 2006. Climatic effects on ice-jam flooding of the Peace-Athabasca Delta. *Hydrol. Processes*, 20, 4031-4050. https://doi.org/10.1002/hyp.6418.

Bouchard, F., Turner, K.W., MacDonald, L.A., Deakin, C., White, H., Farquharson, N., Medeiros, A.S., Wolfe, B.B., Hall, R.I., Pienitz, R., Edwards, T.W.D., 2013. Vulnerability of shallow subarctic lakes to evaporate and desiccate when snowmelt runoff is low. *Geophys. Res. Lett.*, 40, 6112-6117. https://doi.org/10.1002/2013GL058635.

Brock, B.E., Wolfe, B.B., Edwards, T.W.D., 2008. Spatial and temporal perspectives on spring break-up flooding in the Slave River Delta, NWT. *Hydrol. Processes*, 22, 4058-4072. https://doi.org/10.1002/hyp.7008.

Brock, B.E., Yi, Y., Clogg-Wright, K.P., Edwards, T.W.D, Wolfe, B.B., 2009. Multi-year landscape-scale assessment of lakewater balances in the Slave River Delta, NWT, using water isotope tracers. *J. Hydrol.*, 379, 81-91. https://doi.org/10.1016/j.jhydrol.2009.09.046.

Brooks, J.R., Gibson, J.J., Birks, S.J., Weber, M.H., Rodecap, K.D., Stoddard, J.L., 2014. Stable isotope estimates of evaporation: Inflow and water residence time for lakes across the United States as a tool for national lake water quality assessments. *Limnol. Oceanogr.*, 59, 2150-2165. https://doi.org/10.4319/lo.2014.59.6.2150.

Clark, I.D., Fritz, P., 1997. Environmental Isotopes in Hydrogeology (1st ed). *CRC Press*. https://doi.org/10.1201/9781482242911.

Desrochers, N.M., Peters, D.L., Siles, G., Cauvier Charest, E., Trudel, M., Leconte, R., 2023. A remote sensing view of the 2020 extreme lake-expansion flood event into the Peace–Athabasca Delta floodplain—implications for the future SWOT mission. *Remote Sens.*, 15, 1278. https://doi.org/10.3390/rs15051278.

Edwards, T.W.D., Wolfe, B.B., Gibson, J.J., Hammarlund, D., 2004. Use of water isotope tracers in high latitude hydrology and paleohydrology, in: R. Pienitz, M.S.V. Douglas and J.P. Smol (Eds.), Long-term environmental change in Arctic and Antarctic Lakes, *Springer*, 187-207.

Franklin, J.F., Harmon, M.E., Swanson, F.J., 1999. Complementary roles of research and monitoring: lessons from the US LTER Program and Tierra del Fuego. In: *Toward a Unified Framework for Inventorying and Monitoring Forest Ecosystem Resources.* USDA Forest Service Proceedings RMRS-P-12, Guadalajara, Mexico, November 1-6, 1998.

Gibson, J.J., Birks, S.J., Yi, Y., 2016a. Higher tritium concentrations measured in permafrost thaw lakes in northern Alberta. *Hydrol. Processes*, 30, 245-249. https://doi.org/10.1002/hyp.10599.

Gibson, J.J., Birks, S.J., Yi, Y., 2016b. Stable isotope mass balance of lakes: A contemporary perspective. Quat. *Sci. Rev.*, 131, 316-328. https://doi.org/10.1016/j.quascirev.2015.04.013.

Gibson, J.J., Yi, Y., Birks, S.J., 2016c. Isotope-based partitioning of streamflow in the oil sands region, northern Alberta: Towards a monitoring strategy for assessing flow sources and water quality controls. *J. Hydrol.: Reg. Stud.*, 5, 131-148. https://doi.org/10.1016/j.ejrh.2015.12.062.

Intergovernmental Panel of Climate Change (IPCC), 2021. Climate Change 2021: The Physical Science Basis. Contribution of Working Group I to the Sixth Assessment Report of the Intergovernmental Panel on Climate Change. *Cambridge University Press*, Cambridge. https://doi.org/10.1017/9781009157896.

Kay, M.L., Wiklund, J.A., Remmer, C.R., Neary, L.K., Brown, K., Ghosh, A., MacDonald, E., Thomson, K., Vucic, J.M., Wesenberg, K., Hall, R.I., Wolfe, B.B., 2019. Bi-directional hydrological changes in perched basins of the Athabasca Delta (Canada) in recent decades caused by natural processes. *Environ. Res. Commun.*, 1, 081001. https://doi.org/10.1088/2515-7620/ab37e7.

Lamontagne, J.R., Jasek, M., Smith, J.D., 2021. Coupling physical understanding and statistical modeling to estimate ice jam flood frequency in the northern Peace-Athabasca Delta under climate change. *Cold Reg. Sci. Technol.,* 192, 103383. https://doi.org/10.1016/j.coldregions.2021.103383.

Lantz, T.C., Turner, K.W., 2015. Changes in lake area in response to thermokarst processes and climate in Old Crow Flats, Yukon. *J. Geophys. Res. G: Biogeosci.*, 120, 513-524. https://doi.org/10.1002/2014JG002744.

Lindenmayer, D.B., Lavery, T., Scheele, B.C., 2022. Why We Need to Invest in Large-Scale, Long-Term Monitoring Programs in Landscape Ecology and Conservation Biology. *Curr. Landscape Ecol. Rep*., 7, 137–146. https://doi.org/10.1007/s40823-022-00079-2.

MacDonald, L A., Turner, K.W., McDonald, I., Kay, M.L., Hall, R.I., Wolfe, B.B., 2021. Isotopic evidence of increasing water abundance and lake hydrological change in Old Crow Flats, Yukon, Canada. *Environ. Res. Lett.*, 16, 124024. https://doi.org/10.1088/1748-9326/ac3533.

MacDonald, L.A., Wolfe, B.B., Turner, K.W., Anderson, L., Arp, C.D., Birks, S.J., Bouchard, F., Edwards, T.W.D., Farquharson, N., Hall, R.I., McDonald, I., Narancic, B., Ouimet, C., Pienitz, R., Tondu, J., White, H., 2017. A synthesis of thermokarst lake water balance in high-latitude regions of North America from isotope tracers. *Arct. Sci.*, 3, 118-149. https://doi.org/10.1139/as-2016-0019.

Macrae, M.L., Brown, L.C., Duguay, C.R., Parrott, J.A., Petrone, R.M., 2014. Observed and Projected Climate Change in the Churchill Region of the Hudson Bay Lowlands and Implications for Pond Sustainability. *Arct. Antarct. Alp. Res.*, 46, 272–285. https://doi.org/10.1657/1938-4246-46.1.272.

Marsh, P., Lesack, L.F., 1996. The hydrologic regime of perched lakes in the Mackenzie Delta: potential responses to climate change. *Limnol. Oceanogr.,* 41, 849-856. https://doi.org/10.4319/lo.1996.41.5.0849.

Marsh, P., Russell, M., Pohl, S., Haywood, H., Onclin, C., 2009. Changes in thaw lake drainage in the Western Canadian Arctic from 1950 to 2000. *Hydrol. Processes*, 23, 145-158. https://doi.org/10.1002/hyp.7179.

Medeiros, A.S., Wood, P., Wesche, S.D., Bakaic, M., Peters, J.F., 2017. Water security for northern peoples: review of threats to Arctic freshwater systems in Nunavut, Canada. *Reg. Environ. Change*, 17, 635-647. https://doi.org/10.1007/s10113-016-1084-2.

Mikisew Cree First Nation (MCFN), 2014. Petition to the World Heritage Committee Requesting Inclusion of Wood Buffalo National Park on the List of World Heritage in Danger. Accessible at https://cpawsnab.org/wp-content/uploads/2018/03/Mikisew_Petition_respecting_UNESCO_Site_256_-_December_8_2014.pdf.

Narancic, B., Wolfe, B.B., Pienitz, R., Meyer, H., Lamhonwah, D., 2017. Landscape-gradient assessment of thermokarst lake hydrology using water isotope tracers. *J. Hydrol.*, 545, 327-338. https://doi.org/10.1016/j.jhydrol.2016.11.028.

Neary, L.K., Remmer, C.R., Krist, J., Wolfe, B.B., Hall, R.I., 2021. A new lake classification scheme for the Peace-Athabasca Delta (Canada) characterizes hydrological processes that cause lake-level variation. *J. Hydrol.: Reg. Stud.*, 38, 100948. https://doi.org/10.1016/j.ejrh.2021.100948.

Neary, L.K., Remmer, C.R., Owca, T.J., Girard, C.A.M., Kay, M.L., Wiklund, J.A., Imran, A., Hall, R.I., Wolfe, B.B., 2024. Synthesis of a hydrological, water chemistry and contaminants research program in the Peace-Athabasca Delta (Canada) to inform long-term monitoring of shallow lakes. *Environ. Rev.* 32, 688-706. https://doi.org/10.1139/er-2024-0041.

Peace-Athabasca Delta Implementation Committee (PADIC), 1987. Peace-Athabasca Delta Water Management Works Evaluation – Final Report. Peace-Athabasca Implementation Committee, Governments of Alberta, Saskatchewan, and Canada. Accessible at https://publications.gc.ca/collections/collection_2017/eccc/En4-315-1987-eng.pdf.

Peace-Athabasca Delta Project Group (PADPG), 1973. Peace–Athabasca Delta Project, technical report and appendices, Volume 1: Hydrological Investigations, Volume 2: Ecological investigations.

Peace-Athabasca Delta Technical Studies Group (PADTS), 1996. Final Report. PADTS Steering Committee, Fort Chipewyan, Alberta.

Peters, D.L., Prowse, T.D., 2006. Generation of streamflow to seasonal high waters in a freshwater delta, northwestern Canada. *Hydrol. Processes*, 20, 4173-4196. https://doi.org/10.1002/hyp.6425.

Peters, D.L., Prowse, T.D., 2001. Regulation effects on the lower Peace River, Canada. *Hydrol. Processes*, 15, 3181-3194. https://doi.org/10.1002/hyp.321.

Peters, D.L., Prowse, T.D., Marsh, P., Lafleur, P.M., Buttle, J.M., 2006. Persistence of water within perched basins of the Peace-Athabasca Delta, Northern Canada. *Wetlands Ecol. Manage.*, 14, 221-243. https://doi.org/10.1007/s11273-005-1114-1.

Prowse, T.D., Conly, F.M., 2002. A review of hydroecological results of the Northern River Basins Study, Canada. Part 2. Peace-Athabasca Delta. *River Res. Appl.*, 18, 447-460. https://doi.org/10.1002/rra.682.

Prowse, T.D., Conly, F.M., 1998. Effects of climatic variability and flow regulation on ice-jam flooding of a northern delta. *Hydrol. Processes*, 12, 1589-1610. https://doi.org/10.1002/(SICI)1099-1085(199808/09)12:10/11<1589::AID-HYP683>3.0.CO;2-G.

Prowse, T.D., Furgal, C., Bonsal, B.R., Edwards, T.W.D., 2009. Climatic conditions in northern Canada: past and future. *Ambio*, 257-265. https://doi.org/10.1579/0044-7447-38.5.257.

Remmer, C.R., Owca, T., Neary, L., Wiklund, J.A., Kay, M., Wolfe, B.B., Hall, R.I., 2020a. Delineating extent and magnitude of river flooding to lakes across a northern delta using water isotope tracers. *Hydrol. Processes*, 34, 303–320. https://doi.org/10.1002/hyp.13585.

Remmer, C.R., Neary, L.K., Kay, M.L., Wolfe, B.B., Hall, R.I., 2020b. Multi-year isoscapes of lake water balances across a dynamic northern freshwater delta. *Environ. Res. Lett.*, 15, 104066. https://doi.org/10.1088/1748-9326/abb267.

Rouse, W.R., Douglas, M.S.V., Hecky, R.E., Hershey, A.E., Kling, G.W., Lesack, L., Marsh, P., McDonald, M., Nicholson, B.J., Roulet, N.T., Smol, J.P., 1997. Effects of climate change on the freshwaters of arctic and subarctic North America. *Hydrol. Processes*, 11, 873-902. https://doi.org/10.1002/(SICI)1099-1085(19970630)11:8<873::AID-HYP510>3.0.CO;2-6.

Saros, J.E., Arp, C.D., Bouchard, F., Comte, J., Couture, R.M., Dean, J.F., Lafrenière, M., MacIntyre, S., McGowan, S., Rautio, M., Prater, C., Tank, S.E., Walvoord, M., Wickland, K.P., Antoniades, D., Ayala-Borda, P., Canario, J., Drake, T.W., Folhas, D., Hazuková, V., Kivilä, H., Klanten, Y., Lamoureux, S., Laurion, I., Pilla, R.M., Vonk, J.E., Zolkos, S., Vincent, W.F., 2023. Sentinel responses of Arctic freshwater systems to climate: linkages, evidence, and a roadmap for future research. *Arct. Sci.*, 9, 356-392. https://doi.org/10.1139/as-2022-0021.

Sauchyn, D.J., St-Jacques, J-M., Luckman, B.H., 2015. Long-term reliability of the Athabasca River (Alberta, Canada) as the water source for oil sands mining. *Proc. Natl. Acad. Sci. U.S.A.,* 112, 12621-12626. https://doi.org/10.1073/pnas.1509726112.

Schindler, D.W., Donahue, W.F., 2006. An impending water crisis in Canada's western prairie provinces. *Proc. Natl. Acad. Sci. U.S.A.*, 103, 7210-7216. https://doi.org/10.1073/pnas.0601568103.

Schindler, D.W., Smol, J.P., 2006. Cumulative effects of climate warming and other human activities on freshwaters of Arctic and subarctic North America. *AMBIO*, 35, 160-168. https://doi.org/10.1579/0044-7447(2006)35[160:CEOCWA]2.0.CO;2.

Smol, J.P., 2016. Arctic and Sub-Arctic shallow lakes in a multiple-stressor world: a paleoecological perspective. *Hydrobiologia*, 778, 253–272. https://doi.org/10.1007/s10750-015-2543-3.

Smol, J.P., Douglas, M.S., 2007. Crossing the final ecological threshold in high Arctic ponds. *Proc. Natl. Acad. Sci. U.S.A.*, 104, 12395-12397. https://doi.org/10.1073/pnas.0702777104.

Timoney, K.P., 2020. Observations of recent flooding along the lower Peace and Athabasca Rivers and the Peace-Athabasca Delta. Report for BC Hydro, Burnaby, BC.

Timoney, K.P., 2013. The Peace-Athabasca Delta: Portrait of a dynamic ecosystem, The Peace-Athabasca Delta: Portrait of a Dynamic Ecosystem. *The University of Alberta Press*, Edmonton.

Tondu, J.M., Turner, K.W., Wiklund, J.A., Wolfe, B.B., Hall, R.I., McDonald, I., 2016. Limnological evolution of Zelma Lake, a recently drained thermokarst lake in Old Crow Flats (Yukon, Canada). *Arct. Sci.*, 3, 220-236. https://doi.org/10.1139/as-2016-0012.

Tondu, J.M.E., Turner, K.W., Wolfe, B.B., Hall, R.I., Edwards, T.W.D., McDonald, I., 2013. Using Water Isotope Tracers to Develop the Hydrological Component of a Long-Term Aquatic Ecosystem Monitoring Program for a Northern Lake-Rich Landscape. *Arct. Antarct. Alp. Res.*, 45, 594-614. https://doi.org/10.1657/1938-4246-45.4.594.

Turner, K.W., Wolfe, B.B., Edwards, T.W.D, Lantz, T.C., Hall, R.I., Larocque, G., 2014. Controls on water balance of shallow thermokarst lakes and their relations with catchment characteristics: a multi-year, landscape-scale assessment based on water isotope tracers and remote sensing in Old Crow Flats, Yukon (Canada). *Global Change Biol.*, 20, 1585-1603. https://doi.org/10.1111/gcb.12465.

Vannini, P., Vannini, A., 2019. The exhaustion of wood buffalo national park: Mikisew Cree First Nation experiences and perspectives. *Int. Rev. Qual. Res.*, 12, 278-303. https://doi.org/10.1525/irqr.2019.12.3.278.

Walsh, J.E., Ballinger, T.J., Euskirchen, E.S., Hanna, E., Mård, J., Overland, J.E., Tangen, H., Vihma, T., 2020. Extreme weather and climate events in northern areas: A review. *Earth Sci. Rev.*, 209, 103324. https://doi.org/10.1016/j.earscirev.2020.103324.

WHC/IUCN, 2017. Reactive monitoring mission to Wood Buffalo National Park, Canada; mission report March 2017. *United Nations Educational, Scientific and Cultural Organization.* https://whc.unesco.org/en/documents/156893.

WHC/IUCN, 2022. Reactive monitoring mission to Wood Buffalo National Park, Canada; mission report August 2022. *United Nations Educational, Scientific and Cultural Organization.* https://whc.unesco.org/en/documents/200340.

Wintle, B.A., Runge, M.C., Bekessy, S. A., 2010. Allocating monitoring effort in the face of unknown unknowns. *Ecol. Lett.*, 13, 1325-1337. https://doi.org/10.1111/j.1461-0248.2010.01514.x.

Wolfe, B.B., Hall, R.I., Edwards, T.W.D., Johnston, J.W., 2012. Developing temporal hydroecological perspectives to inform stewardship of a northern floodplain landscape subject to multiple stressors: paleolimnological investigations of the Peace–Athabasca Delta. *Environ. Rev.*, 20, 191-210. https://doi.org/10.1139/a2012-008.

Wolfe, B.B., Hall, R.I., Last, W.M., Edwards, T.W.D, English, M.C., Karst-Riddoch, T.L., Paterson, A., Palmini, R., 2006. Reconstruction of multi-century flood histories from

oxbow lake sediments, Peace-Athabasca Delta, Canada. *Hydrol. Processes*, 20, 4131-4153. https://doi.org/10.1002/hyp.6423.

Wolfe, B.B., Karst-Riddoch, T.L., Hall, R.I., Edwards, T.W.D., English, M.C., Palmini, R., McGowan, S., Leavitt, P.R., Vardy, S.R., 2007. Classification of hydrological regimes of northern floodplain basins (Peace-Athabasca Delta, Canada) from analysis of stable isotopes ($\delta^{18}O$, $\delta 2H$) and water chemistry. *Hydrol. Process.*, 21, 151-168. https://doi.org/10.1002/hyp.6229.

Wolfe, B.B., Light, E.M., Macrae, M.L., Hall, R.I., Eichel, K., Jasechko, S., White, J., Fishback, L., Edwards, T.W.D., 2011. Divergent hydrological responses to 20th century climate change in shallow tundra ponds, western Hudson Bay Lowlands. *Geophys. Res. Lett.*, 38. https://doi.org/10.1029/2011GL049766.

Wood Buffalo National Park (WBNP), 2019. World Heritage Site Action Plan. *Parks Canada*. Accessible at https://www.pc.gc.ca/en/pn-np/nt/woodbuffalo/info/action.

Wood Buffalo National Park (WBNP), 2022. Report on the State of Conservation of Wood Buffalo National Park World Heritage Site (Canada) property ID 256 in response to: World Heritage Committee decision 44 COM 7B.190. *Parks Canada*. Accessible at https://whc.unesco.org/en/documents/191641.

Yi, Y., Brock, B.E., Falcone, M.D., Wolfe, B.B., Edwards, T.W.D., 2008. A coupled isotope tracer method to characterize input water to lakes. *J. Hydrol.*, 350, 1-13. https://doi.org/10.1016/j.jhydrol.2007.11.008.

Appendices

Appendix 1 (Chapter 2)

This Appendix presents the available photographs of PAD 18 obtained during fieldwork in 2000-2021 to show that the lake level has remained relatively constant relative to a distinctive former high-water mark on bedrock along the lakeshore. Images are presented from October 2000, June 2002, May 2003, May 2018, May 2019, September 2020, and May 2021.

October 2000





June 2002



May 2003



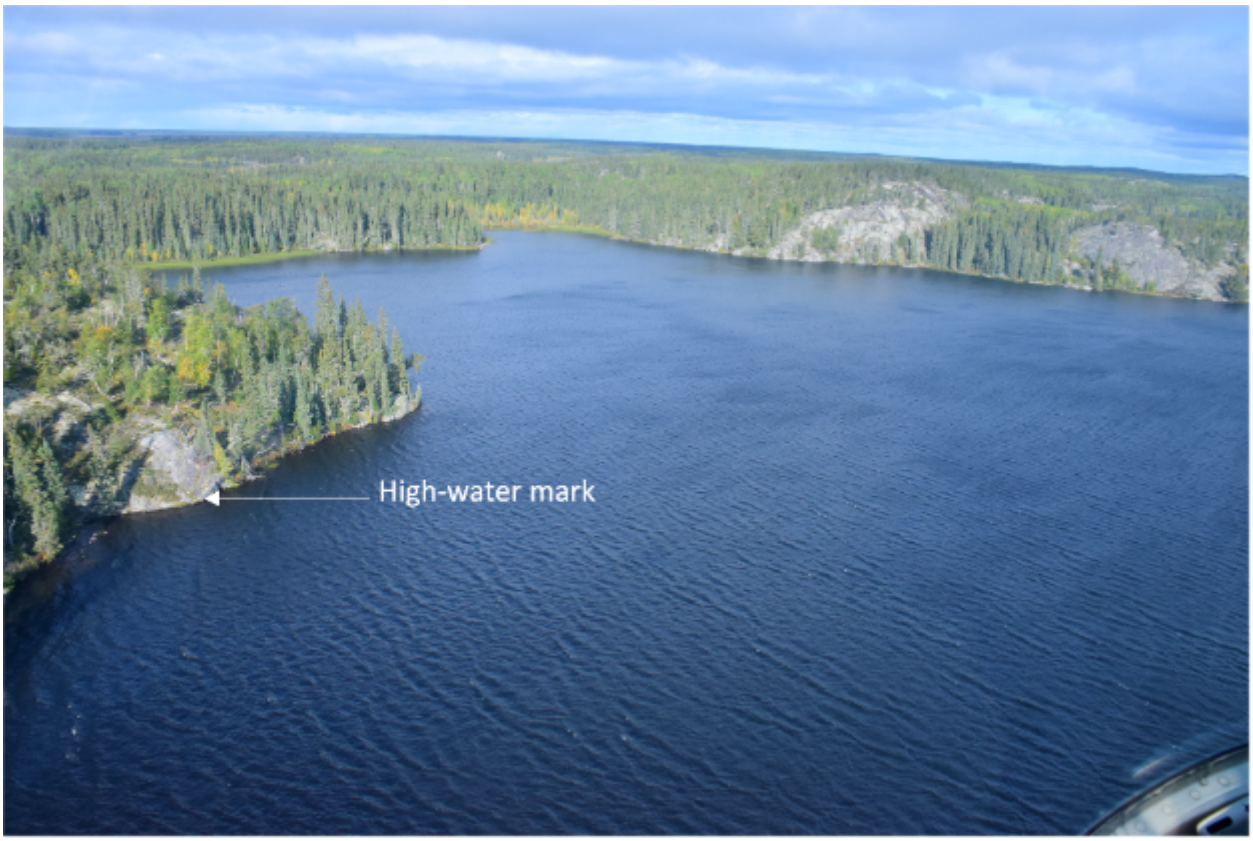
May 2018



May 2019



September 2020



May 2021



Appendix 2 (Chapter 3)

Table A2.1: Water isotope compositions ($\delta^{18}O$, $\delta^{2}H$), *in situ* measurements of specific conductivity (µS/cm) and turbidity (NTU), and key observations contained in field notes collected in May 2020 from 59 lakes and 4 river sites in the Peace-Athabasca Delta, used to determine the flood status of each lake during spring 2020. Turbidity values too low to be quantified, according to the standard, are indicated as below limit of quantification (BLQ).

Site ID	Water isotope composition		Specific conductivity (µS/cm)	Turbidity (NTU)	Field notes	Flood status
	$\delta^{18}O$ (‰VSMOW)	$\delta^{2}H$ (‰VSMOW)				
Peace sector						
PAD 1	-14.81	-132.56	236.1	0.3	Clear, bright brown	No
PAD 2	-17.34	-146.05	179.7	4.9	Clear, brown	No
PAD 3	-17.35	-148.09	189.1	99.4	Clear, light brown	No
PAD 4	-17.27	-147.14	422.6	4	Slightly turbid, dark tea brown	No
PAD 5	-13.42	-127.83	200.4	1.6	Clear, slightly greenish	No
PAD 6	-14.63	-132.27	250.6	7.1	Slightly turbid, greenish brown	No
PAD 8	-18.33	-149.83	145.5	29.3	Slightly turbid, dark brown	Yes
PAD 9	-17.47	-149.02	124.9	0.5	Clear, brown	No
PAD 12	-19.66	-156.82	218.1	182.5	Brown	Yes
PAD 13	-17.61	-147.68	288	0	Clear/brown	No
PAD 14	-15.25	-135.39	91.1	19.2	Slightly turbid, milky brown	No
PAD 15	-18.76	-154.02	206.3	145.3	Clear	Yes
PAD 16	-17.65	-146.66	273.5	5.4	Clear	No
PAD 17	-17.35	-145.71	113	144.4	Clear	No
PAD 18	-10.22	-108.02	148.7	BLQ	Clear, light brown/green	No
PAD 50	-15.55	-138.22	536	25.5	Green, brown	No
PAD 52	-17.76	-150.55	258.2	0	Clear, light brown	No
PAD 53	-15.45	-133.51	183.3	4.5	Brown/green	No
PAD 54	-19.52	-156.89	186.4	100.1	Clear, brown	Yes
PAD 57	-16.33	-141.91	585	22	Clear, brown	No
PAD 58	-17.07	-145.58	333.1	82	Brown, green	No
M15	-13.45	-124.14	157	0.4	Clear	No
M16	-15.01	-133.64	118.9	4	Clear, brown	No
M17	-18.54	-150.49	175.7	38	Brown	Yes
M18	-18.70	-152.51	167.8	78	Brown	Yes
M19	-16.59	-141.16	163.5	2	Clear, brown	No
R2	-18.82	-145.02	N/A	N/A	N/A	Peace River
Athabasca sector						
PAD 19	-14.92	-134.80	96.2	5.9	Clear, greenish	No
PAD 20	-17.06	-143.71	160.9	BLQ	N/A	No
PAD 21	-16.25	-140.41	183	BLQ	Slightly tea coloured	No
PAD 22	-18.25	-150.17	164.1	BLQ	Clear	Yes
PAD 23	-16.32	-139.81	155.1	BLQ	Clear	No
PAD 24	-18.90	-151.45	189.4	9.8	Clear	Yes
PAD 25	-18.80	-151.03	161.3	5.2	Slightly turbid, green tea color	Yes
PAD 26	-18.99	-151.06	166.2	6.2	Silty brown, turbid	Yes

PAD 27	-17.90	-145.84	122.2	2.3	Clear, green tea color	No
PAD 30	-18.34	-146.19	193.1	162.6	Turbid, brown with a milky silty tinge	Yes
PAD 31	-18.30	-145.36	191.5	231.9	Turbid, brown with a milky silty tinge	Yes
PAD 32	-18.41	-149.27	199.4	2.5	Clear	Yes
PAD 33	-19.09	-152.74	206.9	7.3	Slightly turbid, brown	Yes
PAD 36	-18.65	-149.78	182.3	0.8	Clear, greenish brown, some turbidity	Yes
PAD 37	-18.69	-154.27	190.8	BLQ	Clear	Yes
PAD 38	-19.05	-151.82	128.8	26.7	Milky brown, very turbid	Yes
PAD 39	-18.90	-152.28	184.2	1.7	Slightly turbid, greenish color	Yes
PAD 40	-19.12	-153.25	174.3	10.9	Brown	Yes
PAD 45	-18.24	-145.61	175.3	46.3	Turbid, sandy brown	Yes
PAD 46	-18.52	-148.32	198.2	9.4	Turbid, muddy brown	Yes
M1	-18.76	-149.72	188.8	BLQ	brownish, some turbidity	Yes
M2	-18.95	-149.15	66.9	BLQ	Clear	No
M3	-19.30	-153.62	161.7	5.1	Slightly turbid, light brown	Yes
M4	-18.81	-150.82	190.3	7.1	Turbid, weak tea color	Yes
M5	-19.19	-151.65	48.5	BLQ	Clear	No
M6	-18.15	-147.87	167.4	0.7	Clear, dark	Yes
M7	-18.77	-151.10	171	1.2	Clear	Yes
M8	-15.84	-133.71	326.7	1.4	Slightly turbid, greenish	No
M9	-15.06	-129.93	446.1	6.5	Clear, greenish with a tint of brown	No
M10	-17.44	-142.60	277.6	2.8	Slightly turbid, medium brown	No
M11	-17.96	-147.34	211.4	BLQ	Slightly turbid	Yes
M12	-18.51	-147.69	201.1	3.3	Slightly turbid, greenish brown	Yes
M14	-18.77	-148.58	190.2	3.4	Slightly turbid, green, brown	Yes
R5	-17.92	-139.16	N/A	N/A	N/A	Embarras River
R6	-17.56	-136.49	N/A	N/A	N/A	Fletcher Channel
R7	-18.04	-138.99	N/A	N/A	N/A	Mamawi Creek

Table A2.2: Values used for determining isotope framework parameters as reported in Imran et al. (2024).

Parameter	2020-2021 framework
h (%)	70.8
T (°C)	14.72
α^* (^{18}O, ^{2}H)	1.0103, 1.0908
ε^* (^{18}O, ^{2}H) (‰)	10.26, 90.77
ε_k (^{18}O, ^{2}H) (‰)	4.14, 3.64
δ_{As} (^{18}O, ^{2}H) (‰)	-26.89, -203.58
δ_P (^{18}O, ^{2}H) (‰)	-18.4, -142
δ_{SSL} (^{18}O, ^{2}H) (‰)	-10.30, -108.29

Table A2.3: Summary of total number of sites used for analysis of water isotope composition (i.e., flood designation, calculation of input proportion, geospatial analyses), lake-level change (i.e., water-depth data, spatial analysis), and lake-level rise (i.e., for partitioning lake-level rise attributable to snowmelt and river inputs, spatial analyses). Sites were excluded if there was uncertainty in consistent logger placement (†), or if the lake-levels declined in 2020 (‡). For geospatial analyses of lake-level rise, sites where lake-levels declined (‡) were included to improve interpolation.

Analysis type	Sites used (n)	Sites excluded
Water isotope composition	58	PAD 18
Lake-level change	56	PAD 18, PAD 15†, PAD 54†
Lake-level rise	52	PAD 18, PAD 15†, PAD 54†, PAD 19‡, PAD 24‡, M5‡, M14‡

Table A2.4: Estimated isotope composition of input water ($\delta^{18}O_I$, $\delta^{2}H_I$), percent snowmelt input, and percent river floodwater input to the lakes that flooded during the freshet of 2020. These include 6 lakes in the Peace sector and 23 lakes in the Athabasca sector of the Peace-Athabasca Delta.

Site ID	Water isotope composition		% Snowmelt input	% River input
	$\delta^{18}O_I$ (‰VSMOW)	$\delta^{2}H_I$ (‰VSMOW)		
Peace Sector				
PAD 8	-21.15	-162.45	32	68
PAD 12	-21.50	-165.12	37	63
PAD 15	-22.08	-169.44	45	55
PAD 54	-21.79	-167.29	41	59
M17	-21.03	-161.60	31	69
M18	-21.55	-165.46	38	62
Average	-21.52	-165.23	37	63
Athabasca Sector				
PAD 22	-21.34	-164.21	43	57
PAD 24	-20.67	-159.23	35	65
PAD 25	-20.67	-159.25	35	65
PAD 26	-20.38	-157.11	31	69
PAD 30	-19.65	-151.71	22	78
PAD 31	-19.43	-150.07	20	80
PAD 32	-20.66	-159.21	35	65
PAD 33	-20.82	-160.39	36	64
PAD 36	-20.45	-157.64	32	68
PAD 37	-22.24	-170.93	54	46
PAD 38	-20.55	-158.37	33	67
PAD 39	-20.98	-161.04	38	62
PAD 40	-20.98	-161.53	38	62
PAD 45	-19.60	-151.32	22	78
PAD 46	-20.12	-155.21	28	72
M1	-20.26	-156.19	22	78
M3	-20.81	-160.27	30	70
M4	-20.58	-158.56	36	64
M6	-20.57	-158.55	33	67
M7	-20.75	-159.84	33	67
M11	-20.70	-159.51	36	64
M12	-19.91	-153.64	25	75
M14	-19.85	-153.16	25	75
Average	-20.52	-158.13	32	68

Table A2.5: Lake-level change between September 2019 and May 2020 calculated for 56 lakes using lake-depth data. Lake-depth change for 40 lakes is based on availability of logger data from both years. For 16 lakes, a logger was not retrieved in either 2019 or 2020 and a spot measurement of depth (†) collected at the time of water sampling was used to determine lake-depth change. For PAD 45 (‡), spot measurements from 2019 and 2020 were used to calculate lake-level change. Lake-level rise attributable to snowmelt and river floodwater inputs are calculated based on proportion of each input source reported in Table A2.4.

Site ID	Lake-depth (m)		Lake-depth change (m) (from Sept 2019 to May 2020)	Lake-level rise attributable to snowmelt input (m)	Lake-level rise attributable to river input (m)
	September 2019	May 2020			
Peace sector					
PAD 1	0.80	1.18	0.38	0.38	
PAD 2	0.9†	1.38	0.48	0.48	
PAD 3	0.38	0.93	0.54	0.54	
PAD 4	0.44	0.70	0.26	0.26	
PAD 5	0.88	1.00	0.11	0.11	
PAD 6	0.86	1.19	0.33	0.33	
PAD 8	1.25	1.78	0.53	0.17	0.36
PAD 9	0.24†	0.31	0.07	0.07	
PAD 12	0.19	1.30	1.11	0.41	0.70
PAD 13	1.22	1.43	0.22	0.22	
PAD 14	1.32	1.44	0.11	0.11	
PAD 16	0.38	0.70	0.32	0.32	
PAD 17	0.39	0.76	0.38	0.38	
PAD 50	0.02	0.60	0.58	0.58	
PAD 52	0.53	1.02	0.49	0.49	
PAD 53	0.57	1.0†	0.43	0.43	
PAD 57	0.63	0.84	0.21	0.21	
PAD 58	0.31	0.61	0.30	0.30	
M15	0.61	0.91	0.31	0.31	
M16	0.92	1.06	0.14	0.14	
M17	0.72	0.86	0.14	0.04	0.10
M18	1.11	1.33	0.22	0.09	0.14
M19	0.71	0.93	0.22	0.22	
Athabasca sector					
PAD 19	1.01	0.8†	-0.21		
PAD 20	0.54	0.95	0.41	0.41	
PAD 21	0.61	1.1†	0.49	0.49	
PAD 22	0.88	1.99	1.11	0.48	0.64
PAD 23	1.20	1.42	0.22	0.22	
PAD 24	1.30	1.2†	-0.10		
PAD 25	1.29	1.40	0.11	0.04	0.07
PAD 26	1.41	1.99	0.59	0.18	0.40
PAD 27	1.28	1.3†	0.02	0.02	
PAD 30	0.82	1.23	0.42	0.09	0.32
PAD 31	1.27	1.49	0.22	0.04	0.17
PAD 32	0.89	1.02	0.13	0.04	0.08

PAD 33	1.39	1.9†	0.51	0.19	0.33
PAD 36	0.98	1.14	0.16	0.05	0.11
PAD 37	0.11	0.59	0.47	0.25	0.22
PAD 38	1.46	1.85	0.39	0.13	0.26
PAD 39	0.90	1.29	0.40	0.15	0.25
PAD 40	1.2†	1.78	0.58	0.22	0.36
PAD 45‡	1.0†	1.7†	0.70	0.15	0.55
PAD 46	1.41	1.7†	0.29	0.08	0.21
M1	1.22	1.29	0.07	0.02	0.05
M2	1.28	1.42	0.14	0.14	
M3	0.53†	2.04	1.51	0.55	0.96
M4	0.38	1.42†	1.04	0.35	0.69
M5	1.49	1.25	-0.25		
M6	0.41	1.00	0.59	0.20	0.39
M7	1.10	1.44	0.34	0.12	0.22
M8	0.76	1.4†	0.64	0.64	
M9	0.66	1.1†	0.44	0.44	
M10	0.65	1.3†	0.65	0.65	
M11	0.63	2.13	1.50	0.53	0.97
M12	1.09	1.22	0.13	0.03	0.10
M14	1.33	1.22	-0.11		

‡Change in spot depth measurements was verified using change in daily water-level data available at hydrometric station (Mamawi Lake Channel at Old Dog Camp; 07KF003).

Table A2.6: Summary statistics for lake-level rise (m) by input of snowmelt and river floodwater at non-flooded and flooded lakes in the Peace (n = 23) and Athabasca (n = 29) sectors, and at all non-flooded (n = 27) and flooded lakes (n =25) during spring 2020 across both sectors.

Lake-level rise input source (non-flooded/flooded lakes)	N	Median	IQR	Q1	Q3
Both sectors					
Snowmelt (non-flooded)	27	0.32	0.25	0.21	0.46
River floodwaters (flooded)	25	0.26	026	0.14	0.40
Snowmelt (flooded)	25	0.15	0.17	0.05	0.22
Peace sector					
Snowmelt (non-flooded)	19	0.31	0.20	0.21	0.41
River floodwaters (flooded)	4	0.25	0.31	0.13	0.44
Snowmelt (flooded)	4	0.13	0.16	0.07	0.23
Athabasca sector					
Snowmelt (non-flooded)	8	0.43	0.33	0.20	0.53
River floodwaters (flooded)	21	0.26	0.23	0.17	0.40
Snowmelt (flooded)	21	0.15	0.17	0.05	0.22